A Unified Approach to Maximum Power Point Tracking and I-V Curve Determination of Photovoltaic Arrays from Real-time Measurements

ScuDo
Scuola di Dottorato ~ Doctoral School
WHAT YOU ARE, TAKES YOU FAR

Doctoral Dissertation
Doctoral Program in Energy Engineering (29th Cycle)

A Unified Approach to Maximum Power Point Tracking and I-V Curve Determination of Photovoltaic Arrays from Real-time Measurements

By

Jawad Ahmad

Supervisor:
Prof. Filippo Spertino

Doctoral Examination Committee:

Prof. Pierlugi Caramia, University of Napoli Parthenope

Prof. Giorgio Graditi, ENEA Portici Research Centre

Prof. Federico Silvestro, University of Genova

Prof. Giuseppe Marco Tina, University of Catania

Politecnico di Torino
2017

Declaration

I hereby declare that, the contents and organization of this dissertation constitute my own original work and does not compromise in any way the rights of third parties, including those relating to the security of personal data.

Jawad Ahmad

2016

* This dissertation is presented in partial fulfillment of the requirements for **Ph.D. degree** in the Graduate School of Politecnico di Torino (ScuDo).

Contents

Abstract

In recent years we have seen a considerable increase in the installed capacity of Photovoltaic (PV) power generating plants worldwide. This increase is primarily attributed to the decrease in the cost of installation and the awareness towards the sustainable power generation. However, the efficiency of the PV modules is still low. The Current vs. Voltage (*I-V*) characteristics of the PV generators is non-linear and changes with irradiance and temperature. For optimal utilization of PV sources, Maximum Power Point Trackers (MPPTs) are used. When the array is under uniform illumination, there is a single peak on the Power vs. Voltage (*P-V*) curve of the PV array. This peak is easily tracked by conventional MPPTs. However, under Partial Shading Conditions (PSC), multiple peaks appear on the *P-V* curve. Out of these, there is one Global Peak (GP) while the others are Local Peaks (LP). When the MPPT algorithm is trapped at LP, considerable power loss occurs. Special MPPTs are designed for finding the GP when the array is under PSC.

It is also important to periodically find the *I-V* curve of the array under the field conditions for monitoring and control of the PV generators. For this purpose, specialized tests are performed. During these tests, the generation of power from the PV arrays is halted. Similarly, the speed of performance of these tests is also important as the environmental conditions may change quickly during finding of the curve. Any change in the surroundings during the performance of finding the characteristic curve may affect the results.

In this thesis, two algorithms are proposed that perform the MPP tracking and measurement of the *I-V* curve under any kind of irradiance. The first algorithm performs these tasks by using the module voltages as the parameter. In the second method, the input filter capacitor of buck or buck-boost converter is used. Simulation and experimental results confirm the performance of the proposed methods.

List of Figures

Chapter 1 Introduction

The major economies of the world are heavily reliant on natural gas, oil, and coal for meeting their energy requirement. These fuels are limited and an unabated use of these resources will eventually cause them to dwindle. From that point it would be impossible to retrieve these sources. On the other hand, renewable sources like wind and solar energy are replenished. The sunlight can be used for production of electricity, for heating, and for many other industrial applications. The energy from fast moving winds is captured by wind turbines for generation of electricity. Similarly, geothermal is the heat from the earth's interior. Geothermal heat pumps tap into this resource for heating and cooling of buildings. The heat from the earth's interior can also be utilized for the production of electric power. Another important renewable energy source is the tidal energy. The importance of these assets is that we can put them to our benefit on sustainable basis.

With the increasing population and penetration of modern technology in human life, the demand for electrical energy is likely to increase continuously with time. The production of electricity from fossil fuels leads to many environmental problems like [1]:

- Water pollution
- Maritime pollution
- Emission of hazardous air pollutants
- Solid waste
- Ozone depletion

In addition to the above mentioned problems, sustainability is another challenge that the human beings face today. A common definition of sustainability is [2]:

> *"Development that meets the needs of the present without compromising the ability of future generations to meet their own needs."*

A sustainable development in society demands sustainable supply of energy resources. There is an intimate relationship between sustainable development and renewable sources of energy. In this chapter a summary of the Renewable Energy Report for year 2015 is presented to accentuate the fact that the attention of all the stakeholders has shifted towards renewable sources of energy in recent times.

1.1 Summary of the Renewable Energy Report

According to the report [3], the investment in renewable power and fuels worldwide has reached to 285.9 billion USD in 2015. This amount is higher than 273 billion USD in 2014. Most of this investment was earmarked for the production of power. The breakup of the power generated from different renewable means is given in Table 1.1.

Table 1.1 Total installed capacity of renewable sources during years 2014 and 2015

Power	Installed Capacity in 2014	Installed Capacity in 2015
Total renewable power capacity	1701 GW	1849 GW
Hydropower capacity	1036 GW	1064 GW
Bio-power capacity	101 GW	106 GW
Geothermal power capacity	12.9 GW	13.2 GW
Solar PV capacity	177 GW	227 GW
Concentrating solar thermal power capacity	4.3 GW	4.8 GW
Wind power capacity	370 GW	433 GW

As can be seen from the data in table 1.1, wind and solar power accounted for about 77% of the new installations. By the end of the year 2015, renewable capacity in place was able to provide about 23.7% of the global electricity. This increase in capacity is attributed to many factors. The policy makers continue to focus on the renewable power technology and particularly the solar and wind power. In 2015, 110 jurisdictions at the national or state level enacted laws and policies making this the most widely adopted regulatory mechanism for promoting generation of electricity from renewable sources. In the same manner, the advances in modern technologies, increasing environmental awareness, and economic benefits further helped in the increasing trend.

At global level, high profile agreements and announcements were made during the year 2015 encouraging the sustainable energy assets. These include:

1. In their Declaration on Climate Change, the G7 countries committed to

transform the world's energy sector by 2050. At present about 1.2 billion people live without electricity with the majority belonging to sub-Saharan Africa and Asia-Pacific, the declaration also affirmed to encourage access to renewable energy in these regions of the world.

2. Renewables were also on the agenda of G20 Energy Ministers meeting. In the meeting the delegates avowed their commitment to renewable energy and energy efficiency. The participants endorsed an 11 point Communique that included adopting of a toolkit for long-term sustainable and combined approach to renewable energy usage. The ministers also concurred on G20 Energy Access Action Plan for sub-Saharan Africa which emphasize the potential of renewable energy in that part of the world.
3. Sustainable Development Goals (SDG) were adopted by the UN General Assembly in 2015. The goals for the time, contained a dedicated goal on sustainable energy for all. This success was owing to the Sustainable Energy for All initiative which was proactive during the SDG deliberations.
4. In December 2015, UN Climate Change Conference took place in Paris. In the summit, 195 participating countries agreed to limit the global warming to well below 2 degrees Celsius and the countries committed to scale up renewables and energy efficiency.

1.2 Increased Capacity of PV Installation in 2015

In this section we will evaluate the advancements made in the installed capacity of the PV power as given in the report [3]. As given in table 1.1 and Fig. 1.1, the solar PV market was up by 25% over 2014. In terms of the GW a record increase of 50 GW was seen as compared to the previous year. From Fig. 1.1 it is also noticeable that the installed worldwide installed capacity of the PV was only 5.1 GW in 2005. This market expansion is attributed to the increasing competitiveness of the PV generators. According to the report, China had the installed capacity of 44 GW by the end of 2015. In Japan the PV capacity has almost doubled during the period of 3 years from 2012-2015 and it now stands at 34.4 GW. Germany has capacity of 41 GW. In the USA the PV installations have exceeded the natural gas capacity for the first time. The country added 7.3 GW during 2015 and has its tally stood at 25.6 GW by the close of the year. Similarly, for the same period the capacity of Italy and UK was 19.3 GW and 9.1 GW respectively. Fig. 1.2 shows the breakup of the contributions from various countries during the year under review.

As given in Fig. 1.2, Asia's contribution was the highest accounting for about 60% of the global additions. China, Japan and USA remained the top three markets followed by the UK, India and Germany. In order to address the country's severe pollution problems China continued to raise the installation of PV generating plants. Another significant achievement from the world's most populous country was that it overtook Germany in terms of cumulative installed capacity. This increase in capacity was also accompanied by grid congestion problems and interconnection delays in China. During the year the average module prices also fell and the prices of multi-crystalline silicon came down to USD 0.55/Watt.

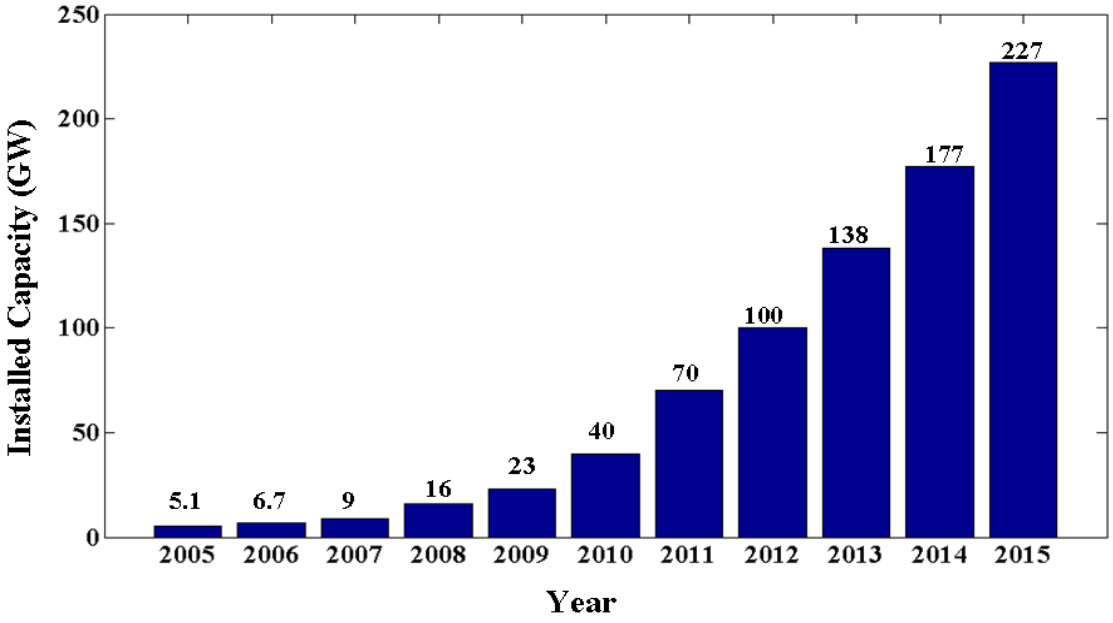

Fig. 1.1 Worldwide PV installed capacity since 2005.

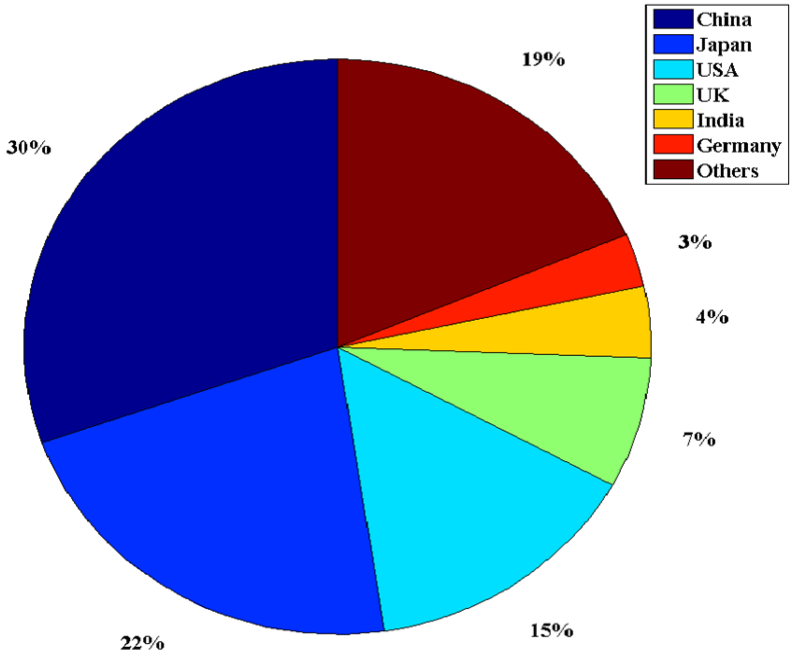

Fig. 1.2 Added capacity of PV by various countries during 2015.

1.3 Challenges in the Development of PV Generation

The PV panels are not the only component of the PV generation system. The other essential components of the PV system include: the array structures, MPPT controllers, inverters, energy storage devices like batteries and supercapacitors, overcurrent protective devices, connectors, and system controllers [4, 5]. It is through the research over the years that the efficiency and reliability of the components involved in the PV plants have improved. Many environment and operation related stresses like humidity, thermal stresses, high voltage bias, the presence of impurities, corrosion etc. affect the performance and lifetime of the PV systems [6].

An essential part of the power processing system is the storage devices which are necessary in many applications. Their usage is not just restricted to the stand-alone but also to the grid tied applications. In critically important applications, for example, industrial control systems, hospitals, telecommunications, and offices; continuous supply is insured. In these applications the storage devices form an integral part of the power supply system [7]. Batteries need to be managed correctly for full utilization and long life. Life reduction owing to misuse can

increase the cost and also affect the stability of the PV generation systems. The design of efficient charge controllers, the proper use of batteries and ultra-capacitor hybrids, and maintaining proper temperature etc. are the primary challenges as far as the storage devices are concerned.

It has been shown in the literature [5, 8, 9, 10] that the inverters form the most fragile part of the system. Over the whole life of the PV systems, the inverter needs to be replaced 3 to 5 times [4]. For example, in [8] it is reported that inverter failures because of the lightning effects and humidity represent about 77% of the system failures. Therefore, it is essential to take climatic conditions into account and improve the lightning protection. Similarly, according to [11], of the total of 139 events of PV system failure about 103 were due to inverters. According to the findings, the main reasons for failures were non-intentional operation of islanding mode. Electrolytic capacitor is also a troublesome component in the switching inverters [12]. The avoidance of electrolytic capacitors and adoption of low ESR capacitor for avoiding overheating can considerably improve the functionality of the inverters. According to [13] another failure prone component is the MOSFET switch. It is recommended in these research papers that the performance and lifetime of the inverters could be improves is slightly overrated MOSFET switches are utilized.

In addition to inverter failure, other challenges in the full utilization of the PV energy include:

- Low conversion efficiency of solar cells.
- Intermittent nature of sunlight.
- Non-linear current vs. voltage characteristics, and dependence of environmental irradiance and temperature.
- Development of current mismatches among the modules as a result of partial shading of PV arrays or change in characteristics due to ageing of the PV modules.
- Obtaining the correct *I-V* curve for control and monitoring the performance of the PV plants

For optimizing the performance of the PV plants, it is important to operate the array at Maximum Power Point (MPP) during any ambient conditions. Maximum Power Point Tracking (MPPT) algorithms are used for extraction of optimal power from the PV systems. For designing a proper MPPT procedure, the system designer must take into consideration the climatic conditions of the locality from the past data. An MPPT method that is designed for the climatic conditions prevalent in desert areas cannot operate efficiently in regions with cyclonic activity. After gaining sufficient knowledge about the climate of the locality,

proper MPPT scheme has to be chosen for ensuring reliability of the system.
Improving the electrical efficiency of the PV plants is the major source of concern in all the applications like, stand-alone, grid connected, remote telecommunications, rural electrifications, and space applications. A judicious choice of the MPPT scheme can help in improving the electrical efficiency manifold [14].
The tracking efficiency and reliability is dependent on the duty cycle perturbation step in some of the famous MPPT algorithms. The higher step size will result in the fast transient response of the algorithm. However, under lower irradiances a higher perturbation step is likely to result in large oscillations around the MPP under steady-state. The small perturbation step reduces the magnitude of the steady-state oscillations. Using a small perturbation step, nevertheless compromises the transient response. Previously, the choice of the proper MPPT scheme also depended upon the parameters that were needed for proper tracking. According to [15], the current sensors were considered to be more expensive and their use was to a large extent discouraged. Similarly, the analog implementation was thought to be a preferred choice. However, owing to the advances is technology this perception has changed. With the development and reduction is price of the microcontrollers, the digital implementation is become feasible. Now the modern microcontrollers are equipped with high speed analog to digital converters and also have a higher number of analog input channels. The ability of these controllers to perform fast and simultaneous conversion of analog into digital quantities has made measurements easy and the number of parameters needed to perform MPP tracking is no more a big hurdle. Similarly, the price and size of the Hall-effect based current sensors have also come down and current measurement has become a lot more convenient.

For fault diagnosis in PV plants two important types of test are performed: the Electroluminescence (EL) and the Infrared Thermographic (IRT) or thermal imaging. In the EL tests the radiative recombination of the charge carriers under forward bias conditions is detected. In the EL image, the resultant light intensity is proportional to the voltage. In this way, any inactive part within the PV module is manifested as dark areas [6]. EL tests can diagnose faults like the cell cracks, shunt paths, Potentially Induced Defects (PID) etc. These tests are performed by halting the normal operation of the PV plants or at night time. The IRT involves the detection and measurement of infrared radiations which are intrinsically emitted by the surface of a body. In the PV applications the IRT tests are performed under real time conditions when the PV generator is operating under

MPP. The IRT provides information about the thermal signature and exact location of the fault. The thermal images can then be used for quantitative diagnosis to calculate the exact power loss as a result of a defect inside a PV module. The main benefit of the thermal imaging test is that the normal operation of the plant is not interrupted. However, these tests are usually quite expensive and may be feasible for large power plants, but for Building Installed PV (BIPV) and plants with relatively smaller capacity frequent performance of these specialized tests may not be cost effective.

Conventional monitoring of the PV plants is performed through the *I-V* curve measurements. An abnormal electrical characteristic curve can be indicative of a defect, but the location of the fault can only be identified by the specialized tests discussed above. However, the *I-V* curve still plays an important role in detecting some of the most common faults if accurate curve is measured. It is the main objective of this text to propose a technique which calculates the accurate *I-V* curve and to identify the module which has potentially developed a defect. The proposed scheme is applied in combination with the MPP tracking algorithm. Thus, the procedure presented in this work executes the MPPT, accurate electrical characteristic curve measurement, and a potential fault diagnosis.

1.4 Organization of Thesis

The main objective of this thesis is to develop algorithms that treat the two issues of MPP tracking and measuring the *I-V* curve simultaneously under the real time field conditions. In the literature these aspects of the PV plant operation are considered as separate subjects, and therefore very little attention is given to adopt an integrated approach towards the two subjects.
This text is further organized as follows:
In chapters 2 and 3 respectively, the literature review of MPPT algorithms and methods of finding the *I-V* curve are given. In chapter 4, a model for PV arrays under partial shading conditions is developed. In chapter 5, properties of PV arrays under partial shading conditions are discussed. In chapter 6, an algorithm for finding the characteristic curve and MPP tracking from on-site measurements is given. This algorithm is based on the assumption that the voltages of the modules inside the array are perfectly matched under nominal conditions. In chapter 7, a method for obtaining the characteristic curve of a solar array and finding MPP is given by taking into consideration the presence of voltage mismatch among modules. Chapter 8 deals with an MPPT and curve finding

procedure by utilizing the input filter capacitor of buck or buck-boost converter.

Chapter 2 Literature Review of the Main MPPT methods

In this chapter literature review about the MPPT algorithms is given. In the first part the main MPPT methods for uniform irradiance conditions are explained. It the second part, the MPPT schemes under non-uniform illumination are discussed. Even though, in the literature many schemes about the MPP tracking have been proposed; we will focus our attention on the famous methods. For further information, the research papers given in the reference list can be useful.

2.1 MPPTs for Uniform irradiance

The well-known MPPT algorithms under uniform irradiance are: Perturb and Observe (P&O) method, Incremental Conductance (IC) method, Ripple Correlation, Fractional Open Circuit voltage, and Fractional Short Circuit Current [15]. Here we will discuss only the most common methods namely: the P&O, and IC algorithms. Some changes to the P&O algorithm for overcoming its shortcomings are also given.

2.1.1 Perturb and Observe method

Among the conventional techniques, P&O is most widely used for its simplicity and ease of implementation. The working principle of P&O technique is that the operating voltage of the PV array is perturbed in a specific direction for example, from point A to B in Fig. 2.1. This is accomplished by changing the duty cycle of the DC-DC converter. If an increase in the output power of the PV system is observed, it suggests that the operating point has moved closer to the MPP and the next perturbation is applied in the same direction, i.e. from point B to C. On the other hand, if the output power is reduced after perturbation, for example from D to E; this means that the operating point has moved away from the MPP and the next perturbation is applied in the opposite direction from E to D. This sequence of perturbing the operating point and observing the variation in power is repeated till the MPP at point P is reached. The system then starts to oscillate around that point. The oscillation of the operating point around the peak is the major drawback of the technique which results in the fluctuation of the out power from

the PV system. The magnitude of this fluctuation can be reduced by decreasing the size of the perturbation step. Unfortunately, the reduction in step size degrades the response of the system to changes in irradiance. Setting large perturbation step results in faster response but it increases the magnitude of oscillations around MPP which increases the steady state power loss.

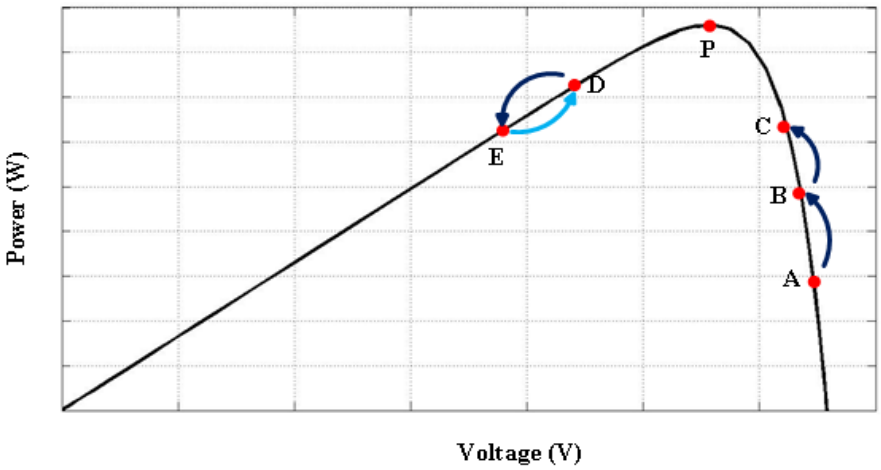

Fig. 2.1 Principle of operation of conventional P&O algorithm.

For obtaining the fast transient response and decreasing the steady-state oscillations, P&O algorithms with variable perturbation step [16], [17], [18] and hybrid MPPT [19] have been reported. In the variable step size P&O algorithm as shown in Fig. 2.2 [20], the size of the duty ratio perturbation (ΔD) is set differently depending upon the location of the operating point of the array. At the start of the algorithm ΔD is kept large in order to accelerate the convergence to the MPP. This is shown by the movement of operating point from A to B and from B to C. After a number of perturbations in a given direction, the operating point of the array passes the peak P which is indicated by the reduction in the PV array's output power from that in the previous sampling period. This is shown by the reduction in power as a result of the movement from point C to E in Fig. 2.2. At this stage the value of ΔD is reduced and the perturbation step is applied from point E to F. Each time the operating point passes the MPP, the value of the perturbation step is decreased. In this way convergence to the MPP is ensured when the value of ΔD falls below a predetermined limit. As given in Fig. 2.3, the during the steady-state operation the value of ΔD is kept at small level for reducing the steady state oscillations around the peak. Thus, the variable step size P&O algorithm overcomes the shortcomings of the conventional P&O method by

employing different size of ΔD depending upon the location of a particular operating point on the *P-V* curve.

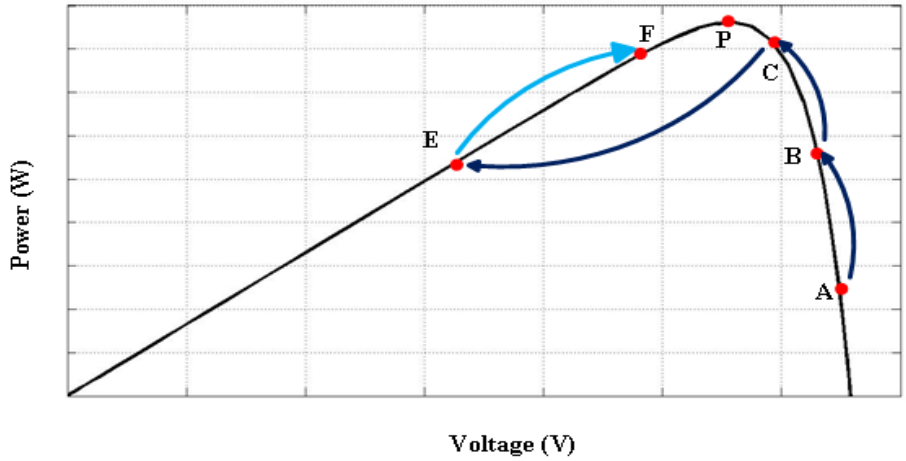

Fig. 2.2 Operation of variable step size P&O algorithm.

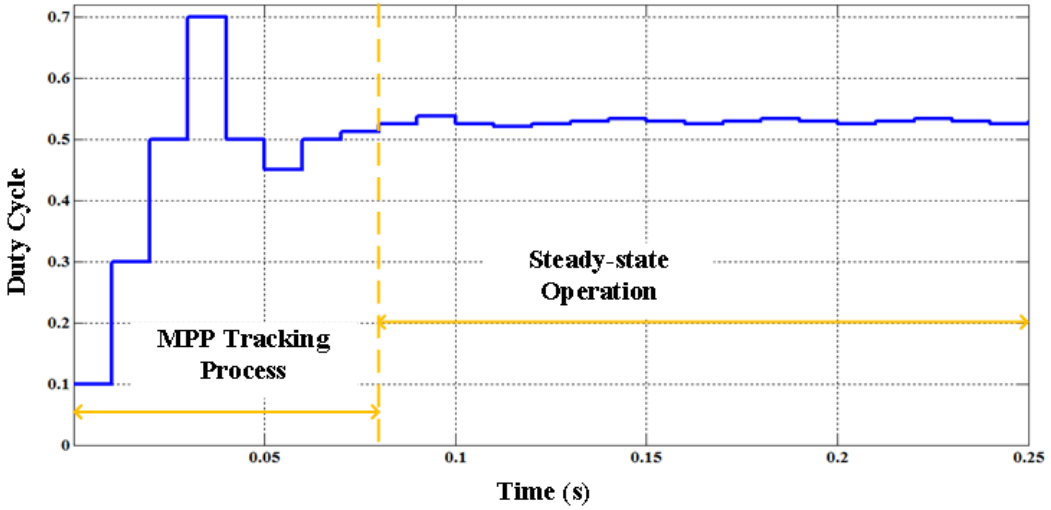

Fig. 2.3 Variation of duty cycle perturbation step during variable step size P&O method.

The method proposed in [16] operates in two modes i.e., the active and the power-down mode. MPP tracking is performed in the active mode and the system operates at this point during the power-down mode. This scheme has a fast tracking speed and also there are no fluctuations around the MPP in the steady-state. However, during rapidly changing irradiance, this method does not instantly respond, as the duration of power down mode is longer than the active mode. Similarly, during the operation of active mode, the operating voltage of the PV

system is changed even in the absence of any change in the MPP which leads to power loss [17]. In [18] also, there are no oscillations around the MPP but the method is strictly applicable to the regions where there is a clear blue sky for the most part of the year and no or very small variations in the sunlight are observed. Ref. [19] also uses the hybrid technique but the method uses additional MOSFET switch in DC-DC converter for disconnecting the PV array for measurement of V_{OC} of the array. The design of high side driver and heat sink for the disconnecting MOSFET switch can be complicated and also expensive. The on-state resistance of the switch also causes some power loss.

The improved forms of the P&O algorithms have better response than the conventional method. It is shown in [20] that the transient response of the variable step size P&O algorithm is three times faster than the conventional P&O. As a consequence of the faster transient response the normalized power loss of the technique is five times smaller. Similarly, by reducing the step size during the steady state operation, its steady-state efficiency is about 99%.

The algorithm proposed in [20] coauthored by the author is further explained with the help of the flowchart shown in Fig 2.4. This technique is specifically developed for the areas which have highly variable weather conditions for most part of the day due to the presence of stochastic cloud cover and frequent cyclonic activity. From the flowchart we see that the scheme operates in two modes: the MPP tracking mode, and the steady-state mode. At the start of the MPP tracking mode ΔD is set to 0.1 and P&O algorithm with monotonically decreasing ΔD (shown as MPP tracking mode in Fig. 2.4) is invoked. This process continues till $\Delta D \leq 0.004$ in case of an 8-bit microcontroller. At this stage the power corresponding to the MPP (P_{MPP}) is measured. Then conventional P&O with ΔD = 0.004, shown as steady state operation, begins.

The output power of the PV module (P_{PV}) is constantly monitored in the steady state for any variations in P_{MPP} outside the range ±3%. The steady state perturbation $\Delta D = 0.004$ is sufficient to maintain the operation of the system around the MPP in the range ±3% of the power corresponding to the MPP tracked under the previous iteration. Any variation in the range ±3% to ±10% (which corresponds to highly variable but stable weather condition) is followed by MPP tracking mode with ΔD initially set to 0.05. Similarly, any variation of PPV above or below 10% is characterized by an unstable weather. In this situation MPP tracking mode is invoked by the algorithm and ΔD is set to 0.1 to track the new MPP. In order to further explain the operation of the method some simulation results are included in this text.

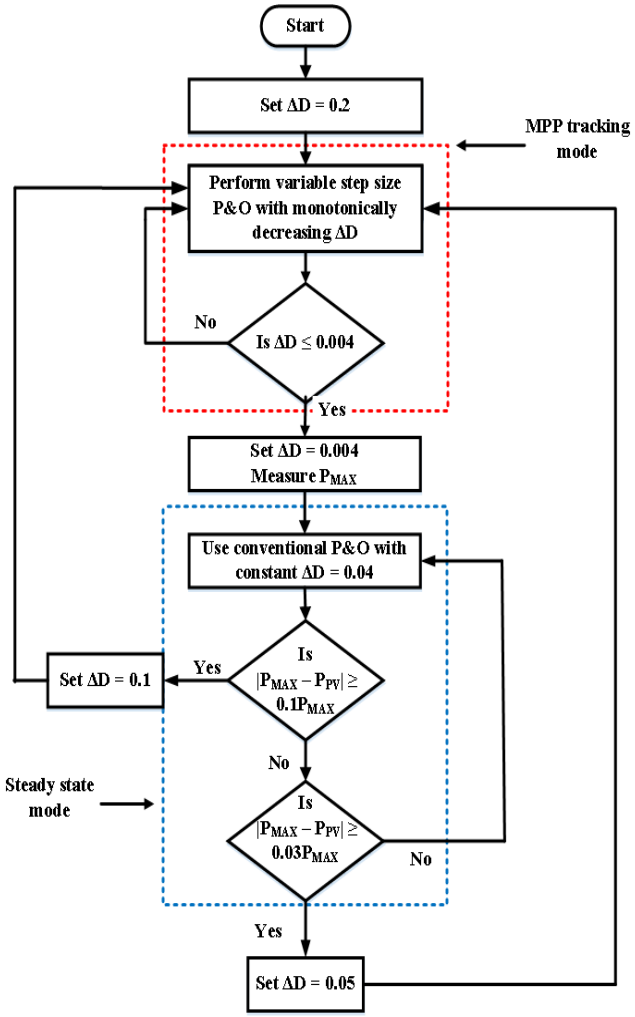

Fig. 2.4 Flowchart of the algorithm given in Ref. [20].

To check the performance of the proposed MPPT algorithm, simulations were performed in MATLAB/SIMULINK. Buck converter with switching frequency of 100 kHz was used. The PV module used in the simulations has V_{OC} and I_{SC} equal to 32.9V and 8.26A respectively. Fig. 2.5 shows the performance of the proposed MPPT in the beginning of the algorithm. For comparison, the operation of the constant step size P&O is shown in Fig. 2.6. The two Figs indicate that the proposed method converges to the MPP much faster than the conventional method. As a result of the faster convergence of the proposed technique, less power loss is incurred. To determine the relative performance of the two algorithms we can use the concept of the normalized power loss (P_{LOSS}) as in [17]. P_{LOSS} for each algorithm can be calculated as

$$P_{Loss} = \frac{(\sum_{i=0}^{k} P_{ideal} - \sum_{i=0}^{k} P_{algorithm})}{\sum_{i=0}^{k} P_{ideal}} \times 100 \quad (2.1)$$

here k is the number of samples [17].

Using (2.1) for the beginning of each algorithm, P_{LOSS} for the conventional and the proposed algorithm was found to be 30.87% and 6.24% respectively. It suggests that the power loss during the beginning of tracking of the proposed algorithm is five times less than the conventional P&O. Eq. (2.1) was also used for calculating the loss due to steady state perturbation under constant irradiance of 1000 W/m^2. It was found that the power loss due to small ΔD was less than 0.08% .

In Fig. 2.7 is shown the response of the proposed algorithm to a ramp increase in the irradiance at 400W/m^{2}s. This figure indicates that the proposed algorithm tracks the MPP during highly variable weather conditions. In Fig. 2.8 is shown the response of the proposed algorithm to a step decrease in irradiance. This situation occurs during unstable weather. The results in Fig. 2.8 indicate that the algorithm is able to converge to the new MPP in about 4 sampling periods. In order to deal with these situations, the method proposed in [19] not only uses additional hardware but also involves frequent disconnection of PV source from the load for measurement of V_{OC} which involves a considerable amount of power loss. Similarly, [16] responds to these changes only in the active mode which makes the method unsuitable for highly variable weather conditions. On the other hand, the proposed algorithm deals with the same scenario quickly and with lesser fluctuations in the output power.

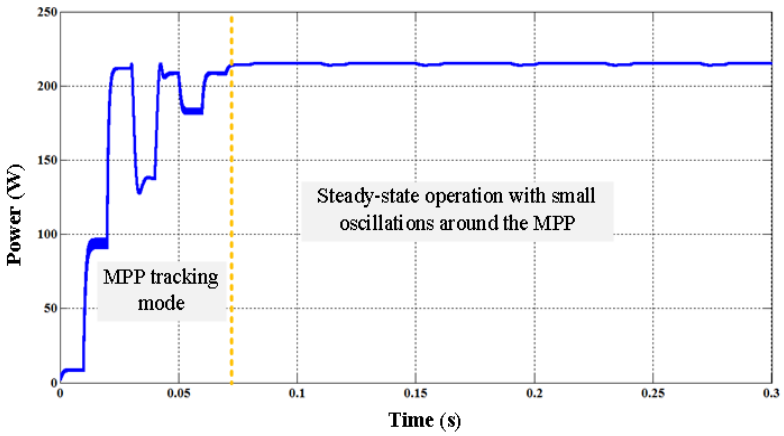

Fig. 2.5 Performance of the algorithm in [20] during the start of the MPP tracking.

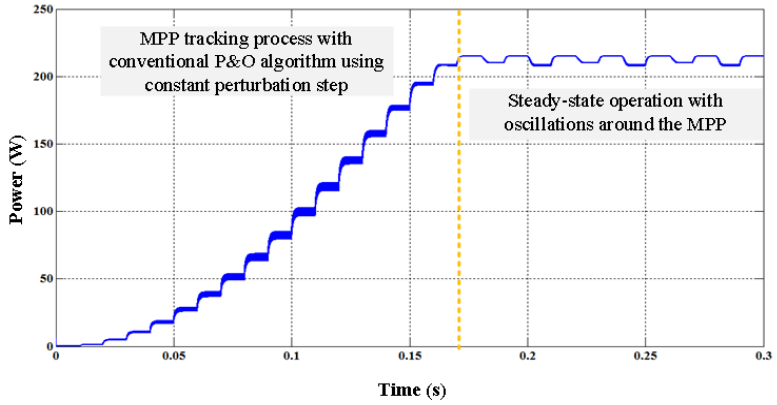

Fig. 2.6 Tracking performance of the conventional P&O algorithm.

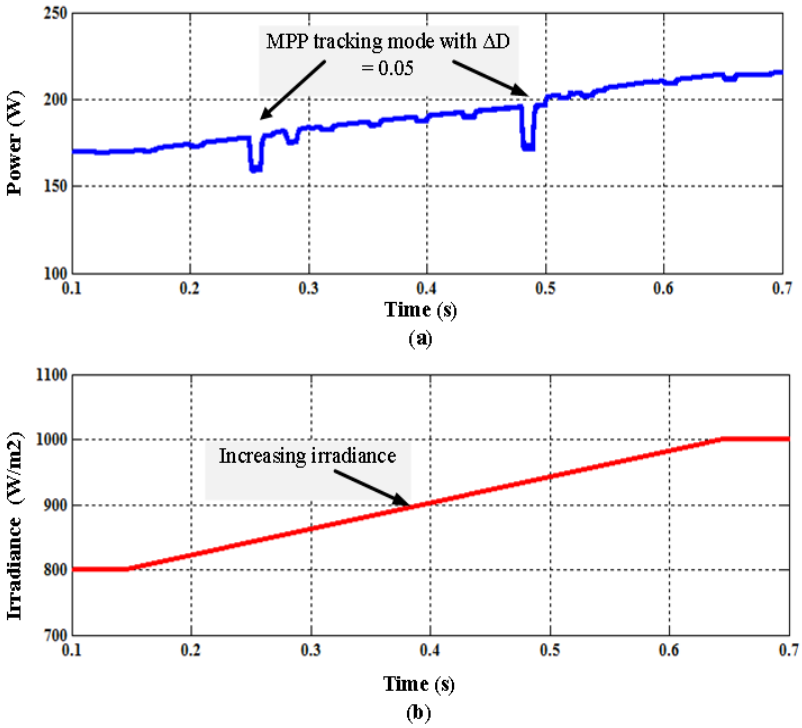

Fig. 2.7 MPP tracking during ramp increase in the irradiance.

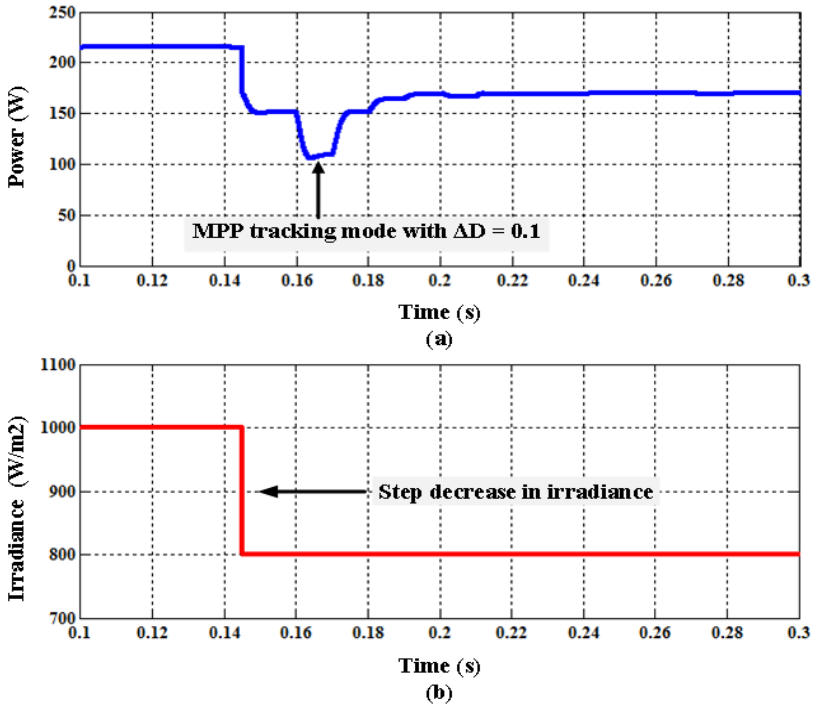

Fig. 2.8 MPP tracking during step variation in the irradiance.

The results given above suggest that the variable step size P&O algorithm has better performance than its conventional version of the MPPT method. In the following section we will discuss another conventional MPPT scheme which is the Incremental Conductance (IC) method.

2.1.2 Incremental Conductance Method

The IC method is based on the comparison of incremental and instantaneous conductance of a PV array. The main idea is that at MPP, the derivative of power w.r.t voltage ($\frac{dP}{dV}$) is equal to zero [21] i.e.

$$\frac{dP}{dV} = \frac{d(VI)}{dV} = I + V\frac{dI}{dV} = 0$$

The above equation can be rearranged as follows

$$-\frac{I}{V} = \frac{dI}{dV} \cong \frac{\Delta I}{\Delta V}$$

Where ΔI and ΔV are the increments of the array current and voltage respectively.

The basic equations of this technique are:

$\frac{dI}{dV} = -\frac{I}{V}$ At MPP

$\frac{dI}{dV} > -\frac{I}{V}$ At the left of MPP

$\frac{dI}{dV} < -\frac{I}{V}$ At the right of MPP

This scheme has a very high efficiency and can reach to about 99%. The flowchart of conventional IC method is shown in Fig. 2.4 [22].

As with the P&O algorithm, some modifications have also been proposed with the IC method for bringing some improvements in the performance. But the amendments in the original technique have not brought about any considerable improvement in the performance as compared to the original version of the algorithm. For example, the variable step size with constant voltage start-up system has a performance of 99.2% while the fixed size method has an efficiency of 98.9% [22]. Thus, with the proper choice of the step size, the conventional IC method can perform satisfactorily without increasing the complexity of the method. In Ref [22] the PI control loop has been eliminated and the duty cycle is controlled directly by the algorithm. This modification has simplified the control loop and the time for tuning the controller has been eliminated.

In this section, two important MPPT techniques have been discussed. The details about other methods for uniform irradiance conditions can found in [15]. The performance of these methods is about 99% when the array is uniformly illuminated. However, when partial shading of the PV array occurs, their performance deteriorates. Partial shading of PV arrays is a common phenomenon particularly in case building integrated PV plants. It is therefore necessary to design MPPTs that can track the MPP under non-uniform illumination. In the following section, we briefly review some of the important MPPT procedures for partial shading conditions.

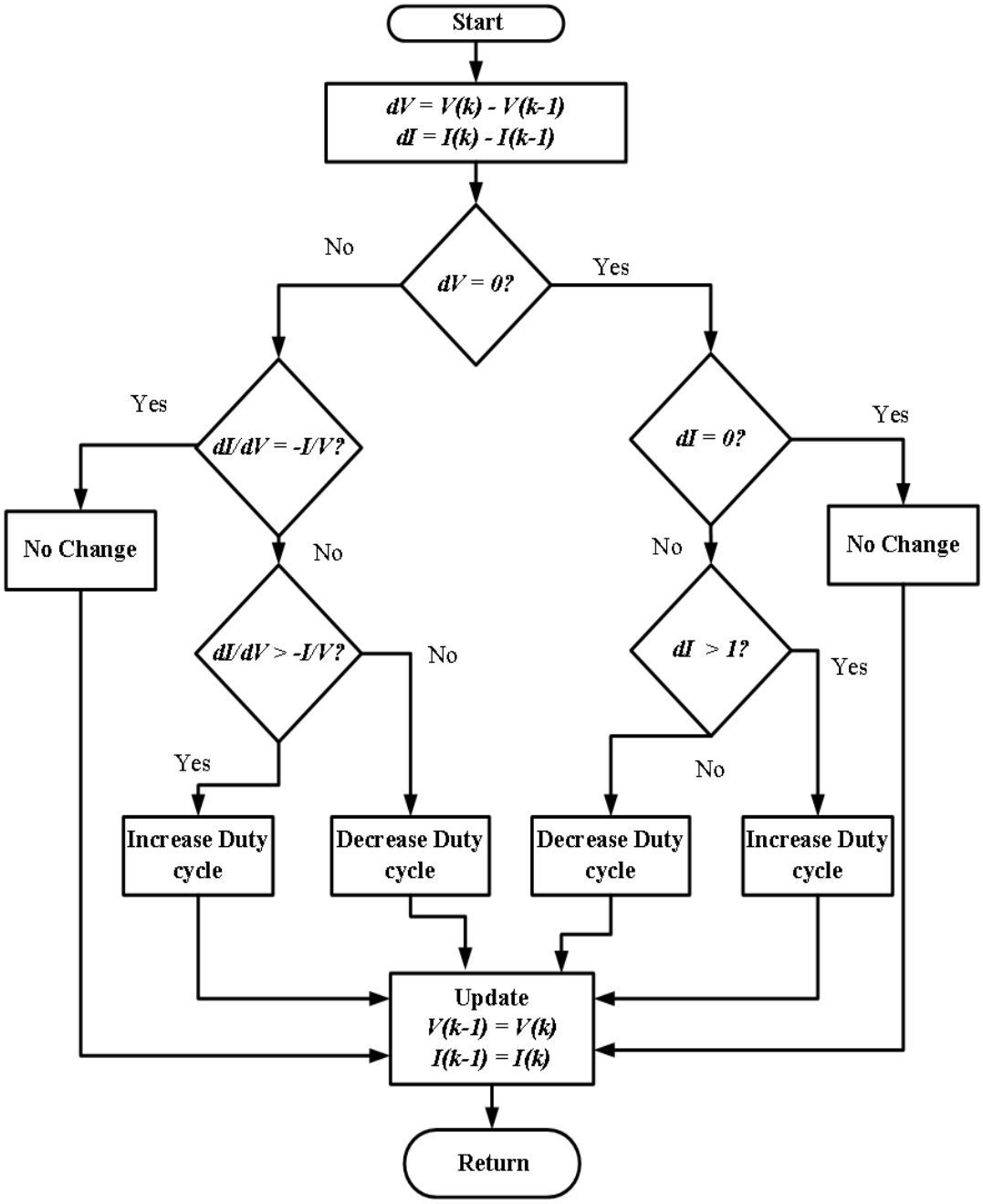

Fig. 2.9 Flowchart of IC method.

2.2 MPPT Techniques for Partial shading

Before discussing some of the most common MPPT schemes which are used under Partial Shading Conditions (PSC), it is important to explain the effects of partial shading in PV arrays.

For obtaining the desired level of power, PV arrays are formed by connecting multiple modules in series, parallel, and series-parallel combination. With the increasing number of modules in an array, its physical size also increases. In practical conditions some of the modules within an array may not receive full solar irradiance due to the shadows of surrounding buildings, trees, dust, etc. It is reported in [23] that out of 1000 building integrated PV systems, installed in Germany, 41% were affected by partial shading. This indicates inevitability of the problem particularly for building integrated PV systems.

It is well known that the photo-generated or the PV current of a cell is proportional to the irradiance according to the relation:

$$I_{ph} = (I_{scn} + K_I \Delta T) \frac{G}{G_n} \tag{2.2}$$

Where I_{ph} is the PV current, I_{scn} is the nominal short circuit current of the cell, K_I is the thermal coefficient of short circuit current in A/K, G is the irradiance received by the cell, G_n is the nominal irradiance and has value of 1000W/m^2, and ΔT is the difference between the cell temperature and the nominal temperature in K.

Let us suppose that some cells inside a series connected string are shaded while the others in the string receive full irradiance. According to Eq. (2.2), the PV current of the shaded cells is reduced whereas that of the unshaded cells is high. Since the current of the series connected cells must be equal, the shaded cells are forced to operate in the reverse region to conduct large current of the unshaded cells [24].

Under PSC the shaded cells behave like a load and consume power instead of producing it because of the reverse polarity. This dissipation of power leads to local overheating and creation of hot spot. Excessive heating can result in the cell burnout and can create open circuit. To overcome the problem of hotspots a bypass diode is connected across a certain number of cells. In a typical module with 60 series connected cells, a diode is connected across 20 cells. These diodes

provide an alternate current path and conduct current when the cells cannot produce the required level of current. Thus, the problem of the formation of hot spot is mitigated. However, due to the action of bypass diodes, multiple peaks appear the *P-V* characteristic of the array under PSC.

Out of these multiple peaks, there is only Global Peak (GP) while the rest are Local Peaks (LP). In this scenario, the tracking of GP becomes quite challenging. The conventional MPPTs like the P&O and IC perform efficiently when the array is under uniform irradiance [25].

When PSC occur the conventional MPPTs may fail to track the GP in the presence of multiple peaks. The failure of the conventional techniques is described in Fig. 2.10. This figure shows the simulated *P-V* curves of a PV generator with six series connected modules. The open circuit voltage of the array under nominal conditions is 73 V and the short circuit current is 8.2 A. Let us assume that the array is under uniform irradiance and its *P-V* curve is represented by dotted line in Fig. 2.10. A conventional MPPT algorithm operates the PV around the peak at point A. Suppose PSC occurs with one of the module now receive irradiance of 300 W/m^2. The *P-V* curve becomes as the one shown by the solid green line. The conventional MPPT may take the operating point to B and will start oscillation around the LP. However, as shown in the Fig. 2.10, point C is the GP. It can be noticed that the power corresponding to point C (P_C) is higher than that at point B (P_B). The power loss P_C-P_B occurs because of the trapping of the conventional MPPT at point B. It is therefore, essential that a MPPT scheme must operate the PV system at the GP when PSC occurs. Referring to Fig. 2.10, we find that the peak shown at point B lies close to the open circuit voltage of the array while the peak C is to its left on the same curve. In this text we will refer to the peak nearest to the open circuit voltage of a PV array as the Right Peak (RP). Depending upon the type of the shade and the number of modules that are shaded, the RP may or may not be the GP.

The location of GP under partial shade depends upon the type of shade and the number of modules that are under the shade [26]. Experiments have been conducted on a 230W PV panel. The panel has 60 series connected cells; one bypass diode is placed across 20 cells and in this way, a string with 3 series connected modules is constituted. In Fig. 2.11, is shown the case in which the shade is cast by a distant object, or in other words the shade is weak. When shading is caused by a distant object, the direct irradiance is prevented from illuminating the surface of the module. However, the diffused irradiance continues to illuminate the shaded part of the array. From the experimental *P-V* curve of the

generator in Fig. 2.12, we see that the peak nearest to the open circuit voltage of the panel (RP) is the GP.

In the field conditions the shading may also be caused by an object that physically covers the surface of the array. This situation is depicted in Fig. 2.13, which shows the case when the shading of the array is caused by an object that is very close to its surface. In this scenario, the cells which are shaded receive very little irradiance. The presence of the object close to the surface does not allow diffused irradiance to illuminate the shaded cells. As given in Eq. (2.2), the photovoltaic current from the shaded cells is very low as compared to the cells which take full irradiance. The *P-V* curve is shown in Fig. 2.14. When the array is operated at the RP, only the shaded module/s operates at its MPP which is characterized by low current. The unshaded modules operate at a current which is well below their MPP currents. Similarly, at P2 the shaded module/s is bypassed and the unshaded modules operate at their respective MPP currents. From Fig. 2.14, we see that the RP (P1) is the LP whereas P2 is the GP.

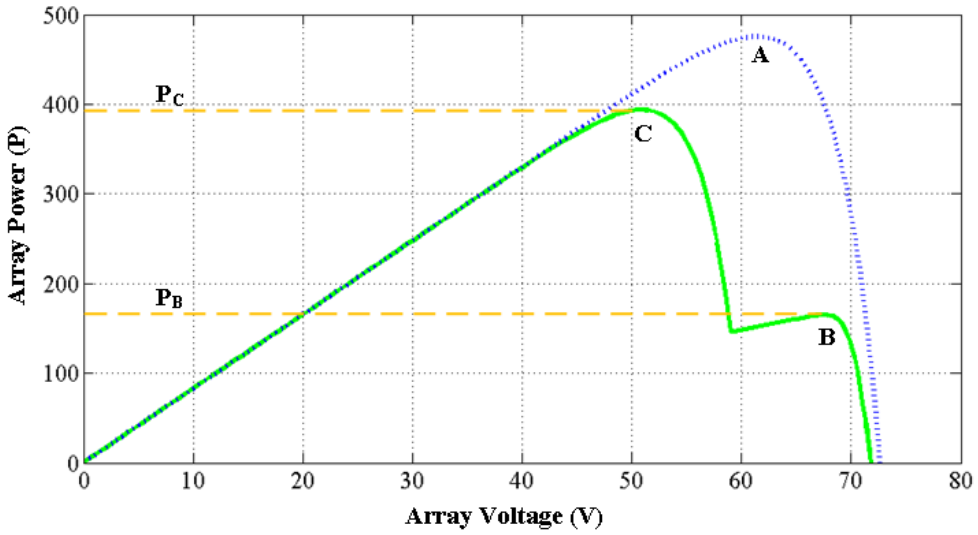

Fig. 2.10 Pictorial representation of MPPT failure under partial shading.

Fig. 2.11 Partial shading caused by a distant object.

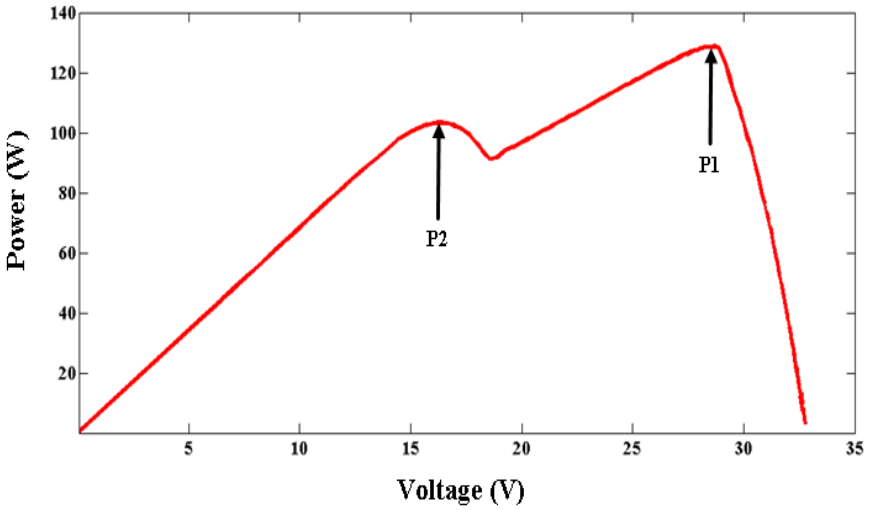

Fig. 2.12 *P-V* characteristic of the array with irradiance pattern given in Fig. 2.11.

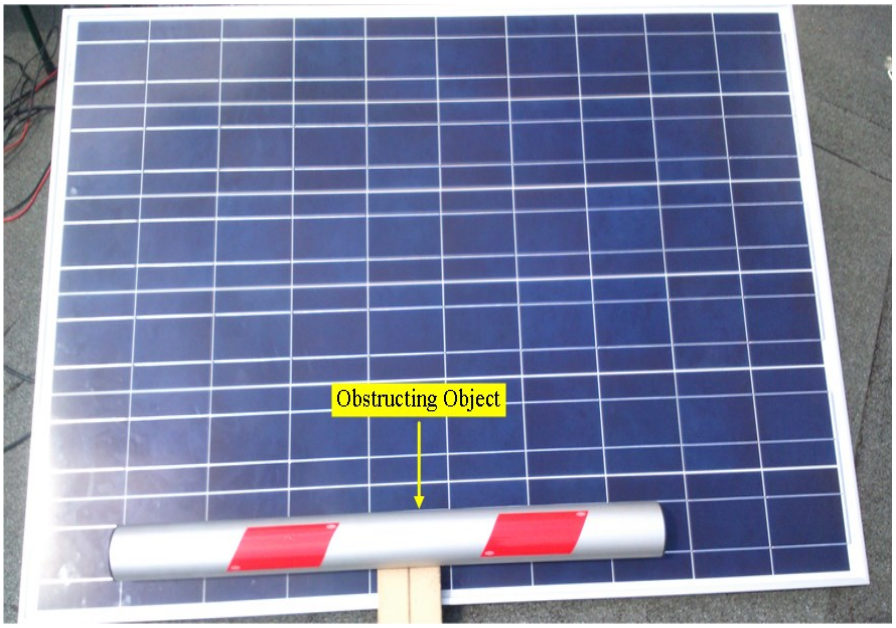

Fig. 2.13 Partial shading caused by object close to the surface of the PV panel.

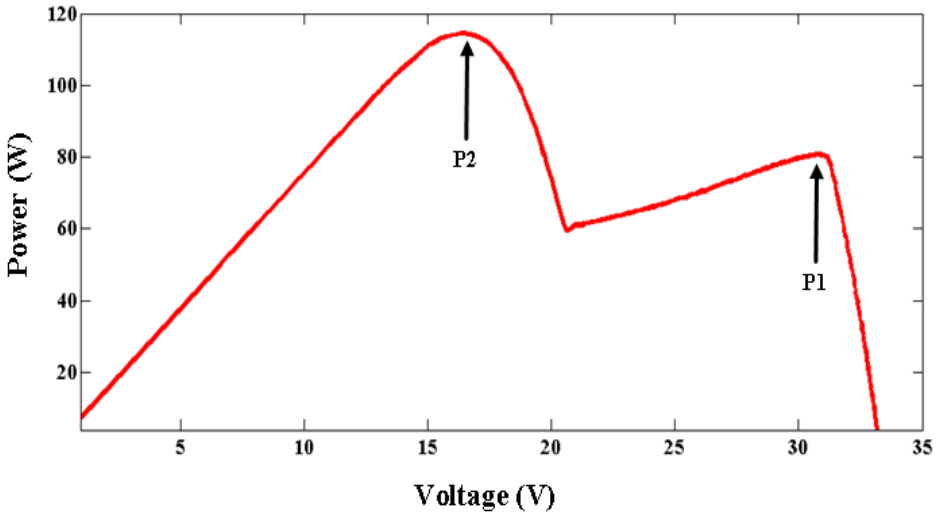

Fig. 2.14 *P-V* characteristic of the array with irradiance pattern shown in Fig. 2.13.

From the above two cases, we can conclude that the location of GP varies in accordance with the type of shade and also the number of modules that are shaded [26]. Hence, a MPPT algorithm should be able to quickly track the GP under any type of shading. Another essential characteristic of MPPT algorithm is that it should be able to sense the presence of PSC.

We now proceed to give brief description of some of the well-known MPPT techniques that are meant to track the GP of a partially shaded PV array.

2.2.1 Two Stages MPPT

In commercially available PV systems the entire *P-V* curve of the array is scanned for finding the GP. This is done by varying the duty cycle of the DC-DC converter in the range [0, 1] in small steps. The GP tracking process is accomplished through this method in several seconds. During the scanning process the array is not operated at the MPP which leads to considerable power loss. In order to reduce the time duration required for completing the scanning of the curve Two Stages MPPT scheme has been proposed in [26, 27, 28]. This method is based on the following assumptions:

1. The peaks on the *P-V* curve occur nearly at the multiples of 80% of V_{OC} of a single module.
2. The minimum displacement between two consecutive peaks is approximately equal to 80% of the V_{OC} of a single module.
3. When the *P-V* curve is traversed either from V_{OC} or from the zero voltage the magnitude of the peaks increases. After converging to the GP, the magnitude of the peaks continuously decreases.

In this method the true MPP is found in two parts: (1) the main program, (2) the GP track routine. To avoid complete scanning of the curve, the search is performed in a certain range of voltage defined by (V_{min}, V_{max}). Then the GP is tracked by performing the search process in the vicinity of voltage points which are at integral multiple of 80% of the V_{OC} of a single module. This mechanism reduces the time duration for performing the MPP search under PSC. However, this algorithm has some shortcomings which are given as follows:

1. This method fails to track the MPP when difference between the irradiances received by the shaded and unshaded modules is high and the

number of shaded modules in the array is greater than the unshaded ones [28].

2. As shown in the work co-authored by this author in [29], the peak on the *P-V* curve does not actually occur at 80% voltage of the V_{OC} of a single module. A more accurate relation is developed which will be presented in subsequent chapters.

2.2.2 External Capacitor Method

This method utilizes an external capacitor for scanning the *P-V* curve according to the physical conditions of the array at a given time [25]. The circuit diagram of this method is shown in Fig. 2.15. As shown in this figure, switch S1 is used to connect the PV array to the DC-DC converter. Under normal operation when the MPP of the array is known, this switch is closed. The purpose of switch S2 is to connect the external capacitor C_{EXT} to the array when it is required to scan its *P-V* curve for finding the GP. During the normal operation of the array, S2 is off. After the execution of the subroutine that finds the GP S2 is turned off and S3 is turned on. Switch S3 is used for discharging C_{EXT} through a resistor R_{EXT}. The time t_C required for charging the external capacitor is given by:

$$t_C = 2C\frac{V_{OC}}{I_{SC}} \tag{2.3}$$

Where C is the capacitance of C_{EXT}, V_{OC} is the open circuit voltage of the array, and I_{SC} is the short its short circuit current.

This algorithm operates in two stages. In the first stage the global MPP of the array is found by means of scanning the *P-V* through C_{EXT}. The operation of this stage is invoked either at the start of the algorithm or if there is a change in irradiance. Let us assume that the array is operating at its MPP, and a sudden variation in the output power of the array is observed due to the occurrence of partial shading. In this situation, it is necessary to find the new GP of the PV generator. As mentioned earlier, the S1 is opened, and S2 is closed for connecting the external capacitor in the circuit. When the capacitor is being charged, the product of the voltage and current of the capacitor are monitored by the microcontroller. When a peak *P-V* curve of the array is observed during the charging evolution of C_{EXT}, the voltage and power corresponding to that point are recorded by the controller as V_{REF}. When any other peak is present due to partial shading, the value of power at the point is compared to the previously recorded

peak. If the value of power corresponding to the new peak is greater than the one which was previously recorded during the scanning, the voltage corresponding to the new one is stored as V_{REF}. After the completion of the scan, the value of V_{REF} corresponding to the GP is obtained by the controller.

In the second stage, the main objective is to take the operating point of the array to the new MPP that has been found in the first stage. To do this S1and S3 are closed, and S2 is opened. The microcontroller produces the necessary PWM signal to operate the array at the desired voltage. The duty cycle of the converter is changed in small steps till the GP is tracked. This method has an advantage of finding the GP in accordance with real condition of the array, but has the following shortcomings:

1. This scheme uses three additional MOSFET switches in its circuit. Of particular importance is the switch S1. The design of driver circuit and heat sink can be challenging and costly. Moreover, the on-state resistance of the switch may also cause power loss in the hardware.
2. The time required for charging the capacitor given in (2.3) is not constant and is mainly dependent upon the irradiance. Some extra arrangement needs to be made in order to account for this variation.
3. After finding the voltage V_{REF}, the procedure proposed in [25] is based on changing the duty cycle of the converter in small steps for operating the array at the GP. This process may take several sampling periods and during the time, the array is not operated at its MPP. This also results in some power loss.

The above mentioned shortcomings of this technique have been addressed in Chapter 8 of this text.

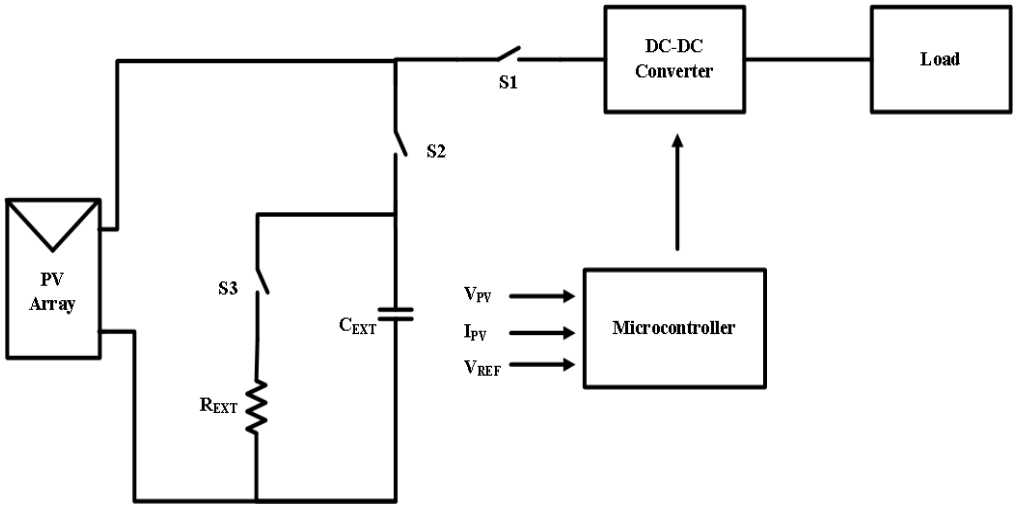

Fig.2.15 Circuit diagram of external capacitor MPPT technique.

2.2.3 Module Voltage Based MPPT

The module voltage based MPPT is based on the principle that the modules that receive different irradiance have different operating voltage [30, 31, 32]. The main motivation behind the development of this technique is that in the two stages MPP procedure discussed previously we do not know about the presence of PSC. Consequently, when the two stages MPPT is used the algorithm performs search in the voltage range (V_{min}, V_{max}). When there is uniform irradiance the MPP procedure performs the search to the left of the RP for a non-existent peak. It is well-known that during the search for a peak, the PV system is not operated at the GP. This results in unnecessary power loss when there is no PSC.

The flowchart of the module voltage based MPPT scheme is shown in Fig. 2.16 [31]. In this mechanism, the PV string is first operated at the peak (RP) which is nearest to the V_{OC} of the array using the P&O algorithm. When the RP is tracked the voltage across each module (each bypass diode) is measured. If the voltage of the modules is same (within a certain limit), it suggests the uniform irradiance. In this case, steady state operating around the MPP begins. However, if the operating voltage of the modules is different at the RP, it means the presence of PSC. It is because when there is PSC, at the RP only the weakest modules operate at the MPP voltage and current. On the other hand, the modules which receive full irradiance function at lower current than their respective MPP currents and their voltages are near to the V_{OC}. For finding the location and the number of peaks the

modules are arranged in various groups on the basis of operating voltage. The modules which have approximately the same operating voltage are placed in the same group. The total number of groups determines the number of peaks present on the *P-V* curve. Then the approximate location of each of the peaks is determined using the relation:

$$V_P \approx \left(1 - \frac{N_B}{N_S}\right) V_{OC} * 0.80 \tag{2.4}$$

Where V_P is the voltage corresponding to a certain peak, N_B is the number of series connected diodes that are bypassed at a certain peak, and N_S is the number of series connected modules in the array. In this way, we can track any number of peaks under PSC. Here, the results of the paper in [31] which is coauthored by this author, are given.

Fig. 2.17 shows a PV generator with four series connected modules. The open circuit voltage and the short circuit current of the generator is 132 V and 8.20 A respectively. The PV source given in Fig. 2.17 is either a small sized array with four series connected modules or is a string in a large array with its independent MPPT. In order to understand the operation of the proposed algorithm with example, consider the case of Fig. 2.17 (b) with the *P-V* characteristic shown in Fig. 2.18. When this situation occurs, the main program calls for the GP track subroutine and the peak P1 is detected using conventional P&O algorithm. The values of the power corresponding to that peak P_{MPP}, the duty ratio of the DC-DC converter D_{MPP}, and voltage V_{MPP} are recorded. The algorithm measures the voltage of each of the series connected modules and finds (VM1 = VM2 = 24.85V, and VM3 = VM4 = 32.01V) which indicates the presence of two irradiance levels. As we can see from the voltage of the modules, M3 and M4 receive the maximum irradiance. We then take the subset which contains the modules that receive lesser irradiance than M3 and M4. This subset is composed of M1 and M2 which means that $N_B = 2$ at peak P2 in Fig. 2.18(a). As M3 and M4 have the same operating voltage, we can therefore conclude that there are only two peaks. The voltage and power at P1 are already known. With $V_{OC} = 132$V the location of P2 is found to be at 56V using Eq. (2.4). The algorithm then proceeds to track this peak using modified P&O algorithm discussed in section 2.1.1 of this chapter. After tracking P2 the power corresponding to the peak is compared to the value at P1 for finding the GP. As the power at the peak P2 is higher than that at P1, this suggests that P2 is the GP. The algorithm then starts operation at the GP in the steady state.

Let us consider the case of Fig. 2.17 (c) with the *P-V* characteristic shown in Fig. 2.19. In the manner discussed previously, the MPPT system first tracks P1. The voltages of the modules are found to be (VM1 = 21.79V, VM2 = 30.64V, VM3 = 31.98V, VM4 = 31.98V). This indicates three different voltage levels which mean that there are three peaks present on the *P-V* curve. Similar to the previous case we obtain NB = 2 for the peak P2 in Fig. 2.19. This means that one of the peaks (P2 in Fig. 2(c)) is at V2 = 56V which is obtained using Eq. (2.4). From the subset containing M1 and M2 we see that M2 receives higher irradiance than M1 from which we see the presence of the peak P3. The location of P3 is found to be approximately at 84V using Eq. (2.4). Having already known the values of power at P1, the algorithm operates the system respectively at P2 and P3. Out of these peaks the GP is determined followed by the steady-state operation.

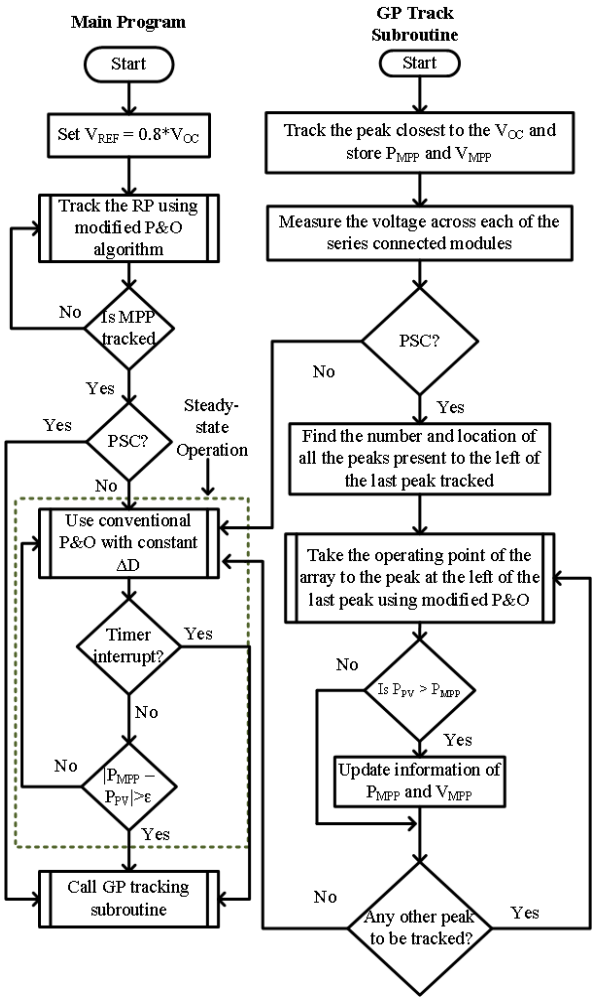

Fig. 2.16 Flowchart of the module voltage based MPPT.

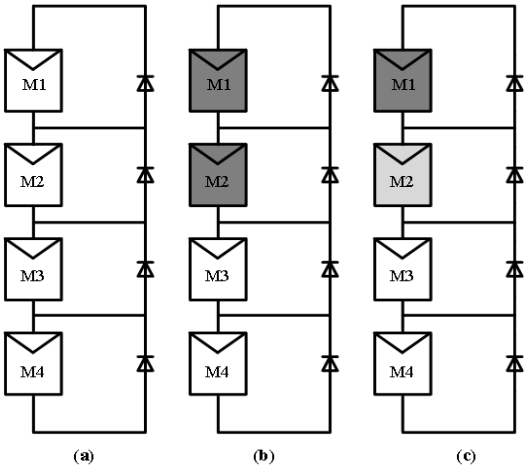

Fig. 2.17 A PV string with four modules under different irradiance.

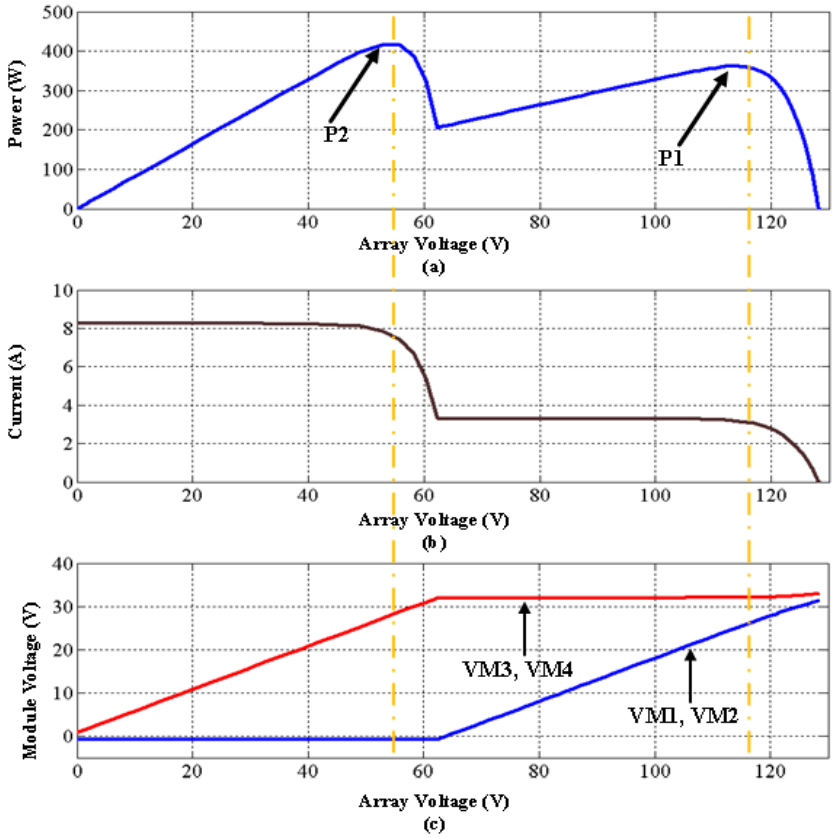

Fig. 2.18 Characteristic curves of the PV generator given in Fig. 2.17 (b). (a) The P-V curve. (b) The I-V curve. (c) Module voltage as a function of the array voltage.

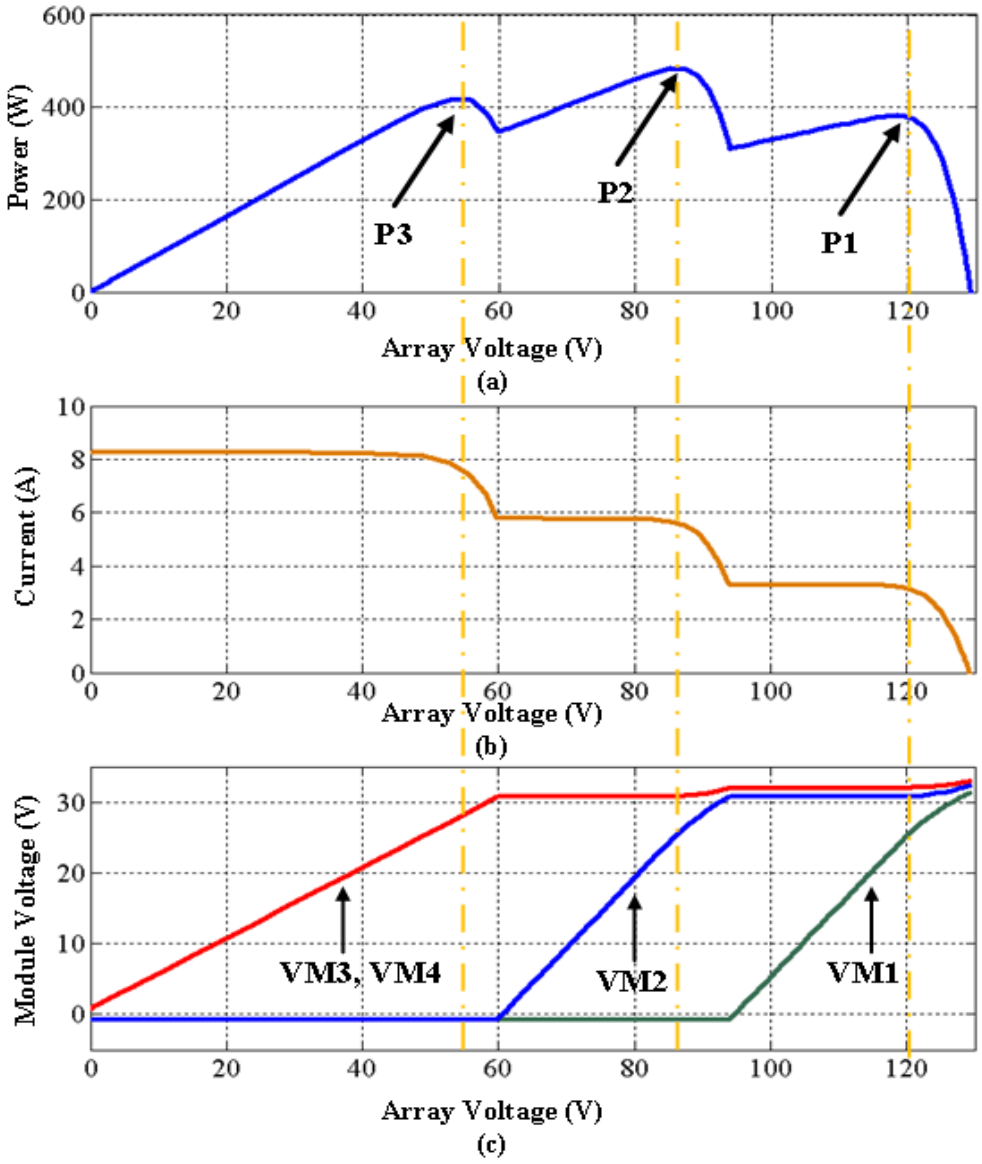

Fig. 2.19 Characteristic curves of the PV generator given in Fig. 2.17 (v). (a) The P-V curve. (b) The I-V curve. (c) Module voltage as a function of the array voltage.

The proposed MPPT algorithm was simulated using MATLAB/SIMULINK. The PV string used in simulations has four series connected modules. The sampling period is 10ms. DC-DC buck converter with switching frequency of 100 kHz is used. The simulation results are shown in Fig. 2.20. Suppose the system is operating at its MPP in the steady state conditions with each of the four modules receiving 1000W/m^2 irradiance. At t1 a step change in irradiance occurs and two of the modules now receive 400W/m^2. This is similar to the situation described in Fig. 2.17 (b) with the corresponding *P-V* curve shown in Fig. 2.18 (a). The

resulting decrease in the array output power is sensed during the next sampling interval at about 0.28s. The GP tracking process starts and the algorithm tracks both the peaks P1 and P2. By comparing the powers at the two peaks, P2 turns out to be the GP and the PV system is operated at this peak in the steady state. The whole process takes about 0.23s. This time duration is far less than 1.1s and 1.2s, taken by the algorithms in [30], and [26] respectively. Fig. 2.21 shows the GP tracking process when three peaks are present. At t = 0.255s a partial shading occurs which is indicated by a sudden decrease in power from the array. The tracking process starts in the next sampling period and lasts till t2 at 0.58s. It means that in the extreme case of three peaks the process takes only 0.32s.
The results obtained from [31] suggest that the time taken for finding the GP is about 0.23s. Under extreme cases, there could be more than two peaks present in the characteristic curve of the PV generator. In such a scenario, the time taken for tracking that many peaks might be longer. The simulation results in [31] suggest that under extreme cases the time required for finding the GP is only about 0.32s.

In addition to reducing the time required to reach the GP under PSC, another benefit of this MPPT is that after tracking RP the existence of PSC if determined from the voltage of the modules. If there is uniform irradiance, the steady state operation begins and the GP track subroutine is not invoked. However, this scheme could be misled if there is a voltage mismatch between the modules due to the development of the potentially induced faults. The shortcomings of this technique are addressed in Chapter 7 of this text. In that chapter it will also be shown that this procedure can also be used for obtaining the current vs. voltage characteristic curve of a PV from onsite measurements.

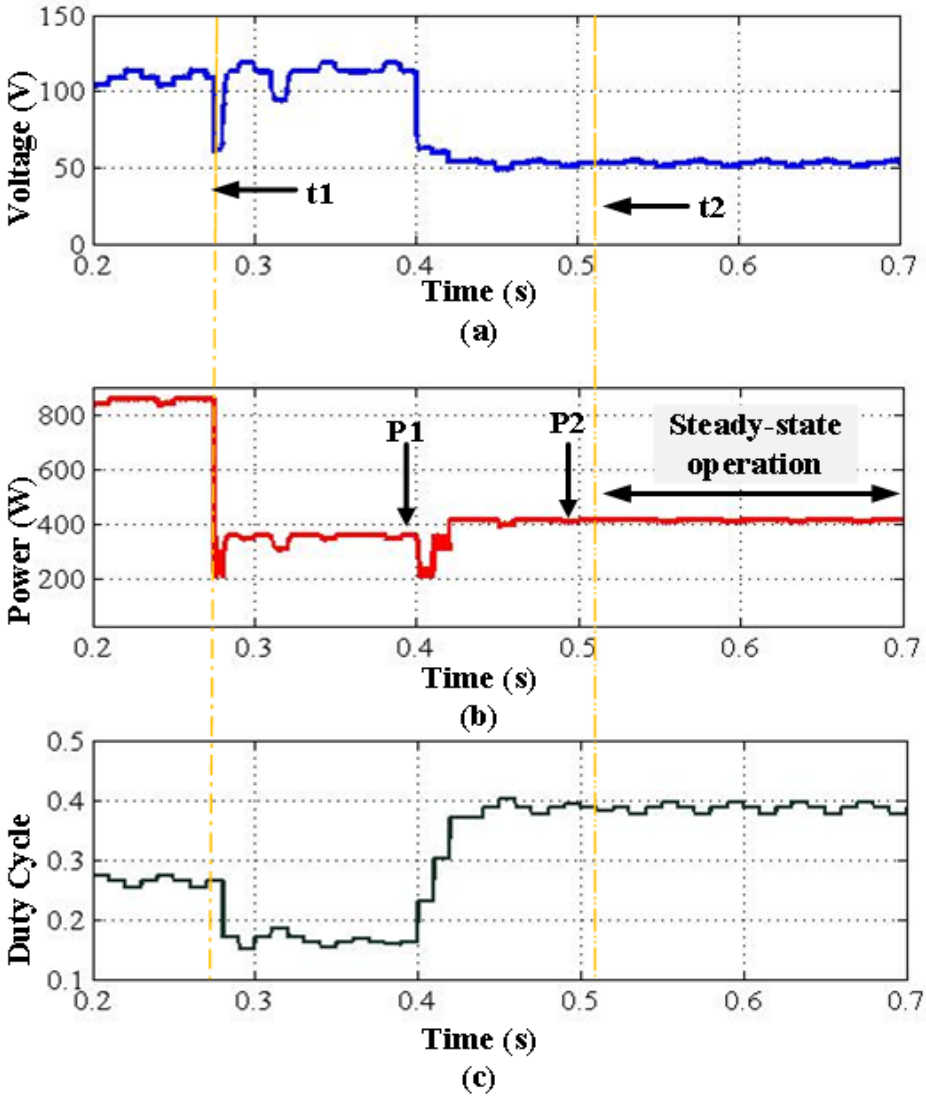

Fig. 2.20 The GP tracking process in case of two peaks.

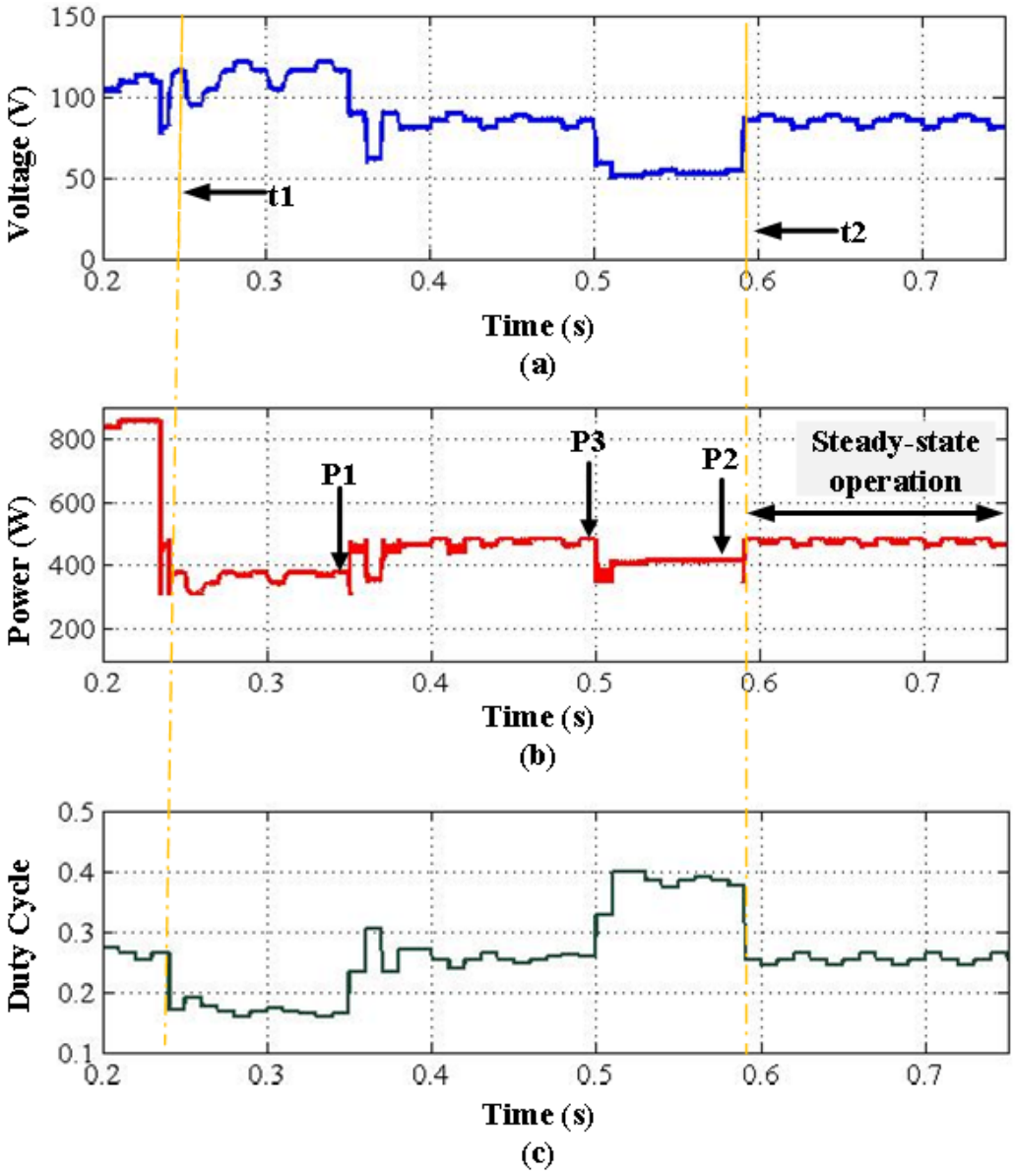

Fig. 2.21 The GP tracking process in case of two peaks.

2.2.4 Artificial Neural Networks

Various authors [33], [34] have used Artificial Neural Networks (ANN) for tracking of MPP under uniform and non-uniform irradiance conditions. The architecture of a generalized 3 layer feedforward neural network is shown in Fig. 2.22. The network consists of input, hidden and output layers. The number of

neurons in the input and output layers depend upon the number of inputs and outputs respectively and may be different from one case to another. For example, [33] needs three inputs namely: the ambient temperature, the I_{SC}, and the position of the Sun. Similarly [34] the array voltage and current are the inputs and in this way, only two input neurons are needed. The number of neurons in the hidden layer is determined by trial and error.

Training of the ANN is first performed, generally by using the back propagation algorithm. During the training process the weights are trained to correctly map the input data to the required output. Training is accomplished to minimize the error between the network output and the desired one. This is done by minimizing the error between the actual output of the network and the required output. At the end of the training process the ANN should be able to find the reference voltage corresponding to the GP.

The ANN could be used for easily finding the MPP under uniform irradiance conditions but its application to the PSC has various limitations. This is because a reliable training dataset is extremely difficult to obtain [21]. Moreover, the method is system specific and the ANN has to be retrained when the characteristics of the array change with time.

Many other MPPT algorithms have also been reported in the literature. These include: Dividing Rectangle Technique [35], Fibonacci Search, Particle Swarm Optimization [24] and Fuzzy Logic [21], etc.

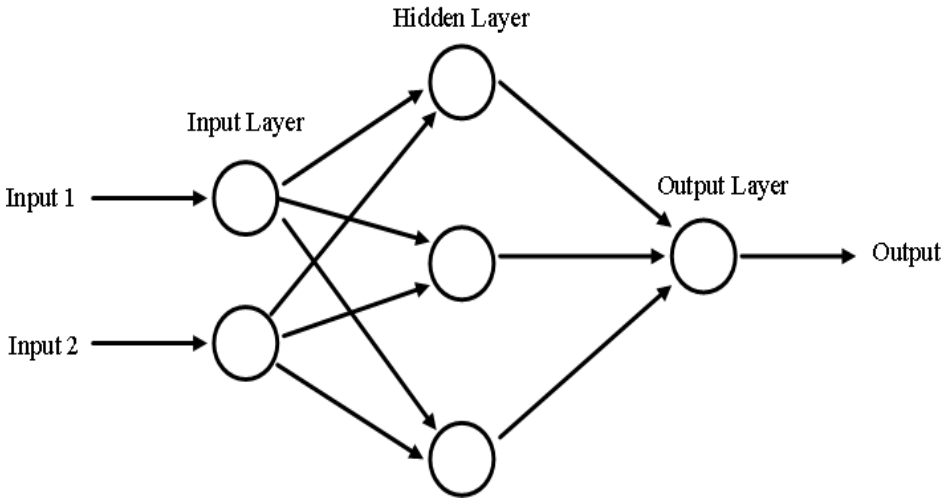

Fig. 2.22 Three layer artificial neural network.

The methods discussed above are categorized as software based MPPTs. To mitigate the effects of non-uniform irradiance, hardware based MPPTs have also been reported in the literature. In the following subsection we discuss some hardware based arrangements which can be used for optimal extraction of power from PV generators under any type of irradiance.

2.2.5 PV System Architecture (Hardware Based MPPTs)

Various types of interconnection of PV modules are utilized in PV arrays for getting a desired level of array voltage, current and power [36-38]. In the series topology shown in Fig. 2.23 (a) the modules are connected in series to form series strings. This is done to achieve a high voltage level required for certain application. Under non-uniform irradiance, the power loss in series topology is high. In another arrangement shown in Fig. 2.23 (b), the modules are connected in parallel to increase the overall current. During the PSC the parallel connected modules produce high power than the series connected configuration of Fig. 2.23 (a).

In the Series-Parallel (SP) connection the modules are first connected in series to form a string. As mentioned before, this is done to get the desired level of voltage required by the load or the inverter. Various strings are then interconnected in parallel to increase the level of current, as shown in Fig. 2.24 (a). Another important configuration is the Total Cross Tied (TCT) connection which is given in Fig. 2.24 (b). In this arrangement the modules are first connected in parallel to form blocks [36]. The blocks are then connected in series. The main advantage of the TCT connection is that it reduces the overall effect of partial shading.

In addition to these arrangements reconfigurable PV arrays have also been reported in the literature. Various forms of reconfigurable arrays are reviewed in [37]. The main objective of reconfiguration of the arrays is to neutralize the effects of non-uniform irradiance. But the main problem with these schemes is the requirement of complex switching matrices. These switches increase the complexity of the hardware.

For ensuring the operation at the MPP various hardware based methods have been reported in the literature, which are summarized in [24]. The most common architecture is the centralized inverter. In this system all the PV strings are connected to the input of a common inverter. Thus the MPPT is performed for the

entire array. In this arrangement, any current mismatch or partial shading will affect the current of the entire array as the current is controlled by the weakest module. For limiting the effects of non-uniform irradiance, bypass diodes are used. The MPPTs which have been discussed previously are primarily designed for this architecture. Depending upon the type of shading, at the GP some of the modules in the arrangement may be bypassed. Similarly in the string inverter architecture, each string has its own MPPT. In the string inverter architecture the performance under PSC is improved as compared to the central inverter. However, the problem of bypass modules still persists.

To avoid bypassing of modules, many researchers have proposed the concept of micro-inverters. A generalized layout of the micro-inverter scheme is shown in Fig. 2.25. In this design, each module is operated at its MPP independently. Similarly, separated DC to AC conversion is performed for each unit. In this system, any shading will only affect the performance of those units which receive lesser irradiance without affecting the performance of other modules. This architecture can increase the energy capture from the PV modules, however they are inefficient because of the high voltage transformation that may be needed for interfacing a single module to the grid.

To overcome this weakness, the concept of series connected DC-DC converter has become popular [39]. In this procedure, each module is operated at its MPP by an independent DC-DC converter. The outputs of the converters are connected in series as shown in Fig. 2.26. In this way, the localized control of module voltage and current is possible. The series connection at the output of the converters enables the designers to have a high DC voltage. This high voltage requires low conversion ratio and therefore, high conversion efficiency is possible.

The possible disadvantages of the hardware based MPPTs are: the increased system cost and complexity, and decreased reliability.

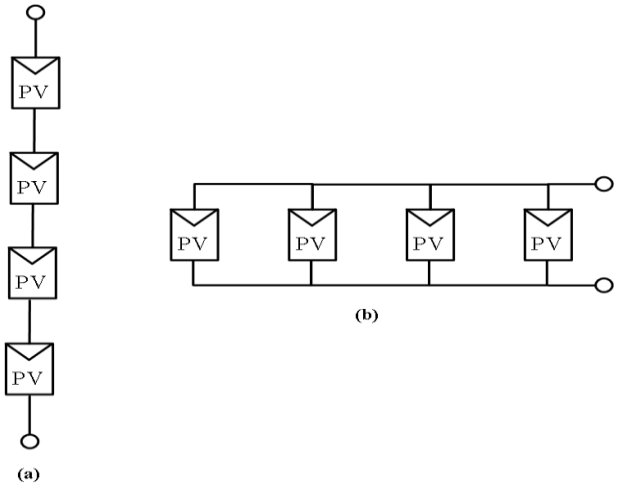

Fig. 2.23 (a) Series configuration of PV modules. (b) Parallel configuration.

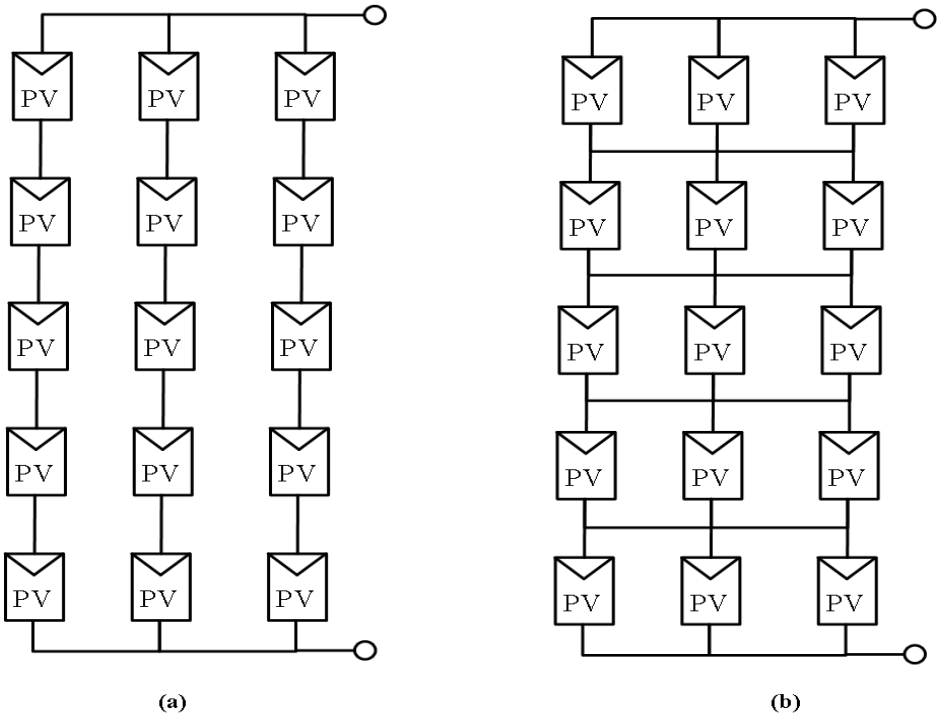

Fig. 2.24 (a) Series Parallel connection. (b) Total Cross Tied connection.

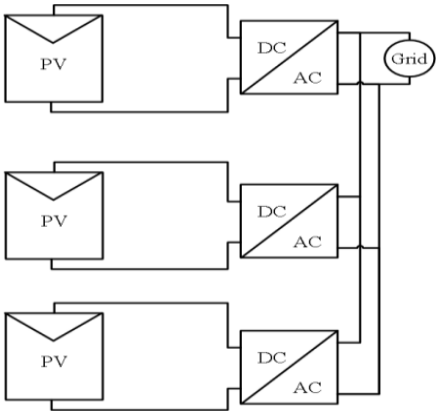

Fig. 2.25 The micro-inverter scheme.

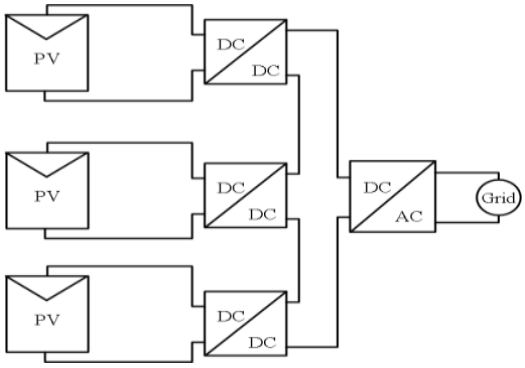

Fig. 2.26 The micro-converter scheme.

In this chapter, we have briefly explained some of the important MPPT methods which have been reported in the literature. In the first part two important MPPT schemes for uniform irradiance have been described. Special emphasis is paid to the improvements made to the P&O algorithm to overcome some of its shortcomings. In the second part, the MPPT methods for PSC have been discussed in brief. In the next chapter the *I-V* curve tracing methods are explained.

Chapter 3 *I-V* Curve Tracing Methods: Literature Review

In this chapter a brief review of some of the well-established procedures that are adopted for finding the I-V characteristic curve are given. This review is essential for establishing the point that these methods involve special tests that usually interfere with the normal operation of PV generator and hence, are dissipative and/or expensive. In the later chapters of this thesis, methods for obtaining the I-V curve of a PV plant from onsite measurements will be proposed.

For monitoring the performance of PV generators, it is essential to obtain the *I-V* characteristic curve under the field conditions. Finding the performance of the PV generators with the help of the characteristic curves is the conventional method. More sophisticated procedures like; the Electroluminescence (EL) and Infrared Thermographic Imaging (IRT) also exist. But these methods are very expensive ones and may not be economically viable in many cases. The basic principle of finding the curve is to change the current of the generator from I_{SC} point to the V_{OC} point (or vice versa) and recording the corresponding values of current and voltage. Various methods for tracing the curve can be found in the literature. In this chapter, some of those methods are given [40].

3.1 Variable Resistor

It is the simplest way of finding the characteristic curve of a PV generator. In this scheme, a variable resistor is connected to the PV array and its resistance is changed from zero to a high value in small steps [41]. In every step the voltage across the variable resistor and its current are recorded. This is a crude and inexpensive method for finding the *I-V* curve, but the manual change of resistance makes the process quite slow. Various quantities, for example the irradiance, may change very quickly during the measurement process and so a true curve may not be obtained.

3.2 Capacitor Charging method

It is a common method for finding the characteristic curve of a PV generator. In this arrangement the PV source is connected to a capacitor which has approximately zero initial charge. The parasitic parameters of the capacitor are assumed to be negligible. When the capacitor is connected to the PV generator, it is initially short circuited. As the charge on the capacitor increases, its current decreases. When the voltage on the capacitor reaches V_{OC}, the current in the circuit falls to zero. The voltage across the capacitor and the corresponding value of the current are recorded and in this way, several points of the *I-V* curve are acquired by the measurement circuit. A typical arrangement for obtaining the curve is shown in Fig. 3.1 [42]. The circuit consists of the following components:

- Multifunction data acquisition device; the device has a high speed A/D converter and a multiplexer.
- Differential probes for measuring the voltage of the PV generator.
- Hall Effect based current probes.
- Personal computer for data storage.

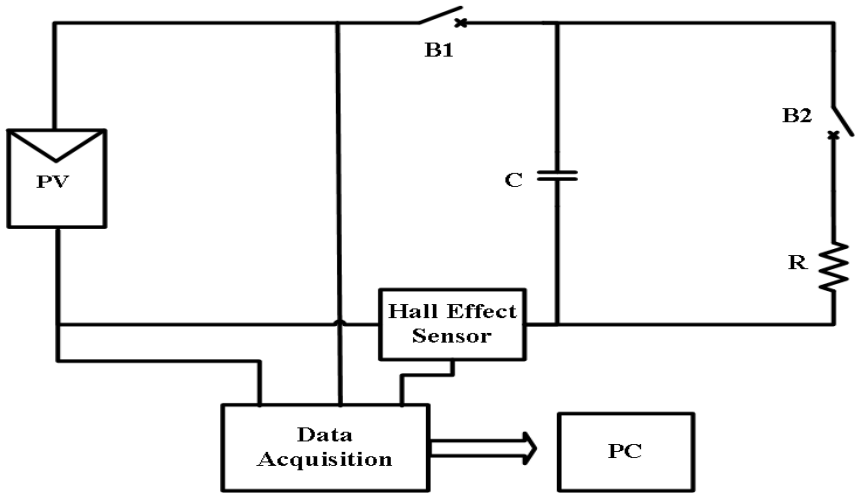

Fig. 3.1 Circuit arrangement for obtaining the I-V curve through capacitor method.

The capacitor C is in Fig. 3.1 is a high quality electrolytic capacitor with low Equivalent Series Resistance (ESR). Due to low the ESR, the capacitor introduces negligible losses in the circuit and ensures a reliable characteristic curve. Breaker

B1 is used to connect the capacitor to the PV device under test. The discharge resistor R is connected to C through breaker B2. The function of R is to discharge C after the test.

Choosing an appropriate value of C is important for obtaining the curve. The equation for calculating appropriate value of the capacitance given the transient duration t_f is calculated as:

$$C = At_f \frac{I_{SC}N_P}{V_{OC}N_S} \tag{3.1}$$

Where A is a dimension-less constant and has a value approximately equal to 0.55, N_S and N_P are the series and parallel connected modules respectively.

The details of derivation of the above equation can be found in Chapter 8 of this text.

3.3 MOSFET Switch Method

In this method the Drain to Source Resistance R_{DS} of power MOSFET is utilized as a variable load for finding the *I-V* curve of an array. In this process the MOSFET is operated in all the three regions of operation, i.e. cutoff, ohmic, and active. A typical circuit arrangement of this method is shown in Fig. 3.2 [43].

As given in Fig. 3.2 , the voltage divider resistors R_1 and R_2 are used to scale the voltage of the array down to an appropriate value. The resistance R_D is used to provide protection to the MOSFET. The current through the circuit is sensed across the current sensing resistor R_{Sense}. A Hall Effect current sensor can also be used instead of the resistor. A low frequency triangular wave is applied to the gate of the MOSFET. An oscilloscope is used to display the *I-V* curve of the PV generator. Peak Detector PD1 is used to record the maximum voltage of the generator i.e. V_{OC}. PD2 is used to record the short circuit current I_{SC}. The current and voltage of the array are multiplied by analog multiplier and its output is fed to a peak detector PD3. During the scanning process, if peak is detected by PD3, it triggers the sample and hold amplifiers S&H 1 and S&H 2 to sample the value of voltage (V_{MPP}) and current (I_{MPP}) corresponding to MPP. The value of MPP power (P_{MPP}) is recorded by PD3.

Through this method the characteristic curve of the array is easily obtained; however, the main drawback of this method is that a high amount of power is dissipated in the MOSFET and the design of its heat sink can also be complicated. Another shortcoming is the drain resistance R_D which results in power dissipation as well as affects the accuracy of the curve.

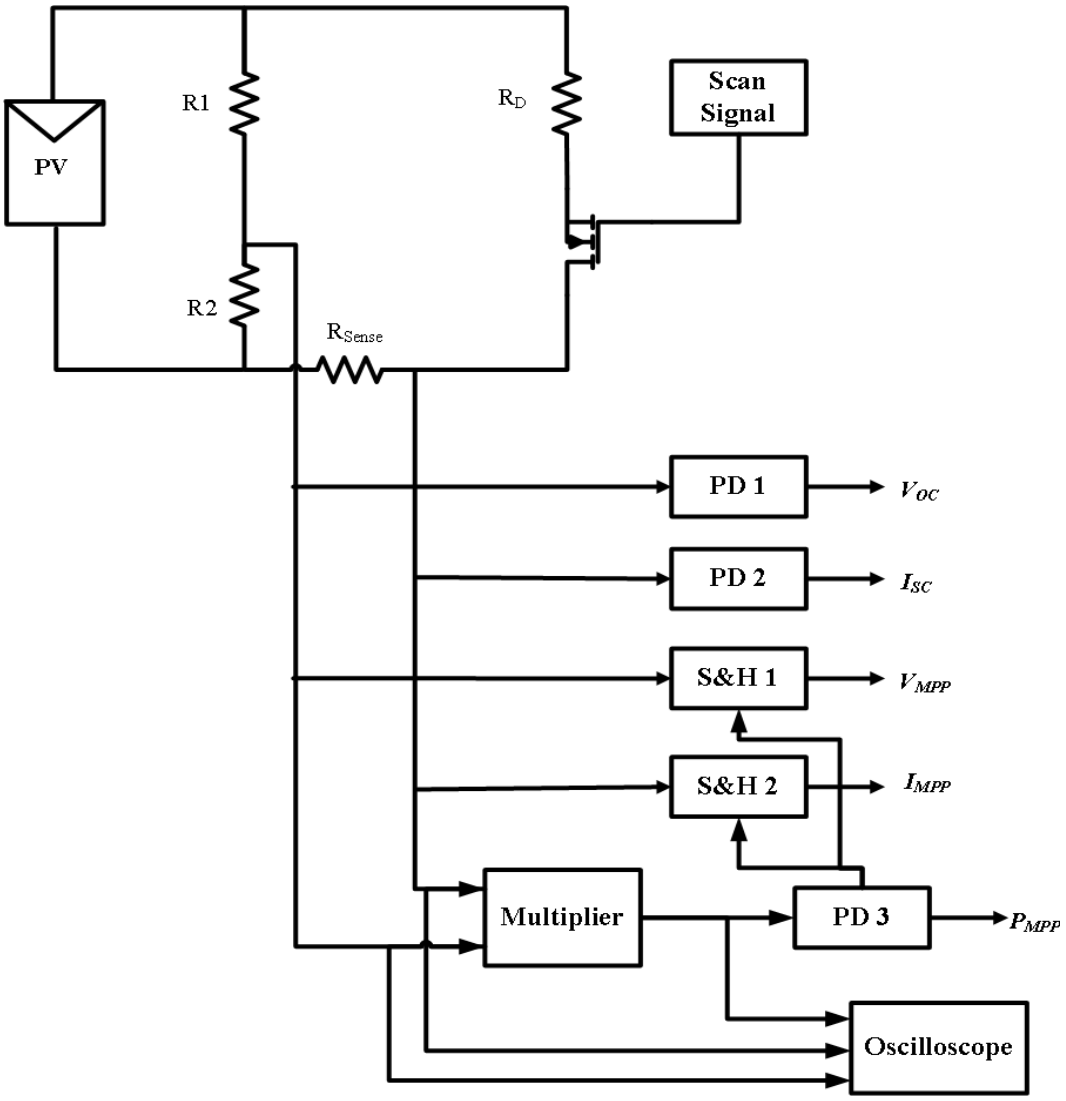

Fig. 3.2 Circuit arrangement for getting the *I-V* curve through MOSFET method.

3.4 Varying the Duty Cycle of DC-DC Converter

In this method the duty cycle of DC-DC converter is varied in the range [0, 1] for tracing the *I-V* curve of the array. In many commercially available PV systems, this process is employed for finding the GP under any type of shading condition. The primary objective is to track the true MPP of the PV array, however the characteristic curve can also be traced in this manner.

In [44] various converter topologies have been studied. Theoretically, the buck-boost converter is the only basic converter topology suitable for finding the complete characteristic curve. Buck converter does not allow tracing of the correct curve near to I_{SC}. On the other hand, the boost converter cannot trace the points on the curve in the vicinity of the V_{OC}. However, some modification to the basic buck and boost converter allows us to find the curve in the vicinity of the two extreme points i.e. V_{OC} and I_{SC}. For example, the circuit shown in Fig. 3.3 allows the operation in buck as well as boost mode [45, 46]. Suppose the main converter that is used in the application is the buck converter. Let us assume that all the points on the curve from the V_{OC} to a certain low voltage have been obtained. However, the relatively high value of R_L in Fig. 3.3 does not allow us to operate the array at lower voltage in the buck mode. In this case, the switch S1 is held in ON state while S4 is OFF. The switches S2 and S3 temporarily assume the role of controlling the converter [24]. Thus, the topology is transformed from buck to boost mode temporarily and the duty cycle is changed such that the points near to the current I_{SC} are obtained.

The limitation of this arrangement is that it requires several seconds and during the process the array is not operated at the MPP which leads to power loss.

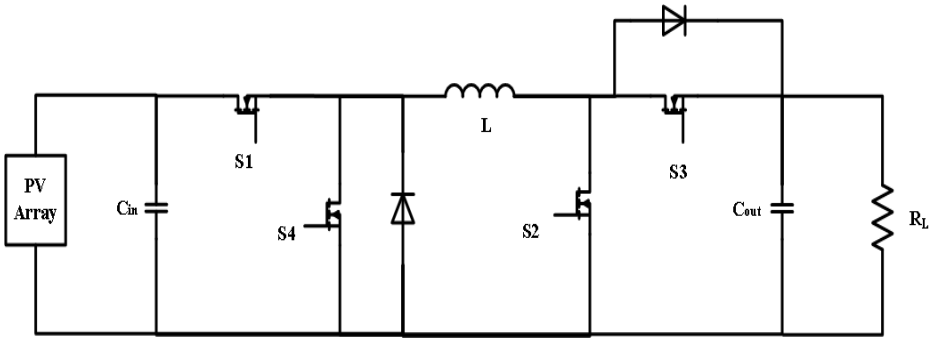

Fig. 3.3 Special converter topology that operate in buck and boost mode.

3.5 Four Quadrant Power Supply

A four quadrant power supply can source as well as sink current with bipolar voltage [47]. It is usually desirable to obtain the characteristic curve of the array in the first quadrant. The added advantage of the four quadrant power supply method is that the characteristics of the array can be extrapolated to the second and the fourth quadrant as well. This may be an important diagnostic tool for detecting possible mismatching in PV arrays. This mechanism has high flexibility and fidelity, but it is an expensive tool.

In the above discussion we have given a brief description of the algorithms that are used for measuring the characteristic curve of the array under field conditions. One common problem with these schemes is that during the measurement of the curve the normal operation of the PV system is disturbed. The objective of this thesis is to put forward a method that finds the characteristic curve as well as perform the MPP tracking.

Chapter 4 Modelling of PV Generators under Uniform Irradiance and Partial Shading Conditions

This chapter deals with the development of a model for PV arrays under any type of irradiance conditions. In the first part of this chapter modelling under uniform irradiance is explained. On the basis of this, a mathematical model for partial shading conditions is developed. The developed model is useful in finding the I-V curve of arrays from on-site measurements.

4.1 Modelling of PV Arrays under Uniform Irradiance

Basically a PV cell is a *p-n* junction diode fabricated in a thin layer of semiconductor. Sunlight consists of photons of different levels of energy. Those photons which have lower energies than the bandgap energy of the semiconductor do not lead to the production of charge carriers. If the energy of the incident photons of light is greater than the bandgap energy of the semiconductor, only those photons produce photovoltaic current. This current is proportional to the solar irradiance. Semiconductors that have lower bandgap energy may utilize a large proportion of solar irradiance for the production of electrical energy but the generated voltages are usually lower.

An ideal PV cell is modeled by a current source with a parallel diode. As shown in Fig. 4.1 (a), a practical PV device has a series resistance R_S and a parallel resistance R_P. R_S is dependent upon the contact resistance of the front metal base with the *p* semiconductor layer, and the resistances of *p* and *n* bodies [48]. The existence of R_P is mainly due to the leakage current of the *p-n* junction and depends on the fabrication of process of the PV cell. Therefore, these two resistances are usually included in the modelling of PV devices. In the present text we will use the model shown in Fig. 4.1 (a) for developing the model of PV array under PSC. Various authors have expanded the model given in this figure present more accuracy. For example, in [36] and [38], an additional current source is added to the model to represent negative breakdown operation. This model is

given in Fig. 4.1 (b). Similarly, an extra diode can be added to the model to represent the effect of the recombination of carriers.

A PV module is formed by stacking together various cells in series or series/parallel combination. The series combination of cells increases the voltage level of the module while stacking the cells in parallel leads to increase in current of the module. A mathematical equation which describes the *I-V* characteristic of a practical PV module is given by:

$$I = I_{ph} - I_0 \left[\exp\left(\frac{V+R_S I}{n_s a V_t}\right) - 1\right] - \frac{V+R_S I}{R_P} \tag{4.1}$$

$$V_t = \frac{kT}{q} \tag{4.2}$$

Where I_{ph} is the photovoltaic current without taking into consideration the effects of R_S and R_P. I_0 is the diode saturation current, V_t is the thermal voltage, a is the diode ideality constant, q is the electron charge and has the value of 1.602179×10^{-19} C, k is the Boltzmann constant with the value $1.3806503 \times 10^{-23}$ J/K, T is the temperature of the *p-n* junction in kelvin, and n_s is the series connected cells in the module. Similarly, n_s is the number of series connected cells in the module. It is important to mention here that if there are n_p cells in parallel to each cell in the module, then we have to multiply the RHS of Eq. (4.1) by n_p.

I_{ph} depends linearly on solar irradiance (G) and is also influenced by temperature according to the equation:

$$I_{ph} = (I_{scn} + K_I \Delta T)\frac{G}{G_n} \tag{4.3}$$

Where I_{scn} is the short circuit current of the module under nominal conditions (T_n = 298K, G_n = 1000W/m^2), K_I is the short circuit current coefficient in A/K, G_n is the nominal irradiance (1000W/m^2), and ΔT is the difference between the array temperature T and the nominal temperature Tn.

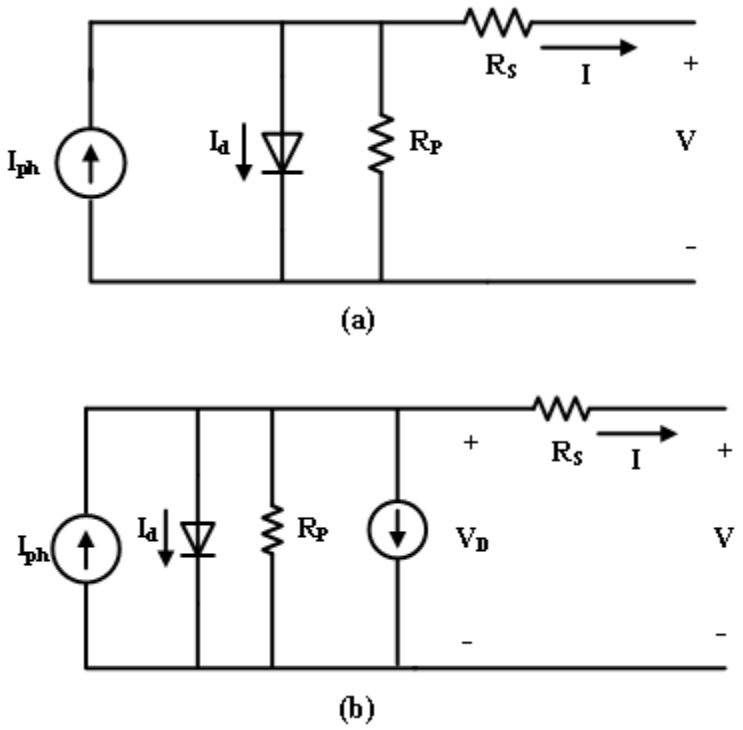

Fig. 4.1. (a) Single diode model of a photovoltaic cell. (b) Single diode model with additional current source for representing the negative diode breakdown operation.

The diode saturation current I_0 and its dependence upon the temperature is given by the relation :

$$I_0 = \frac{I_{scn}+K_I\,\Delta T}{exp\left((V_{ocn}+K_V\,\Delta T)/aV_t\right)-1} \tag{4.4}$$

Where V_{ocn} is the nominal open circuit voltage of the module, and K_V is the open circuit voltage coefficient. Ref [49] has proposed a relation for the calculation of I_0 as:

$$I_0 = \frac{I_{sc}-V_{oc}/R_{sho}}{\exp\left(\frac{V_{oc}}{(aV_t)}\right)-1} \tag{4.5}$$

Where R_{sho} is the reciprocal of the slope of the *I-V* curve of the module at $I = I_{sc}$ in Ω.

The value of the diode ideality constant affects the curvature of the *I-V* curve. A relationship for finding the value of *a* is given by [50]:

$$a = \frac{K_V - \frac{V_{ocn}}{T_n}}{n_s V_{tn}\left(\frac{K_I}{I_{phn}} - \frac{3}{T_n} - \frac{E_g}{kT_n^2}\right)} \tag{4.6}$$

Where V_{tn}, I_{phn}, and T_n are the thermal voltage, the photovoltaic current and the temperature under nominal conditions respectively. E_g is the bandgap energy for the semiconductor material, for crystalline silicon it is 1.12 *eV*.

In practical PV devices the resistance R_S is quite low and R_P is high and therefore we can neglect these resistances to simplify the model. Therefore, by neglecting these resistances and inserting the value of I_0 in (4.1), we get:

$$I = I_{ph} - \frac{I_{scn} + K_I\,\Delta T}{exp\left((V_{ocn} + K_V\,\Delta T)/aV_t\right) - 1}\left[\exp\left(\frac{V}{n_s V_t a}\right) - 1\right] \tag{4.7}$$

Another consequence of neglecting the series and parallel resistances of a module is that the photovoltaic current I_{ph} becomes approximately equal to I_{SC} [48, 49, 50].

When the PV array is under uniform irradiance, the model discussed above can be used to represent the array. However, when there is PSC, different approach is adopted for modelling purposes. In the following subsection, a model for PV array under PSC is developed.

4.2 Modelling of PV Arrays under Partial Shading

In the previous section, a model based on [48] has been discussed. In this section we make the essential modifications to the equations given in the last section to account for non-uniform illumination.

When some cells in a PV module are shaded, those cells cannot produce the amount of current and hence, power that is produced by the unshaded cells. This difference in the ability to produce power leads to difference in voltage among the shaded and unshaded cells. If an attempt is made to drive high current through a shaded cell, its voltage becomes zero and begins to consume power instead of producing it. If the consumed power exceeds a certain limit, hotspot problem may occur which can cause permanent damage to the shaded cells. The use of bypass diodes allows the current to flow in the correct direction even if some of the cells do not take full irradiance, but it complicates the electrical characteristics of the PV array. Multiple peaks appear in the *P-V* characteristics of the array under non uniform irradiance. Similarly, the *I-V* characteristic of the array has multiple mini *I-V* curves. Fig. 4.2 shows a PV array under different shading conditions. It should be noted that the six series connected modules in Fig. 4.2 combine to form a single string. In this text we assume that the PV string either represents a PV array consisting of series connected modules or it is a string in a large PV array with its independent MPPT. The latter is commonly referred to as the string inverter based MPPT [51]. The array has six series connected modules. The number of series connected cells in each of the modules is 20 and it has rated V_{OC} and I_{SC} 12.2V and 8.2A respectively. The rated V_{OC} of the array is 73.2V. For modelling the array, we take into consideration the irradiance pattern of Fig. 4.2 (b) in which the modules receive three different irradiances. From Fig. 4.3(a) we see that there are three mini curves in the *I-V* characteristics. For modelling of this array we first group the modules together that have the same irradiance [27]. Group 1 consists of modules M5 and M6 which means that the number of modules inside this group is $N_1 = 2$, group 2 has M3 and M4, so the number of modules in the group is $N_2 = 2$. Similarly, M1 and M2 make group 3 with $N_3 = 2$.

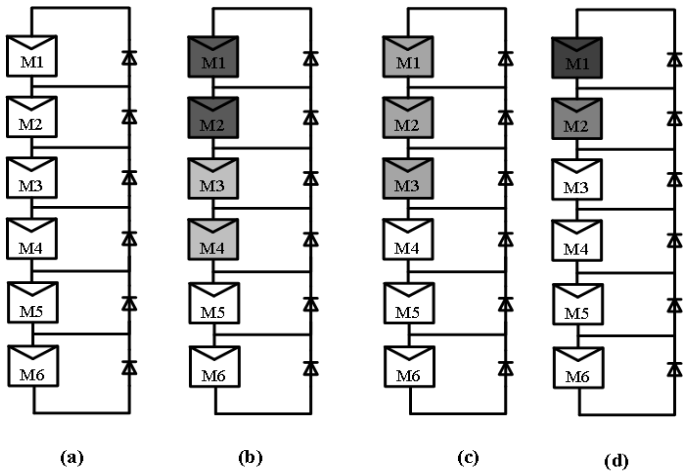

Fig. 4.2 A PV string under different shading conditions. (a) All the modules receive uniform irradiance of 1000 W/m^2. (b) Module M1 and M2 receive 300 W/m^2, M3 and M4 receive 600 W/m^2, M5 and M6 receive 1000 W/m^2. (c) M1, M2, and M3 have 300 W/m^2 irradiance; M4, M5, and M6 has 1000 W/m^2 irradiance. (d) Partially shaded array with M1 receiving 300W/m2, M2 receiving 500W/m^2, and M3-M6 receiving 1000W/m^2.

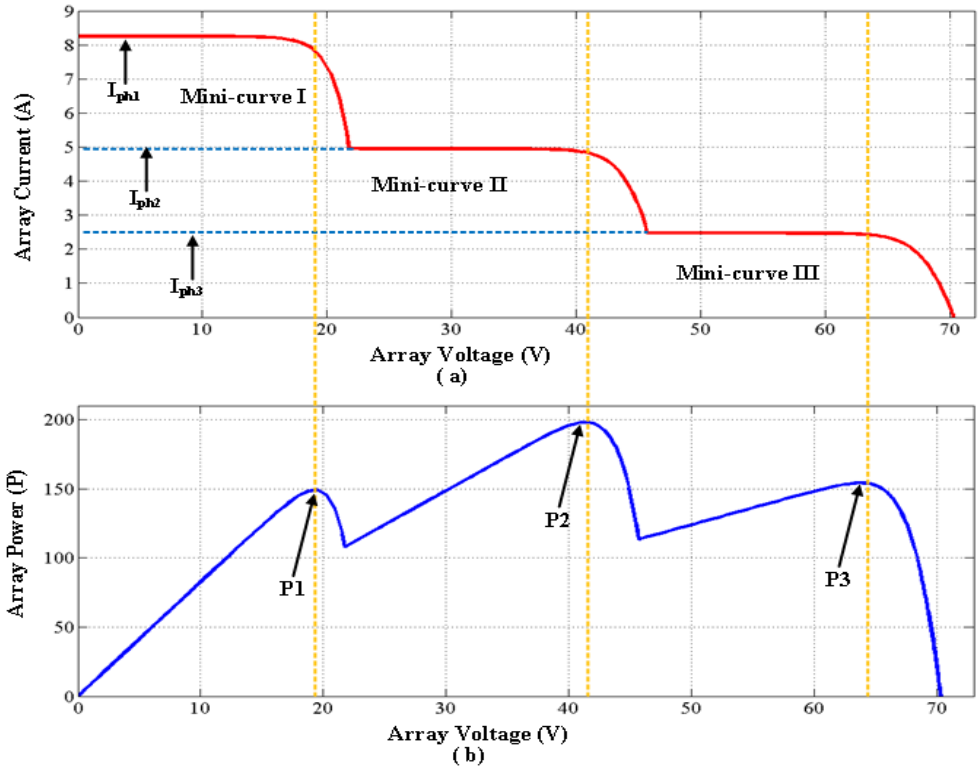

Fig. 4.3 Characteristic curves of partially shaded string shown in Fig. 4.2 (b) with three distinct irradiances. (a) The *I-V* curve. (b) The *P-V* curve.

a. Mini Curve I. In this part of the curve the modules M5 and M6 supply power while the remaining i.e. M1─M4 cannot produce the desired amount of current and are bypassed. The equation representing the array's terminal voltage V in this region of the curve is:

$$V = N_1V_1 - (N_2 + N_3)V_d \tag{4.8}$$

Where V_1 is the voltage of single module in group 1 and its value is in the range ($0 \leq V_1 \leq V_{Max1}$), V_d is the bypass diode voltage drop. V_{Max1} is the maximum voltage of single module in group 1.
The current in this part of the curve is determined as:

$$I_1 = I_{ph1} - I_0 \left[exp\left(\frac{V + (N_2+N_3)V_d}{aN_1V_t}\right) - 1\right] \tag{4.9}$$

$$I_{ph1} = (I_{scn} + K_I\Delta T)\frac{G_1}{G_n} \tag{4.10}$$

Where G_1 is the irradiance of the modules in group 1.
The voltage (V_{MPP1}) at which the peak $P1$ occurs is determined by the relation:

$$V_{MPP1} = 0.8N_1V_{Max1} - (N_2 + N_3)V_d \tag{4.11}$$

b. Mini Curve II. In this part of the characteristic curve, the modules M3─M6 are supplying power to the load while M1 and M2 cannot produce the required level of current and so these are bypassed. However, the current of the entire sring is controlled by modules M3 and M4. The modules M5 and M6 operate at a current below their MPP current and their voltage is approximately equal to their respective V_{OC} or V_{Max1}. The voltage equation in this region is given as:

$$V = N_1V_{Max1} + N_2V_2 - N_3V_d \tag{4.12}$$

Where V_2 is the voltage of one module in group 2 and has value in the range ($0 \leq V_2 \leq V_{Max2}$).
The equation for current I_2 in this region is given by:

$$I_2 = I_{ph2} - I_0 \left[exp\left(\frac{V+N_3V_d-N_1V_{Max1}}{aN_2V_t}\right) - 1\right] \quad (4.13)$$

The current I_{ph2} is proportional to the irradiance G_2 received by the modules in group 2 and is given by:

$$I_{ph2} = (I_{scn} + K_I\Delta T)\frac{G_2}{G_n} \quad (4.14)$$

The voltage corresponding to the peak P2 in this part is determined using the relation:

$$V_{MPP2} = N_1V_{Max1} + 0.8N_2V_{Max2} - N_3V_d \quad (4.15)$$

c. Mini Curve III. In the same manner as given above we can find the relationships for voltage and current in this region of the main *I-V* curve as:

$$V = N_1V_{Max1} + N_2V_{Max2} + N_3V_3 \quad (4.16)$$

$$I_3 = I_{ph3} - I_0 \left[exp\left(\frac{V-(N_1V_{Max1}+N_2V_{Max2})}{aN_3V_t}\right) - 1\right] \quad (4.17)$$

$$I_{ph3} = (I_{scn} + K_I\Delta T)\frac{G_3}{G_n} \quad (4.18)$$

Where V_3 is the voltage across each of the modules in group 3 and is in the voltage range ($0 \leq V_3 \leq V_{Max3}$), G_3 is the irradiance of the modules that constitute group 3.
The voltage value at the peak P3 is calculated by:

$$V_{MPP3} = N_1V_{Max1} + N_2V_{Max2} + 0.8N_3V_{Max3} \quad (4.19)$$

Similarly, we can model a PV string under PSC with any number of different irradiances falling on it. In general, characteristic equation for modelling the PV array in a certain region *j* of the *I-V* curve is:

$$I = N_P I_{phj} - N_P I_0 \left[exp\left(\frac{N_C V + N_B V_d - \sum_{i=1}^{i=k-1} N_{LCi} V_{Maxi}}{a N_C V_t} \right) - 1 \right] \quad (4.20)$$

$$I_{phj} = (I_{scn} + K_I \Delta T) \frac{G_j}{G_n} \quad (4.21)$$

where N_B is the number of modules bypassed by the diodes, N_P is the number of parallel connected strings. In the present case we have taken $N_P = 1$ for simplicity. N_C is the number of series connected modules controlling the current of the PV generator in a particular region of the *I-V* curve, I_{phj} is the PV current of the *jth* group, and G_j is the irradiance of the *jth* group.

Ref [26] has used a simulation model for studying the effects of partially shaded PV arrays. A significant outcome of the observations is that two consecutive peaks on the *P-V* curve of the array under partial shading is the integral multiple of 80% of V_{OC} of a single module and the minimum possible displacement between two consecutive peaks is $0.8V_{OC}$. This is only an approximation but the accurate value of a voltage at which a peak occurs of the curve can be generalized from (4.12), (4.15), and (4.19). By observing these relations we can generalize the possible existence of a peak on the *P-V* curve as [59]:

$$V_{MPP,k} = \sum_{i=1}^{k-1} N_{LCk} V_{Max,k-1} + 0.8 N_{CC} V_{Max,k} - N_{B,k} V_d \quad (4.22)$$

Where $V_{MPP,k}$ is the MPP voltage of the *kth* peak and N_{LC} is the number of modules that are operating at a lower current than their respective MPP current.

In this chapter, a model of PV generators operating under non-uniform illumination has been presented. The equations derived in this chapter will be used in finding the *I-V* curve of a PV generator from onsite measurements. The method for calculating the characteristic curve will be presented in Chapter 6 and Chapter 7. In the next chapter, we discuss the properties of PV array under non-uniform illumination.

Chapter 5 Properties of PV Generators under PSC

As discussed in the previous chapters, when PSC occurs the characteristics of PV generator change. This change is brought about mainly by the conduction of bypass diodes. In this chapter, the characteristics of PV generators under PSC are explained with the help of a simulated model. The variation of module voltage as a function of the string voltage is of particular importance in the development of algorithms which simultaneously obtain the I-V curve and perform MPP tracking under different shading conditions.

5.1 Properties of Partially Shaded PV Arrays

Majority of the MPPT methods reported in the literature for finding the MPP under Partial Shading Conditions (PSC) are unable to ascertain two essential information at the outset of performing the search for true MPP. One is the presence of the PSC, and the other is the number of peaks that are present as a result of PSC. For getting the knowledge of the presence of PSC and the number of peaks present in the *P-V* characteristic curve, it is important to discuss some of the properties of PV strings under non-uniform irradiance conditions. These properties are also important for the purpose of finding the characteristic curve of the array under field conditions.

Let us consider the PV generator shown in Fig. 4.2(a) in which all the modules receive uniform irradiance of 1000 W/m^2. Each module has now 54 series connected cells and has rated V_{OC} and I_{SC} equal to 32.9 V and 8.26 A, respectively. The rated V_{OC} of the array is 197.4 V. The characteristic curves are shown in Fig. 5.1. Fig. 5.1(a) shows the *I-V* curve, in Fig. 5.1(b) is shown the *P-V* curve, and in Fig. 5.1(c) are drawn the module voltages (VM1─VM6) as a function of string voltage. Let us assume that the voltages of all the modules are completely matched under nominal conditions. When the PV is under uniform irradiance, all of the series connected modules have identical operating voltage, current, and output power [30]. This can be seen in Fig. 5.1(c) However, when there is partial shading this situation changes.

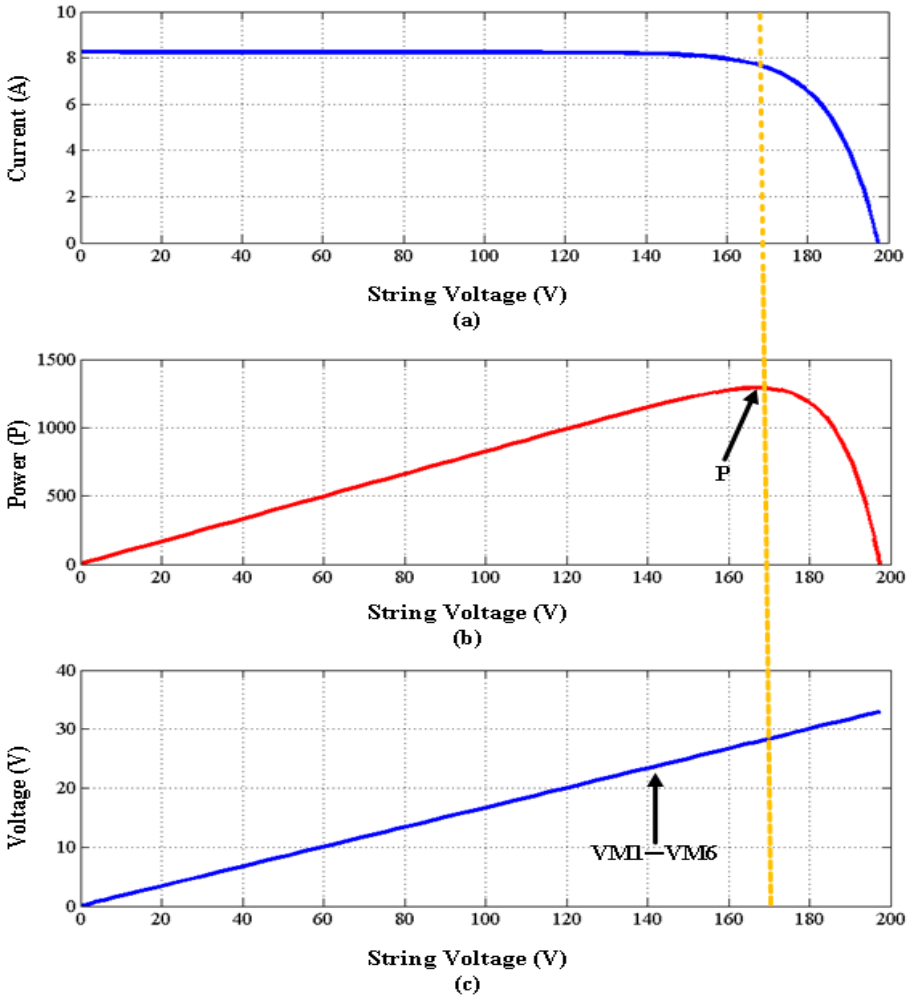

Fig. 5.1 Characteristic curves of the array under the irradiance pattern given in Fig. 4.2 (a).

For studying the behavior of the module voltages under PSC, consider the case in Fig. 4.2(c) in which the modules M1, M2, and M3 receive 600W/m^2 while M4, M5, and M6 get the illumination of 1000W/m^2. The corresponding characteristic curves are shown in Fig. 5.2. It can be noticed from this figure that the *I-V* curve has two regions, similarly two peaks P1 and P2 can be observed in *P-V* curve. When the operating point of the array is at P1, its current is higher than the maximum current supplied by the modules M1, M2, and M3. These modules are, hence, bypassed and the voltage across them is equal to the forward bias voltage of the diode with negative sign. At P1, the modules M4, M5, and M6 supply power to the load. On the other hand, when the string is operating at peak P2 all the modules M1─M6 supply power. However, the current is controlled by the modules M1─M3. Notice from Fig. 5.2(c) that at P2 the voltage across the

modules M1─M3 is lower than that across M4─M6. The reason for the difference in voltage is because, M1─M3 are operating at their MPP current under the present irradiance condition. On the other hand, the modules M4─M6 operate at lower current than their respective MPP currents. The operation at smaller current means that the modules have operating voltages which are nearly equal to their V_{OC}.

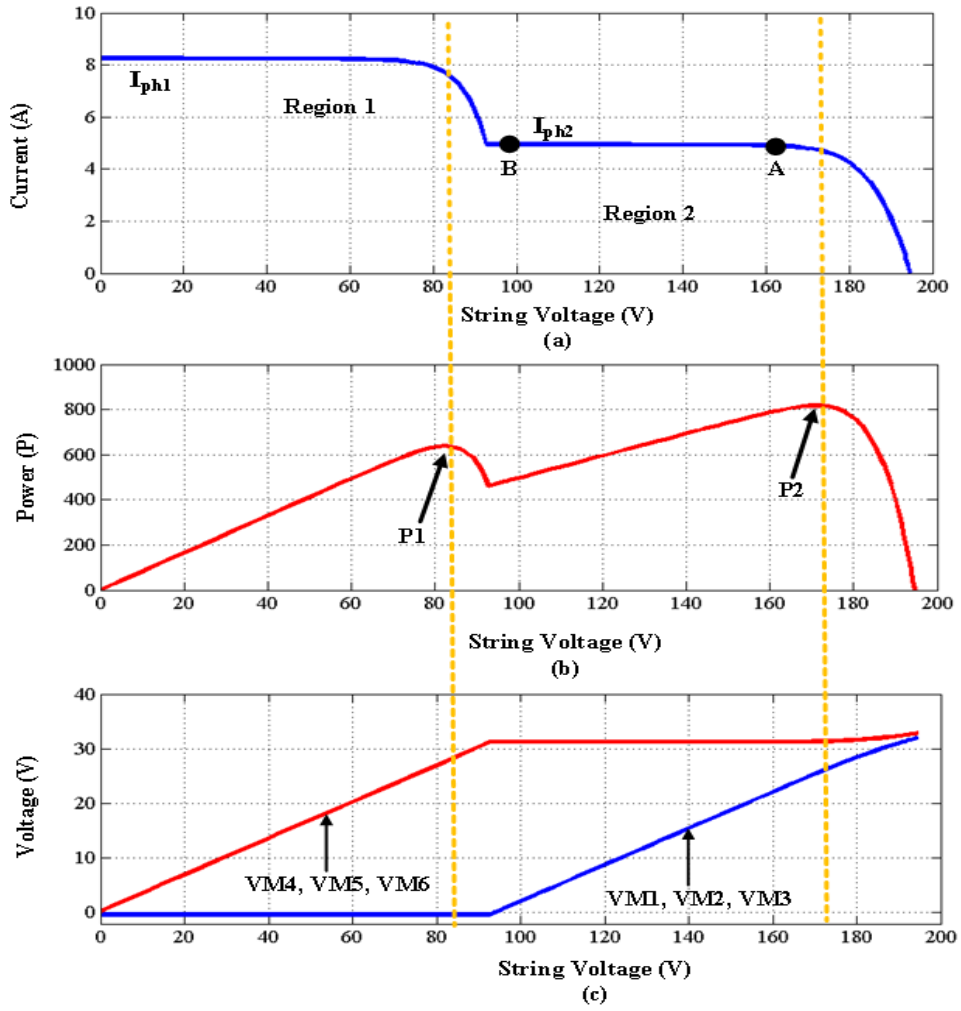

Fig. 5.2 Characteristic curves of the array with irradiance pattern given in Fig. 4.2(c).

Let us consider the case shown in Fig. 4.2(d). As given in this figure, the modules M1 is getting 300 W/m^2, M2 receives 500 W/m^2, while the remaining four modules take 1000 W/m^2 irradiance. The *I-V* curve of this array will have three regions (or three mini *I-V* curves) and *P-V* will have as many peaks. Fig. 5.3 shows the characteristic curves of the array corresponding to the irradiance pattern given in Fig. 4.2(d). An important thing to observe is the difference in the voltages of the modules at peaks P1, P2, and P3.

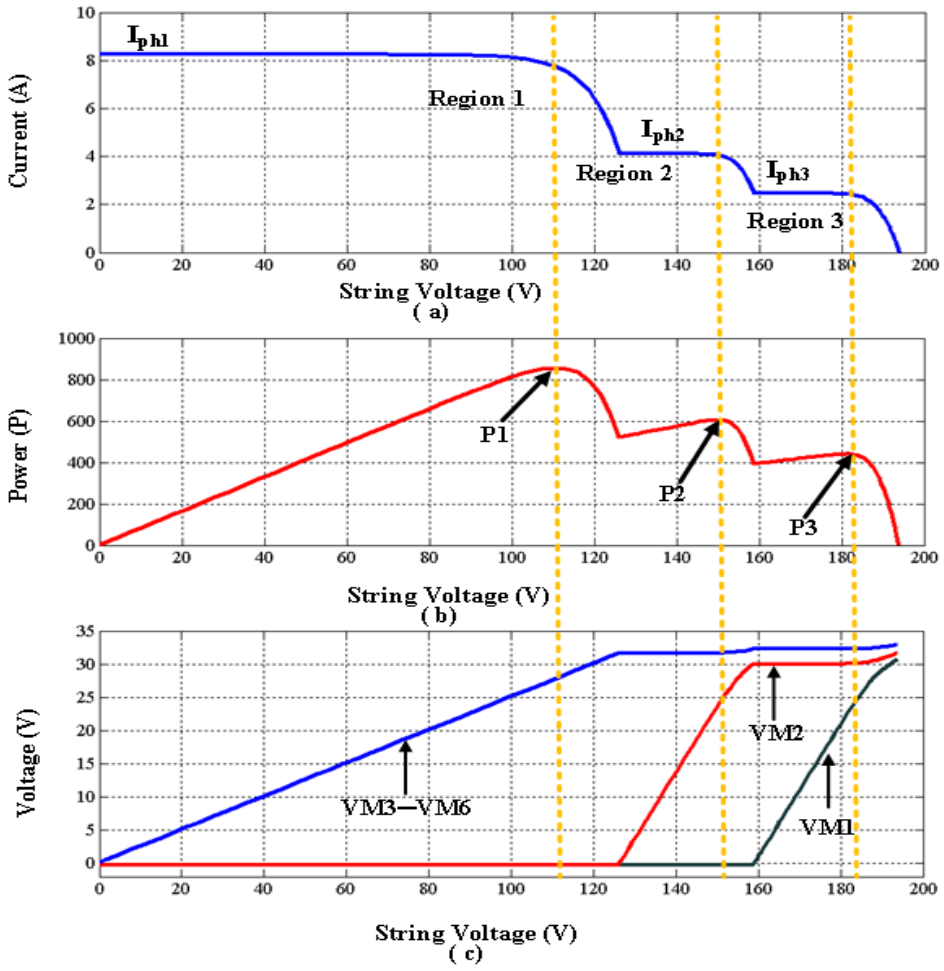

Fig. 5.3 Characteristic curves of the string with irradiance pattern shown in Fig. 4.2(d).

Another important thing to notice from the above figures is that each of the peaks on the *P-V* curve occurs at a voltage V_{LP} which is approximated by the relation [26], [30]:

$$V_{LP} \approx \left(1 - \frac{N_B}{N_S}\right) V_{OC} * 0.80 \tag{5.1}$$

Where N_S is the total number of series connected modules in the string and N_B is the number of series connected modules that are bypassed.

The above equation provides a reasonable estimate for finding the location of a peak and is helpful when used for MPP tracking schemes which are based P&O or incremental conductance algorithm [26]. Though, a more accurate relation for calculating the voltage at which a certain peak occurs is given by Eq. (4.22).

We can see from Fig. 5.2 and Fig. 5.3, that there is a constant current part to the left of each peak. For example, in Fig. 5.2(a) this constant current part lies between points A and B. In the constant current part the value of the current remains almost constant as a function of voltage. In this part of the curve, the current is equal to the short circuit current of the modules that are controlling the current. For example, between points A and B in Fig. 5.2(a) the value of current is equal to the short circuit current of modules M1, M2, and M3. The PV modules usually have high parallel resistance and very low series resistance, therefore the effect of these resistances is neglected [48]. As a consequence of this simplification, the value of short circuit current and the photovoltaic current become equal . Thus, the value of current between points A and B is equal to the value of the photovoltaic current I_{ph2} of the modules M1─M3.

From the above discussion some important properties of solar generators under PSC are:

1. Under uniform illumination, single peak is present in the *P-V* characteristic curve of a solar array. As observed from Fig. 5.1, at any operating point all the modules in the array have almost identical voltage. Tracking of the single peak is not challenging for a conventional P&O or IC algorithm.

2. Under PSC, the *P-V* curve has multiple peaks. The *I-V* curve is characterized by multiple regions as given in Fig. 5.1 and Fig. 5.2.
3. There is a constant current part to the left of each peak. Tracking a point in the constant current part is comparatively easier than tracking a peak on the *P-V* curve under non-uniform irradiance. It is because the constant current part is spread over a relatively wider voltage range, while a peak occurs at a single voltage point.
4. When a partially shaded array is operated at the peak nearest to the array's V_{OC} (termed as the Right Peak (RP)) all the modules supply power to the load. However, the array current is controlled by the modules that receive the lowest irradiance.
5. When the array is operated at the RP under PSC the modules receiving different irradiances have different voltages across them; similarly, the modules that receive the same irradiance have the same voltage. This assertion is based on the assumption that the voltages of the modules are perfectly matched under the nominal conditions.
6. After operating the array at a certain peak, the series connected modules can be classified in different groups on the basis of the voltage across them. In such an arrangement, the modules that have the same voltage (receiving the same irradiance) are placed in the same group.
7. The approximate location of each peak depends upon the number of modules that are bypassed and the V_{OC} of the array according to (5.1). A relation which accurately calculates the location of a peak is given by (4.22).

On the basis of these observations above we develop a mechanism for obtaining the characteristic curve of the array in the following chapter.

Chapter 6 Obtaining the *I-V* Curve and Tracking the MPP with no Voltage Mismatch among the Modules

In this chapter a method for obtaining the characteristic curve and finding the MPP under any shading conditions is discussed. The scheme presented in this chapter assumes that the voltages of the modules are perfectly matched under nominal conditions or STC (1000 W/m^2, 298 K). Though, the issue of voltage mismatch among the PV modules is dealt with in chapter 7; however, the material given in this chapter is important for conceptual purposes. Based upon the material presented in this chapter a complete algorithm will be proposed in the next chapter.

6.1 The Curve Tracing and MPPT Algorithm

As pointed out in Chapter 5, when the string is operated at the RP the modules that have the same irradiance have the same operating voltage. Similarly, when the array is under partial shade, the modules that are shaded have low operating voltage as compared to those which are getting full illumination. For finding the *I-V* curve, the array is first operated at the RP, and then the voltage of each of the modules is measured. The modules are arranged into groups according to their operating voltage. It is pertinent to mention here that if the array is under uniform irradiance, all the modules will have approximately the same operating voltage and will be placed in the same group. The total number of groups gives the number of regions in the *I-V* characteristics. Likewise, the number of modules in each of the group is also determined. The value of I_{ph} for each of the group is obtained from the following equation [29]:

$$I_{ph} = I + \frac{I_{scn}+K_I\,\Delta T}{exp\left((V_{ocn}+K_V\,\Delta T)/aV_t\right)-1}\left[\exp\left(\frac{V}{n_sV_ta}\right) - 1\right] \quad (6.1)$$

Where I, and V indicate the values of current and voltage at the RP.

Having calculated the values of I_{ph} for each of the regions in the characteristic curve using the above equation, the values of N_B, N_{LC}, and N_C for each of the regions are also determined. These quantities are arranged in the form of vectors. For the case shown in Fig. 4.2 (b) and Fig. 4.3, these vectors are given as:

$$I_{ph} = \left[I_{ph1}, I_{ph2}, I_{ph3}\right] \quad (6.2)$$

$$N_C = \left[N_{g1},\ N_{g2},\ N_{g3}\right] \quad (6.3)$$

$$N_B = [N_{g2} + N_{g3},\ N_{g3}, 0] \quad (6.4)$$

$$N_{LC} = [0,\ N_{g1},\ N_{g1} + N_{g2}] \quad (6.5)$$

After finding the vectors for I_{ph}, N_C, N_B, and N_{LC}, the process proceeds to acquire the *I-V* curve. This mechanism is described with the aid of the flow chart given in Fig. 6.1. In this figure, the first seven blocks deal with operating the array at the RP, finding the I_{ph} for each of the regions in the characteristic curve, and obtaining the vectors given in equations 6.2─6.5. From block 8 onwards the characteristic of the array is traced by the algorithm numerically. The first value in each of the vectors given in equations 6.2─6.5 are assigned to $I_{ph}(n)$, $N_C(n)$, $N_B(n)$, and $N_{LC}(n)$ respectively in block 8. In block 9 the value of array voltage, I_{MPP}, and V_{MPP} are initialized to zero. In block 10, the array voltage is incremented by 0.1V from its previous value and the new value is given to the variable *V(k)*. The value of the array current *I(k)* is calculated for the corresponding value of voltage *V(k)* using equation (4.20) in block 11. In block 12, the products $V(k)I(k)$ and $V_{MPP}I_{MPP}$ are compared. If the product of current and voltage in the iteration k is greater than the product of MPP voltage and current that is stored in the memory of the microcontroller, the algorithm updates I_{MPP} and V_{MPP} to *I(k)* and *V(k)* respectively.

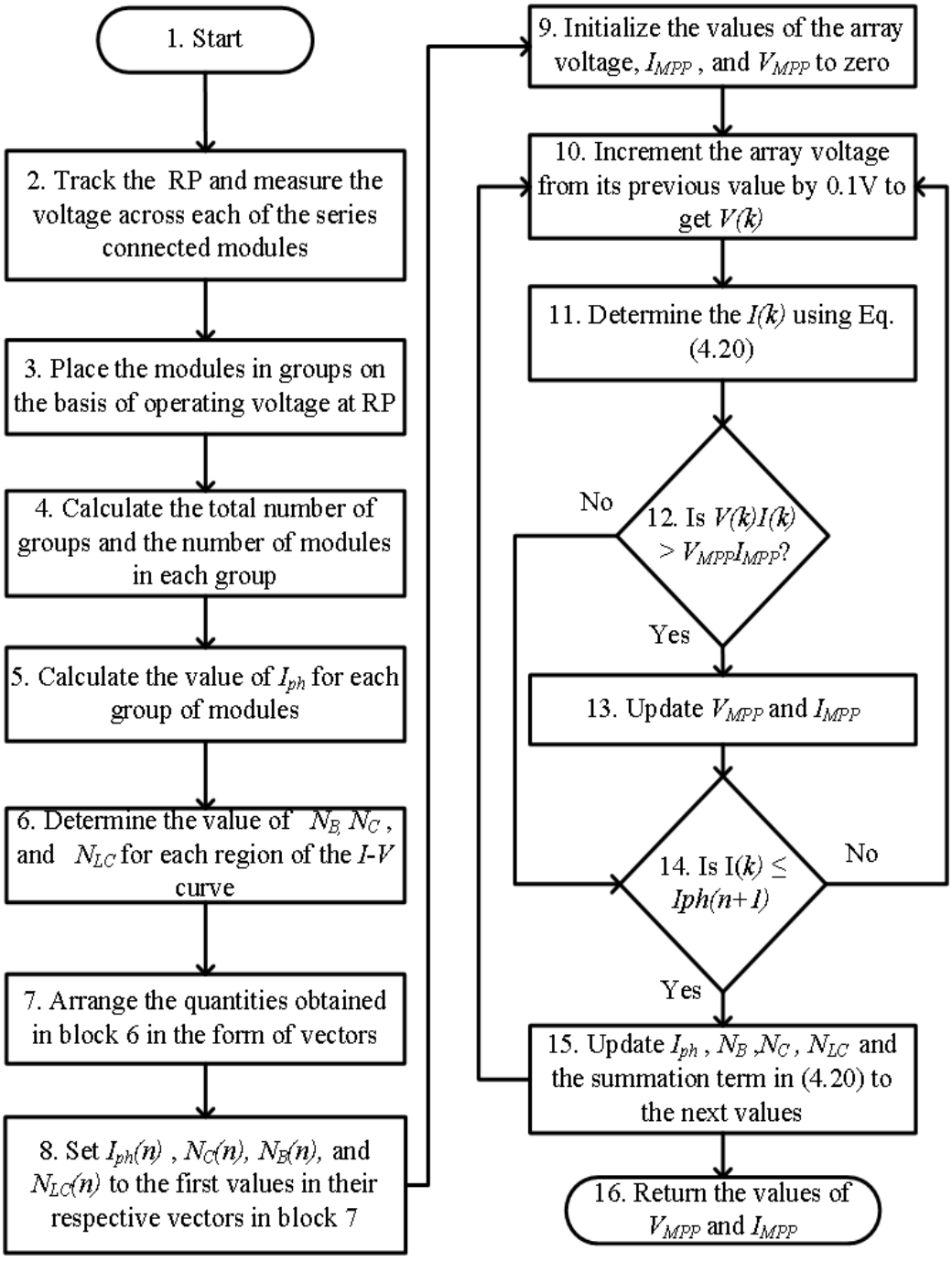

Fig. 6.1 Flowchart of the algorithm for obtaining the *I-V* curve from onsite measurements.

In block 14 the value of *I(k)* is compared to the next value of the photovoltaic current in Eq. (6.1) i.e. $I_{ph}(n+1)$. If the condition is false, then the algorithm goes back to block 10 for the next iteration. If the condition in block 14 is true, it suggests the inception of the next region of the *I-V* curve. In this case, I_{ph}, N_C, N_B, and N_{LC} are updated to their next values in the vectors in Eq. 6.2─6.5, respectively. It is particularly important to mention that for updating the summation term ($\sum_{i=1}^{i=k-1} N_{LCi} V_{Mi}$), the present value of *V(k)* is put in Eq. (4.20). The algorithm then reverts back to block 10. This process continues until the entire *I-V* curve is obtained. At the end of this routine, the values of I_{MPP} and V_{MPP} are also returned.

6.2 Simulation Example of the Proposed Scheme

The proposed algorithm has been simulated in MATLAB/SIMULINK. The PV generator in this case consists of four series connected modules as shown in the Fig. 6.2. Each of the module has 54 series connected cells with rated V_{OC} = 32.9 V, and I_{SC} = 8.26 A. As given in Fig. 6.2, modules M1 and M2 are getting 1000 W/m^2, while M3 and M4 are taking 500 W/m^2 and 300 W/m^2 respectively. The characteristic curves of the array are shown in Fig. 6.3. The switching frequency of DC-DC buck converter is set to 100 kHz and load resistance of 1Ω is used. The sampling period of the MPPT controller is 10ms. Fig. 6.4 shows the GP tracking process for the PV array with shading pattern shown in Fig. 6.2. The algorithm first tracks the RP (i.e. P1 in Fig. 6.3). After converging to the RP at t = 0.1s, the voltage of each of the series connected modules is measured to be VM1 = VM2 = 32.27V, VM3= 30.03V, and VM4 = 23.08V. From the voltages of the modules it can be seen that there are three groups: group 1 consists of modules M1 and M2; group 2 comprises of M3; and group 3 has M4. The vector for I_{ph} , N_C, N_B, and N_{LC} for each of the regions in the *I-V* curve are [8.212A, 4.039A, 2.386A], [2, 1, 1], [2, 1, 0], [0, 2, 3] respectively. After defining these vectors, the algorithm obtains the *I-V* characteristic curve. After the end of the subroutine, the values of I_{MPP} and V_{MPP} are returned. The algorithm, then, calculates the value of D_{MPP} = 0.365. As shown in Fig. 6.4, at t = 0.1s the duty cycle of the DC-DC converter is set to the value of D_{MPP} to begin the steady state operation. Thus the proposed algorithm takes about 0.1s to converge to the GP.

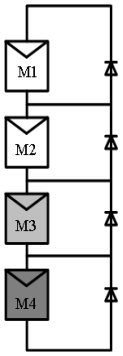

Fig. 6.2 PV array used in the simulation example.

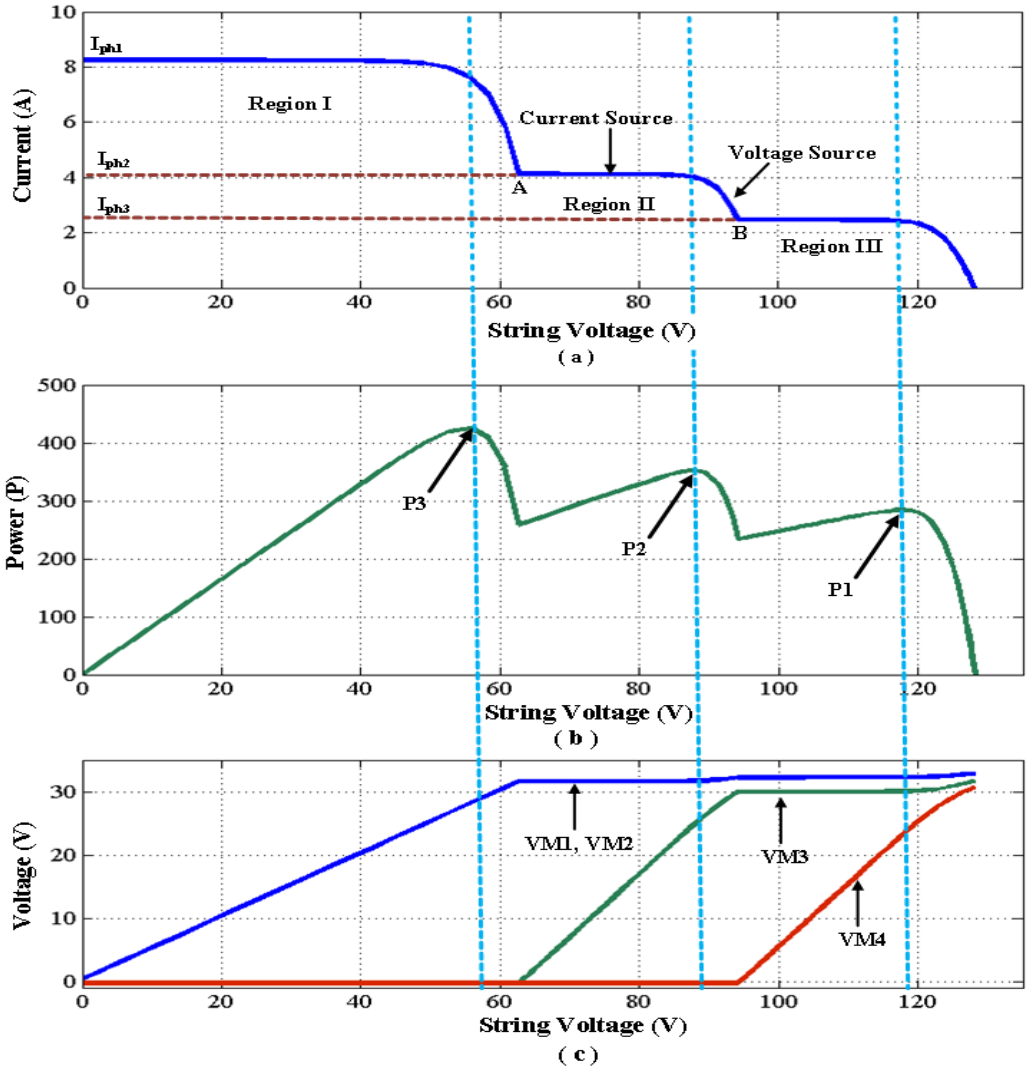

Fig. 6.3 Characteristic curves of the string given in Fig. 6.2.

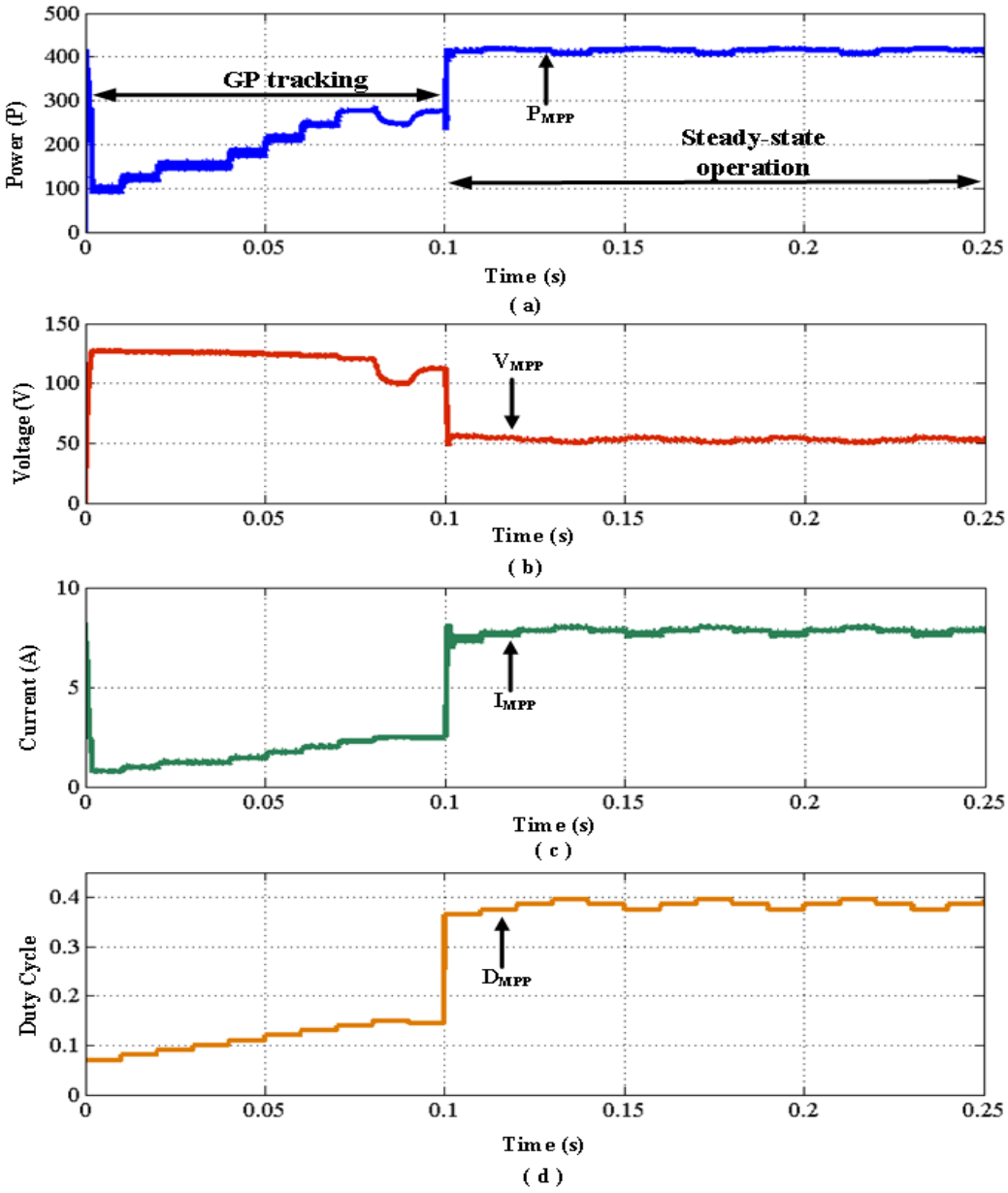

Fig. 6.4 GP tracking process of the PV array given in Fig. 6.2.

6.3 Shortcomings of the Algorithm

The aforementioned procedure finds the characteristic curve of the array by operating it at the RP. Accurate curve is obtained in the case in which the voltages of the modules are perfectly matched under nominal conditions. In the real time situations owing to deterioration as a result of ageing, and also because of manufacturing defects, voltage mismatch among the modules may be present. By reason of this mismatch the procedure discussed in this chapter may not be able to sketch the correct curve. This state of affairs is demonstrated in Fig. 6.5 in which the characteristic curve for the array in Fig. 5.2 is re-drawn. But, in the present instance, the module M4 has lower voltage (under nominal conditions) than M5 and M6. The module M4 gets the same irradiance as M5 and M6 but its lower voltage may be due to any of internal faults. When the array is operated at the RP, the present algorithm categorizes the modules in three groups on the basis of operating voltages (instead of two). By following the procedure given in this chapter, an *I-V* curve with three regions is obtained. Thus, the present algorithm cannot sketch the true curve in the event of a high inequality of voltage among the modules. Refs [30, 31, 32] have proposed MPPT techniques that follow more or less the same mechanism that is expressed in this chapter. Even though these MPPTs might eventually converge to the GP in spite of their inability to recognize the voltage mismatch; however the time taken for convergence could be longer. For this purpose it is necessary to make some modifications to the present mechanism so that a true curve is traced even when the voltages of the modules inside the array are not perfectly matched. The necessary modification to the algorithm is made in Chapter 7.

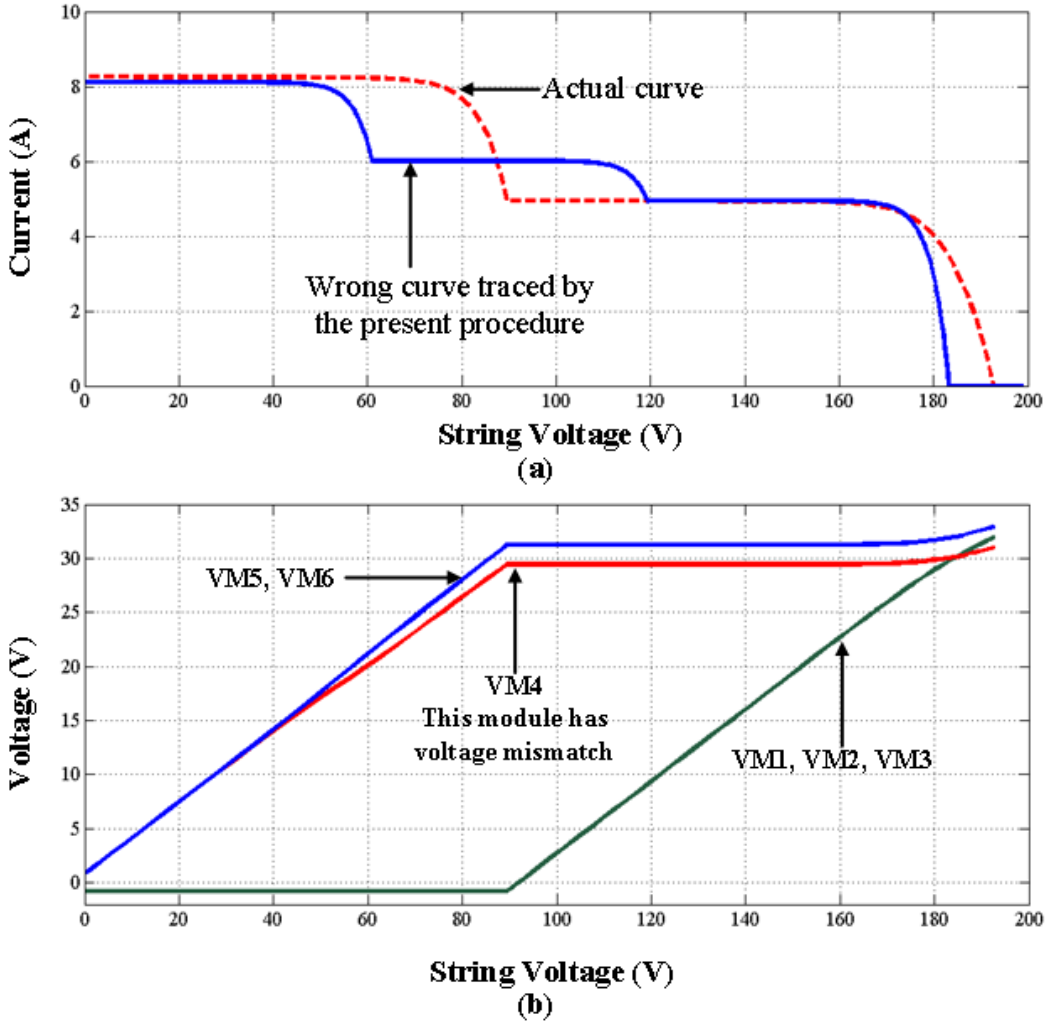

Fig. 6.5 Finding of incorrect *I-V* curve in case of mismatch among the module voltages under nominal conditions.

Chapter 7 Obtaining the Characteristic Curve and MPP Tracking in the Presence of Voltage Mismatch Among the Modules

This chapter deals with the development of MPPT and curve tracing algorithm in case of the existence of voltage mismatch among the modules under nominal conditions. Equations for computing the duty cycle for buck converter are also derived. The performance of the presented method is also verified with the help of simulations and experiments.

7.1 Modified Algorithm

Before presenting the algorithm for the curve tracing and MPP tracking to account for the problems in the PV array discussed in the previous chapter, it is important to discuss the behavior of the module voltages in the presence of voltage mismatch. For this purpose, we take into consideration the string with the irradiance pattern shown in Fig. 4.2(b). In the present case the module M3 has a voltage mismatch of about 3V as compared to the other modules under STC. The new characteristic with the voltage mismatch is now given in Fig. 7.1. Notice the variation of the module voltages VM3 and VM4 in Region 2 of the characteristic curve. When the array operation is performed to the right of point B, the difference between voltage of M3 (i.e. VM3) and voltage of module M4 (VM4) is higher. However, at point B VM3 and VM4 become almost equal and we can say that these modules receive the same irradiance. We can observe from this figure that when the operating point of the string is at the RP (P3), the voltage of M3 is close to the voltage of M1 and M2. When the algorithm discussed in the previous chapter is used, M3 will be placed in a different group from M4. From the irradiance pattern shown in Fig. 4.2(b), the module with voltage mismatch should be placed in the same group with M4. This will result in the calculation of wrong *I-V* curve. It is, therefore, mandatory to make some changes in the previous algorithm to account for any voltage mismatch among the modules. The modified algorithm is discussed below.

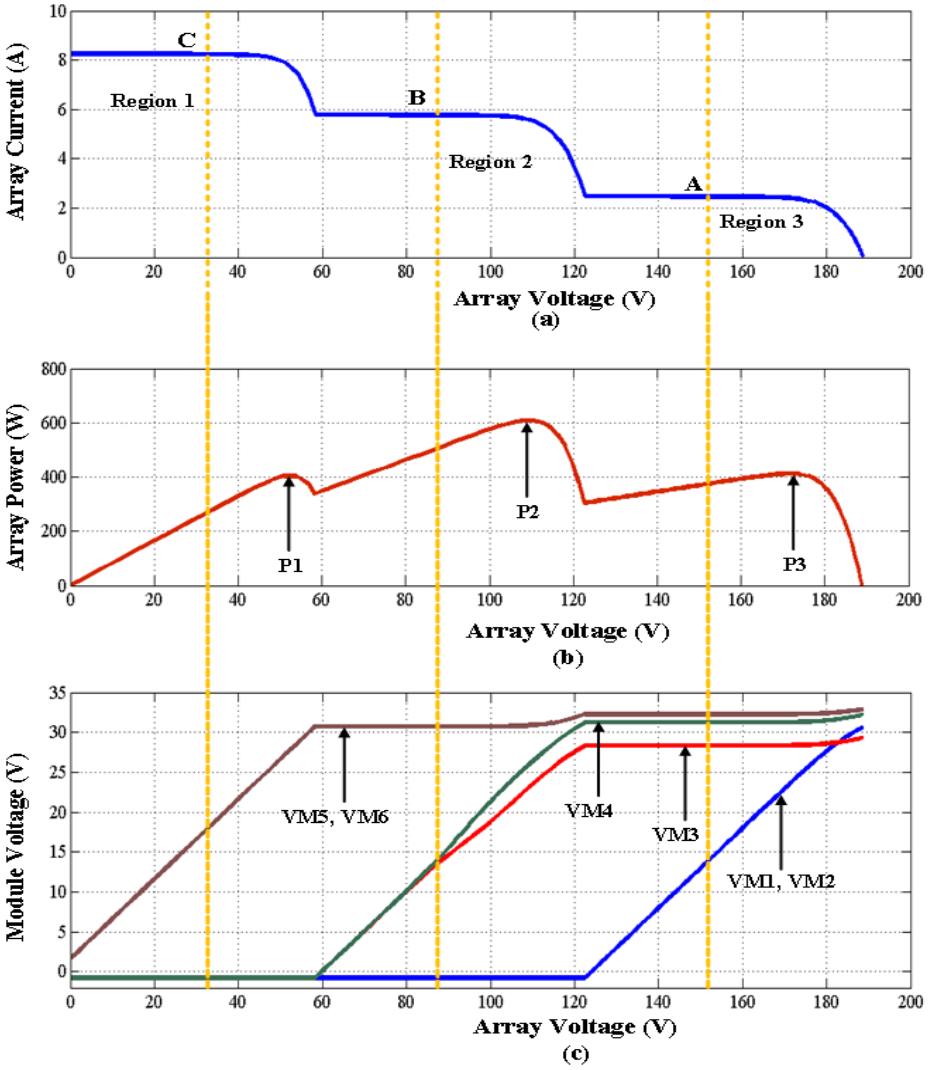

Fig. 7.1 Characteristic curves of the array with the irradiance pattern shown in Fig. 4.2 (b). There is voltage mismatch between modules M3 and M4.

In the mechanism defined in the last chapter, the string is operated at RP and the classification of the modules is implemented. In the modified procedure, the array is first operated to the left of the RP, for example at point A in Fig. 7.1 (a). The flowchart of the modified algorithm is shown in Fig. 7.2. After operating the array close to point A, the grouping of the PV modules is executed. This grouping is different from the previous case. Now, the modules are placed in three groups on the basis of the operating voltages. In the first group, the bypassed modules are placed: in this group the operating voltage of the modules is lower than 0V. Group 2 contains the modules that are controlling the current of the string. The operating

voltage of these modules is higher than those of Group 1. Group 3 is composed of the modules that operate at current below their MPP currents: or in other words, operate close to their respective V_{OC}. The difference in the operating voltages of the modules in the three groups is now higher. In this way, the classification is much easier. As will be shown in the following paragraphs, the new algorithm is able to perform correct classification even in the presence of voltage mismatches among the modules.

For the specific case of Fig. 7.1, when the string functions close to point A, the classification under new procedure is performed as follows:

- Group 1 has no modules, as none of those is bypassed.
- Group 2 contains M1 and M2. This is because the voltage of these modules is higher than those in Group 1 and much lower than those in Group 3.
- Group 3 consists of the remaining four modules M3 ─ M6. We can see that M3, even though has lower voltage under STC, is placed in this group because its operating voltage is still higher than M1 and M2.

The current of the string is stored as I_{ph} for the corresponding region (region 3 in the present case). The number of modules in Group 1 is stored as N_B, the number of modules in Group 2 is recorded as N_C, while that of Group 3 as N_{LC} for this region of the characteristic curve. As the number of modules in Group 3 is greater than zero, it means that there is at least one peak to the left of the present operating point and the search process has to be performed for finding a point to the left of that peak.

The next step is to make the string function at point B in Fig. 7.1. The process of expediting the process of taking the point of operation from A to B will be discussed later in this chapter. But for now assume that the array is functioning close to point B. The modules are again divided into three groups as:

- Group 1 consists of modules M1 and M2.
- Group 2 comprises of M3 and M4.
- Group 3 has M5 and M6.

As done in the previous case, the current of the array is stored as I_{ph} for this region. N_B for this region is equal to 2 as M1 and M2 are bypassed and placed in Group 1. N_C for this part of the curve is also 2 as M3 and M4 form Group 2. Likewise, from the number of modules in Group 3 we set N_{LC} equal to 2. As the

number of elements in the third group is greater than zero, it indicates the present of another peak to the left of point B.

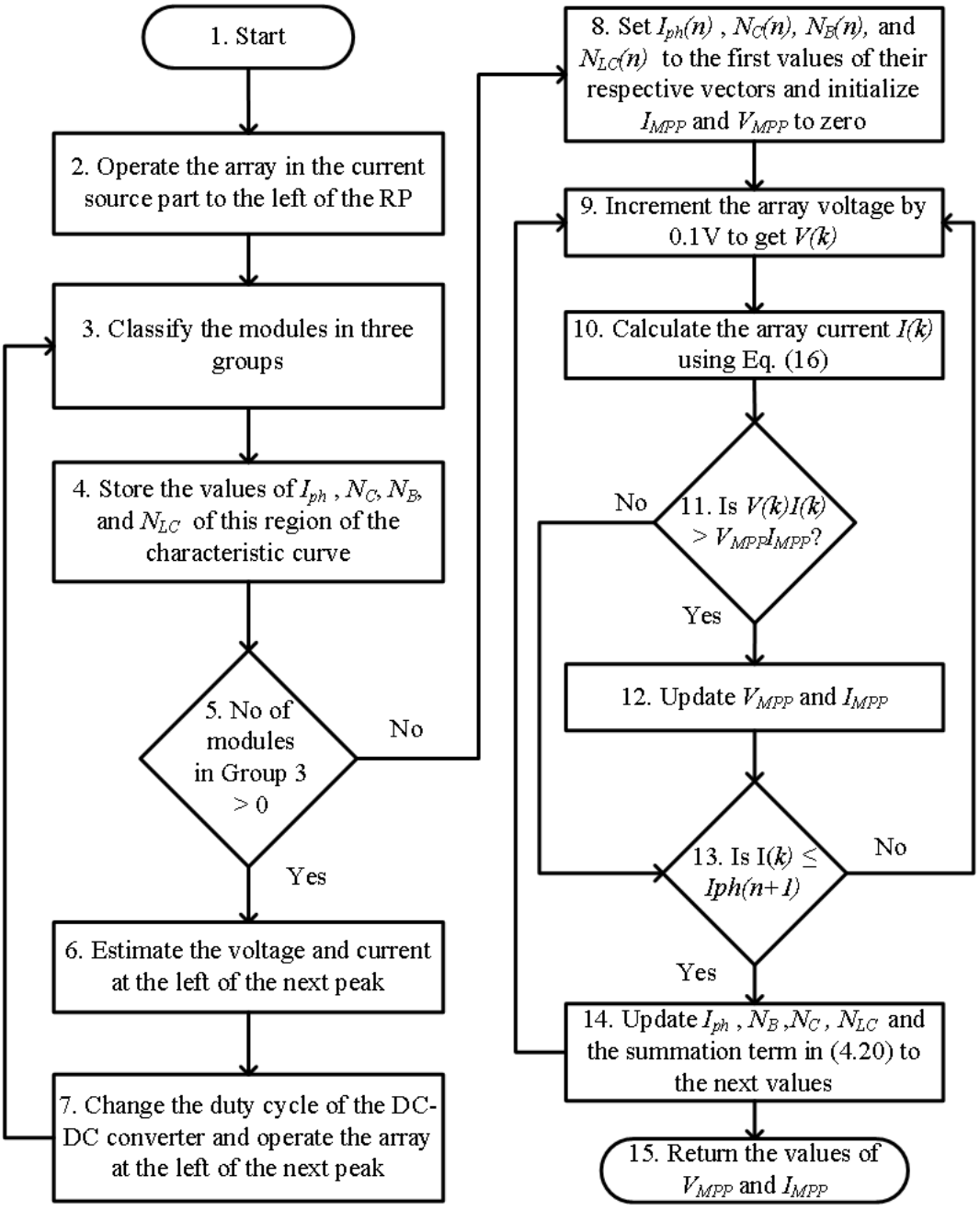

Fig. 7.2 Flowchart of the modified algorithm.

The functioning point of the string is then brought near to point C in Fig. 7.1. The same process is repeated here. The number of modules in Group 1 will be equal to 4 i.e. $N_B = 4$, the number of modules in Group 2 is equal to 2 ($N_C = 2$). The third group will now contain no elements ($N_{LC} = 0$) and hence, no further search is performed. At this stage all the quantities of I_{ph}, N_B, N_C, and N_{LC} corresponding to each region of the curve are arranged in the form of vectors given in Eqs. 6.2─6.5, respectively.

After obtaining the vectors, the new algorithm proceeds to calculate the characteristic curve of the array in identical manner as given in the previous chapter as can be seen in the flow chart shown in Fig. 7.2.

7.2 Duty Cycle Computation for Fast Convergence to the MPP

As given above, after obtaining the *I-V* curve, the values of V_{MPP} and I_{MPP} are also returned. We then need to operate the array at this voltage. For taking the point of operation to the MPP, the duty cycle of the DC-DC converter is varied in a certain direction. Typically, this is accomplished by changing the duty cycle in small steps as is done in [30]. This naturally affects the convergence speed of the MPPT scheme. For that reason, it is important to use a relation for calculating the duty cycle of the converter in order to accelerate the convergence to the MPP. In this section the relation for finding the duty cycle of a stand-alone buck converter with resistive load is given. For other converter topologies and applications, this relation can be found in the literature [28].

Suppose the array is functioning at a point with voltage V_{PV} and I_{PV} with duty cycle D_{PV}. The proposed algorithm obtains the characteristic curve of the array and also returns I_{MPP} and V_{MPP}. For converging to the GP, the equation for calculating the duty cycle corresponding to the MPP (D_{MPP}) is given in the following text

For buck converter the relationship between the input and output voltages (*Vi* and *Vo*) and currents (*Ii* and *Io*) are given by:

$$V_i = \frac{1}{D} V_o \tag{7.1}$$

$$I_i = DI_o \tag{7.2}$$

From the above equations we get

$$\frac{V_i}{I_i} = \frac{V_o}{D^2 I_o} \tag{7.3}$$

Here $\frac{V_o}{I_o}$ represents the load resistance R_o , solving (7.3) for R_o we get

$$R_o = D^2 \frac{V_i}{I_i} \tag{7.4}$$

The value of R_o is found operating the array at an appropriate point and inserting the value of duty cycle, voltage and current at that point in (7.4).

Assuming that R_o is constant, when the PV array is at the MPP, the input and the output resistances of the converter are related by the equation [19]:

$$R_{MPP} = \frac{1}{D_{MPP}^2} R_o \tag{7.5}$$

Where $R_{MPP} = \frac{V_{MPP}}{I_{MPP}}$ and D_{MPP} is the value of duty ratio at the MPP. Solving (7.5) for D_{MPP} and putting the relation of R_{MPP} we get

$$D_{MPP} = \sqrt{\frac{R_o I_{MPP}}{V_{MPP}}} \tag{7.6}$$

The values of V_{MPP} and I_{MPP} are obtained from the subroutine which calculates the points on the characteristic curve given in the flowchart. From the present point of operation of the array, we can calculate the value of R_o. Then Eq. 7.6 is used to calculate the D_{MPP}. By setting up the duty cycle of the converter to this value, the GP of the array is tracked.

Let us refer back to the previous section 7.1. During the searching process for finding the values of the vectors in Eq. 6.2─6.5, it is desirable to shift the operation of the array from point A and B and then from B to C quickly. One way of doing so is to change the converter's duty cycle in small steps. As mentioned previously, this will cause an undesirable delay in the process. To expedite this process, Eq. (7.6) can be utilized for buck converter applications. For understanding the procedure, let us consider the string is operating at point B, in Fig. 7.1 and we want to proceed to point C. The value of R_o is found from the duty cycle, voltage, and current of the array at the present point. The value of current at C is equal to the I_{ph} of the modules M5 and M6 which can be estimated using (6.1). In Eq. (7.6) this value of current is used instead of I_{MPP}. For approximating the voltage at C we make use of (5.1) or (4.22). We can see that the voltage at which the peak P1 occurs in Fig. 7.1, is estimated as:

$$V_{P1} = 0.80\left(1 - \frac{N_B \; at \; point \; C}{N_S}\right) V_{OC}$$

$$= 0.80\left(1 - \frac{Number \; of \; modules \; in \; Groups \; 1 \; and \; 2 \; at \; pointB}{N_S}\right) V_{OC} \qquad (7.7)$$

The voltage of point C is estimated to be a few volts less than V_{PI}. Then, these values are inserted in eq. (for D_{MPP}) to calculate the duty cycle close to a point near C. For insuring that the array is operating in the current source region, the duty cycle of the array is changed in small steps and if the current as a result of the perturbation is virtually constant, it means that the string operates close to the desired point.

7.3 Application of the Proposed Method for MPP Tracking

The scheme presented in this text can be utilized to perform MPP tracking as well as finding the characteristic curve of the array under uniform irradiance and partial shading conditions. In this section, the application of the proposed method for MPP tracking is expressed. The procedure is explained with the help of the block diagram shown in Fig. 7.3.

Referring to Eq. 7.6, it is important to determine the value of V_{OC} of the array for convergence to a specific point of operation of the array during the subroutine

given in Fig. 7.3. Calculation of V_{OC} is accomplished from the reading of the temperature sensor. The equation used for computing the value of V_{OC} is given as:

$$V_{OC} = V_{OC,n} + K_V \Delta T \tag{7.8}$$

Once the value of the open circuit voltage is found, the next step is to calculate the *I-V* characteristic curve of the PV source. This is accomplished through the algorithm described in the section 7.1. The whole procedure is executed in block 3. As has been mentioned in the previous sections, the values of V_{MPP} and I_{MMP} are returned to the main program after finding the characteristic curve. In block 4, the D_{MPP} is calculated. In block 5, the duty cycle of the DC-DC converter is set to D_{MPP}. After confirming that the array has converged to the desired point, the steady state operation commences.

Blocks 6, 7, and 8 represent the steady-state operation. This operation is based on the conventional P&O algorithm. One of the disadvantages of the P&O algorithm is that it oscillates around the MPP. To minimize these oscillations, the value of the duty cycle perturbation (ΔD) should be kept to a small value. As given in the work of the author in [20], when the value of ΔD is kept to about 0.4, the efficiency of the algorithm under the steady-state conditions reached up to 99.92%. A small amount of oscillations is also important to alter the functioning point of the PV in the face of small variations in the ambient conditions. As given in block 7, a timer overflow interrupt could also be enabled for triggering the process of finding the new MPP and the characteristic curve. In block 8, the output of the power from the PV generator is monitored after every sampling period. If the absolute difference between the output power of the array P_{PV} and the power of the array corresponding to the last MPP tracked (P_{MPP}) exceeds a certain limit ε, the algorithm goes back to block 2 to re-initiate the whole procedure.

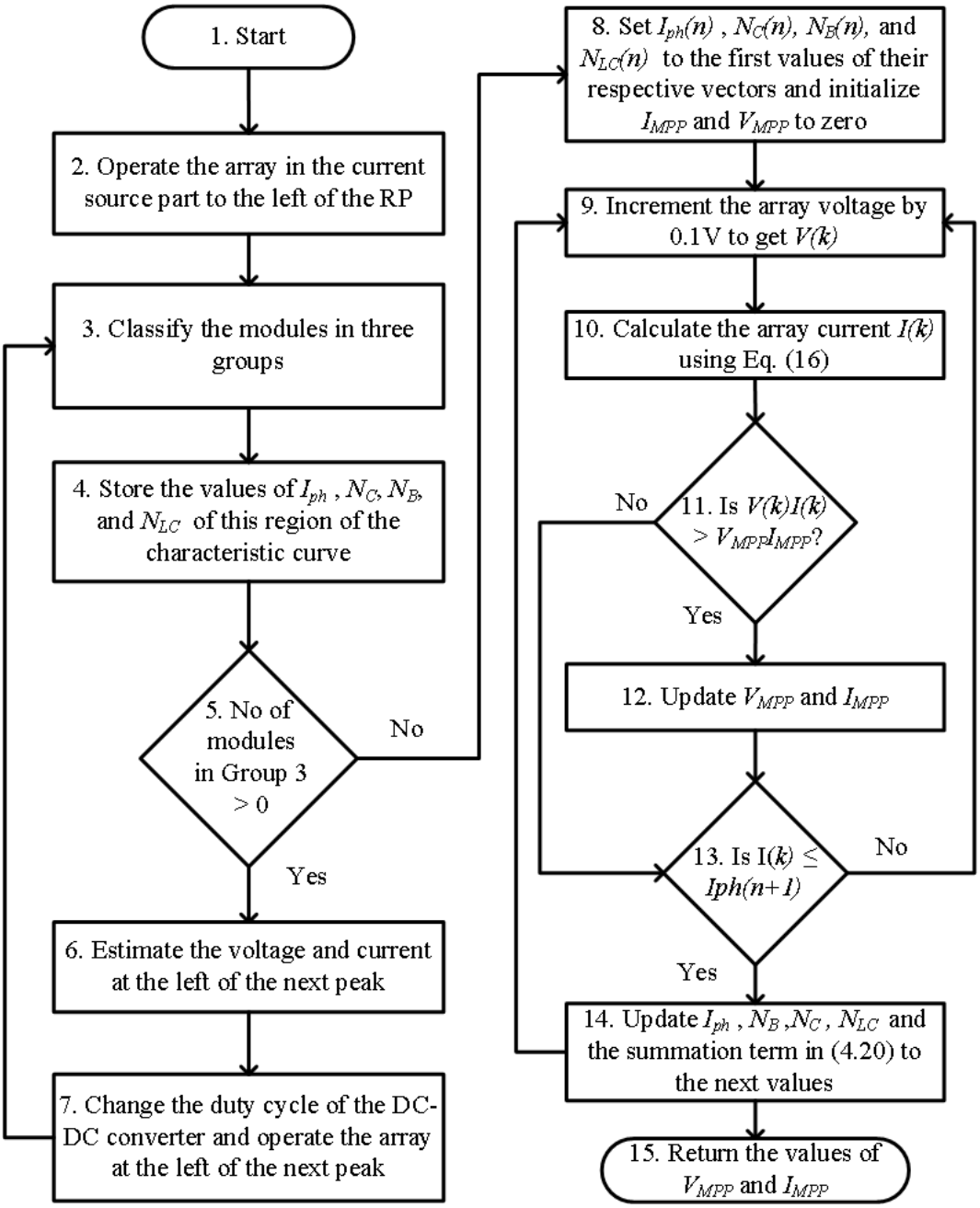
1. Start
2. Operate the array in the current source part to the left of the RP
3. Classify the modules in three groups
4. Store the values of I_{ph} , N_C, N_B, and N_{LC} of this region of the characteristic curve
5. No of modules in Group 3 > 0
No
Yes
6. Estimate the voltage and current at the left of the next peak
7. Change the duty cycle of the DC-DC converter and operate the array at the left of the next peak
8. Set $I_{ph}(n)$, $N_C(n)$, $N_B(n)$, and $N_{LC}(n)$ to the first values of their respective vectors and initialize I_{MPP} and V_{MPP} to zero
9. Increment the array voltage by 0.1V to get $V(k)$
10. Calculate the array current $I(k)$ using Eq. (16)
11. Is $V(k)I(k) > V_{MPP}I_{MPP}$?
No
Yes
12. Update V_{MPP} and I_{MPP}
13. Is $I(k) \leq Iph(n+1)$
No
Yes
14. Update I_{ph} , N_B ,N_C , N_{LC} and the summation term in (4.20) to the next values
15. Return the values of V_{MPP} and I_{MPP}

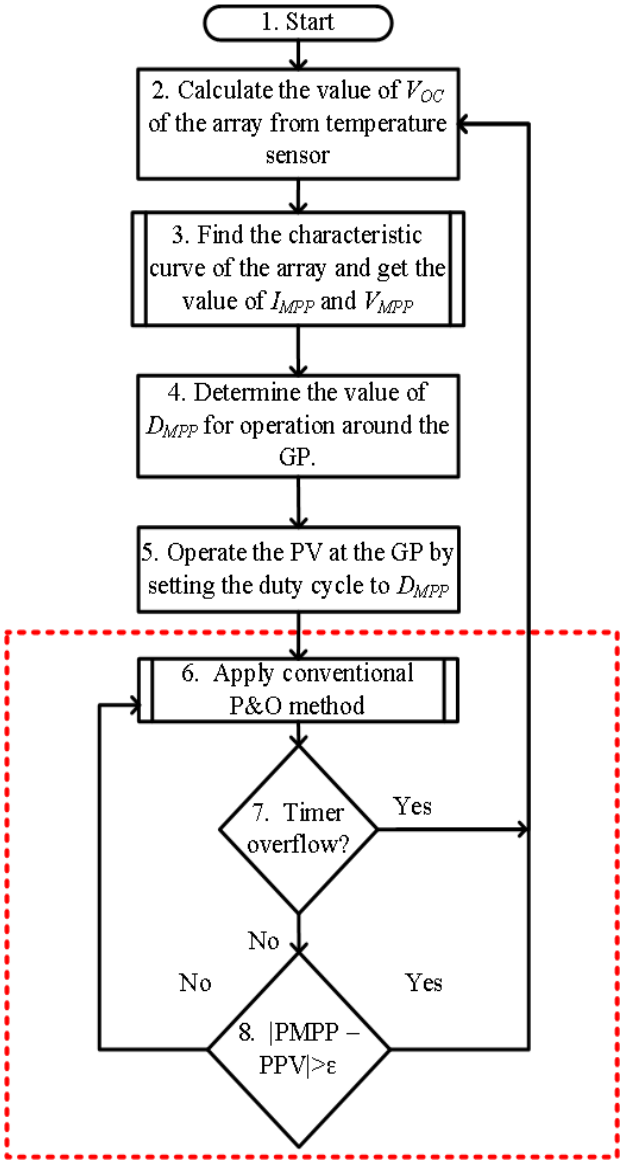

Fig. 7.3 Flowchart of the proposed MPPT.

7.4 Simulation Results

To check the performance of the method presented in this chapter, simulations have been conducted using MATLAB/SIMULINK. The specifications the PV string are the same as have been shown in Chapter 5. DC-DC buck converter is used in the simulations. The switching frequency of the converter is 100 kHz and the load resistance is 1Ω. The sampling period of the MPP controller is 10 ms.

The performance of the scheme was checked under various shading conditions. First, the case given in Fig. 7.1 is considered. As given in this beginning of this chapter, there is also a mismatch between the voltage of M3 and the rest of the modules in the array under nominal conditions. The simulation results are shown in the Fig. 7.4. A vertical green dotted line divides each of the subplot in Fig. 7.4 in two portions. To the left of the dotted line the part of the algorithm in which it performs the search for various parameters given in vector form in Eq. 6.2─6.5. From t = 0.0 s to 0.05 s the algorithm tracks the RP (or P3 in Fig. 7.1). After doing so, the modules are classified into three groups as expressed in section 7.1. The algorithm finds the presence of another peak (P2) to the left of the RP. As expressed previously, the voltage and current corresponding to point B (in Fig. 7.1) are found by the algorithm. The approximate location of the voltage point is easily found by using Eq. (7.7). For finding the approximate value of current, the algorithm takes the modules with the lowest voltage in group 3, which is M3. As M3 has lower voltage so the use of Eq. (6.1) will give a lower value of current. Thus, for getting close to point B, the duty cycle of the converter is changed in small steps. This can be seen in Fig. 7.4 (d) in the interval from t = 0.05 s to 0.1 s. The point of operation of the array is easily taken to the current source part to the left of P1 from t = 0.1 s to t = 0.12 s. At this stage the characteristic curve of the array, I_{MPP}, and V_{MPP} are found and from these values D_{MPP} is calculated. The steady state operation begins at t = 0.13 s.

Thus, from these results we can conclude that the proposed scheme converges to the MPP under non-uniform irradiance in about 0.13 s. This time duration is far less than [26, 28, 30]. These MPPTs take about 1 s for finding the GP. The method proposed in this chapter performs additional function measuring the characteristic curve of the array from on-site measurements.

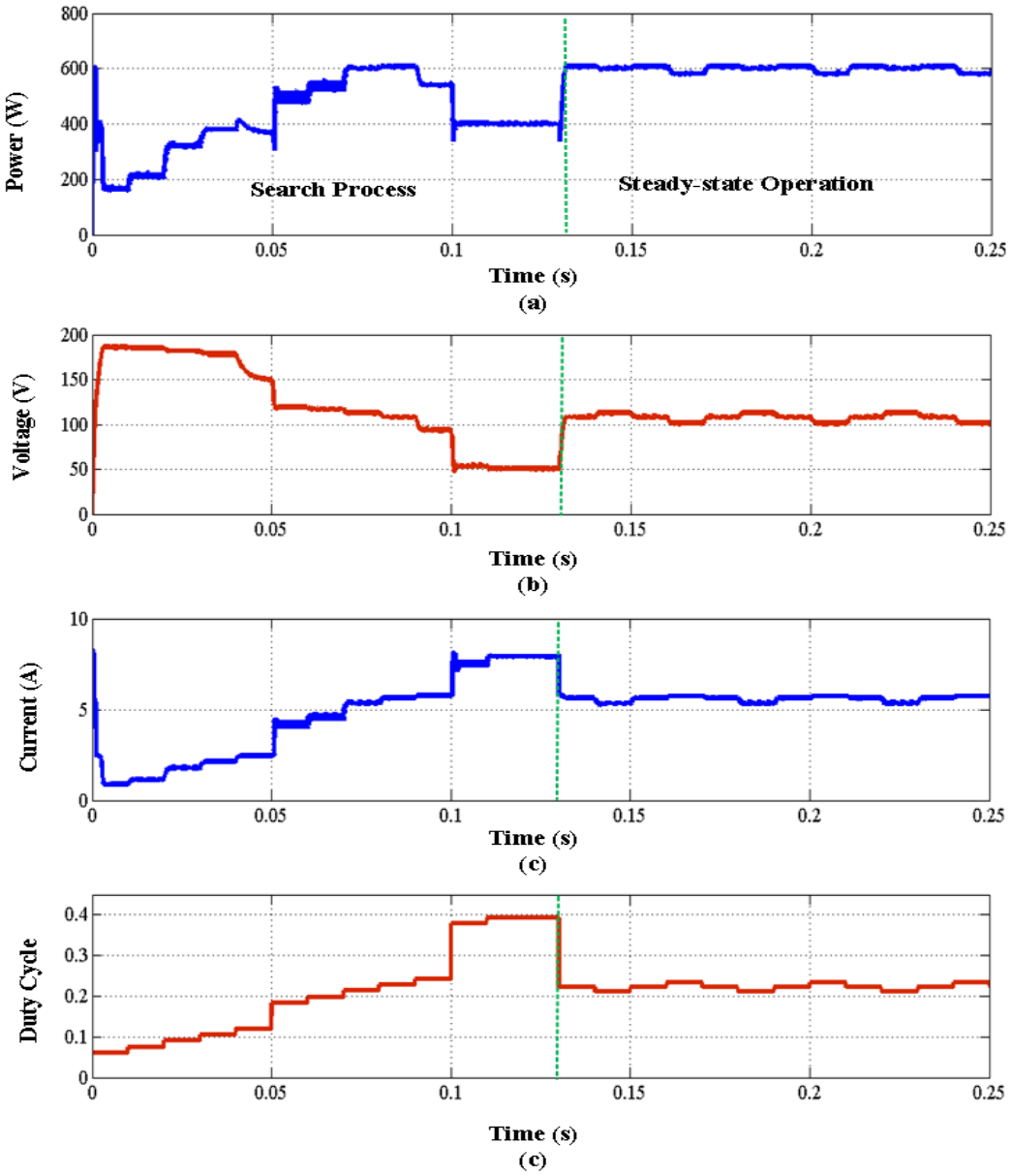

Fig. 7.4 GP tracking process using the proposed algorithm for MPP tracking.

7.5 Experimental Results

For confirming the ability of the proposed algorithm to get an accurate *I-V* curve, experiments were conducted for partially shaded PV arrays. The scheme presented in this chapter is compared to the capacitor-charging based curve tracing method given in [42]. The PV source used for experiments is a 230W panel which is made of 60 PV cells connected in series. Inside the panel, 20 cells are protected by same bypass diode. Thus, we have a PV string with three modules M1, M2, and M3 as given in Fig. 7.5. The experimental setup consists of: multifunction data acquisition device with high speed ADC; a PC for storing the experimental data; differential probes for measurement of voltage; and Hall effect based current probes. Switch S1 is used to connect the capacitor to the PV source. Switch S2 connects the discharge resistor R to the capacitor after performing the test.

The essential parameters that are required for the finding of the *I-V* curve through the proposed method are the vectors containing the PV current, the number of modules that control the current of the array in each region of the characteristic curve (N_C), the number of modules which are bypassed in each region (N_B), and the number of modules that operate at lower current than their MPP currents (N_{LC}). These vectors are given in Eqs. 6.2─6.5, respectively. These vectors were easily found from the capacitor charging method by means of programing in LABVIEW. The vectors were then used by the proposed algorithm to trace the characteristic curve.

The module M1 in Fig. 7.5 was put under partial shade which is shown in Fig. 7.6. Experiments were performed for finding the *I-V* curve with the help of capacitor charging method. The experimental results are shown in Fig. 7.7. In this figure, subplot (a) shows the current, (b) indicates the voltage of the PV array, and (c) indicates to the submodule voltages VM1, VM2, and VM3. All these quantities are drawn as a function of time and were acquired during the charging of the capacitor. As shown in Fig. 7.7, in Region 1, the capacitor draws the maximum current from the PV source. In this region, M1 is unable to supply the current due to partial shading and therefore, the module is bypassed. In this region of the curve, the modules M2 and M3 control the current of the generator. The values of quantities in the form of vectors were recorded. At point A, the current drawn by the capacitor decreased to a value just below the maximum current of M1 could supply. From that point, all the three modules started to supply power to

the load. The values of the essential parameters were also recorded in the second region.

Fig. 7.8 shows the characteristic curves obtained from the two methods. The blue curve in Fig. 7.8(a) shows the one obtained from the capacitor charging method and the red curve shows the one obtained from the proposed scheme. The close resemblance of the two curves could be seen which indicates the effectiveness of the proposed method in obtaining the accurate characteristic curve of the array from on-site measurements. Similarly, Fig. 7.8 (b) shows the *P-V* curves obtained from the proposed (red curve) and the capacitor charging method (blue curve). The figure shows that the proposed method can return accurate values of I_{MPP} and V_{MPP} and hence, it can also be utilized for GP tracking under any irradiance conditions.

An important point to consider here is that the model which is developed in Chapter 4 is based on the assumption that all the cells in a PV module get the same irradiance. However, PV array given in Fig. 7.6 shows that only a certain number of cells are under the shade. The model developed in chapter 4 is also applicable to the case shown in the Fig. 7.6. It is because when some of the cells in a module are shaded, the current of the entire module is controlled by the shaded cell. It is also well known that the voltage of a PV cell is logarithmically related to the irradiance. As a result of it, the difference in irradiance causes a small difference in the voltages among the cells. Considering Fig. 7.8 (a) which shows the curves obtained from capacitor charging method and the one obtained from the proposed procedure, it can be seen that the portion of the curve in which the module M1 is bypassed, the two curves match with each other between points A and B. The two curves are also identical between points B and C. The small divergence between the two curves from point A to C is because of the fact that in the proposed model R_S and R_P of the PV panel have been neglected. Now from point C to D, we see that the *I-V* found from the proposed procedure intersects the voltage axis at a slightly lower voltage than the one obtained from the capacitor charging method. This difference between the two curves is owing to the fact that proposed scheme is based on the assumption that all the cells in submodule M1 are taking the same amount of sunlight, whereas in reality some of the cells in the module are shaded. It is, however, important to notice that the region between point C and D is of lesser significance for MPP tracking and even diagnostic purposes. The two curves are almost identical between points A and C which are important for practical purposes.

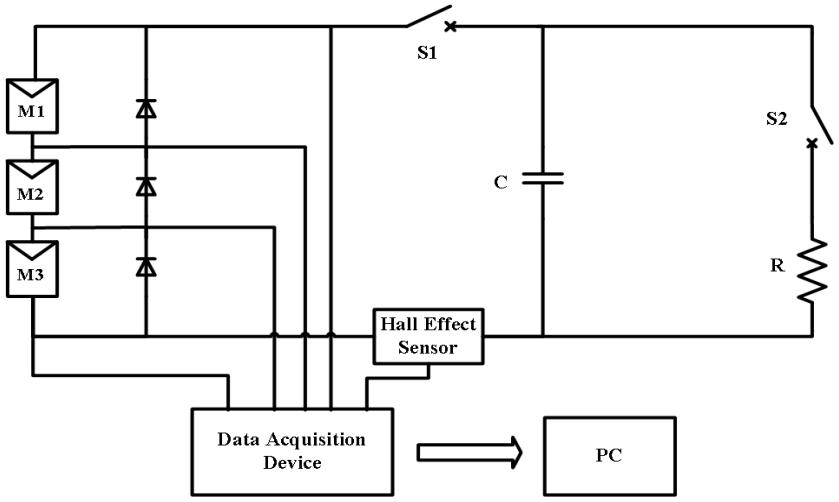

Fig. 7.5 Circuit diagram of the experimental setup.

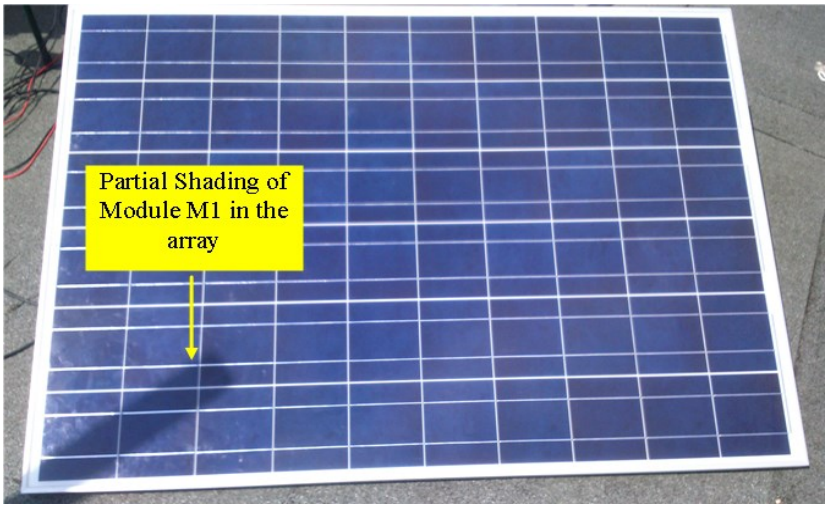

Fig. 7.6 PV array under partial shade.

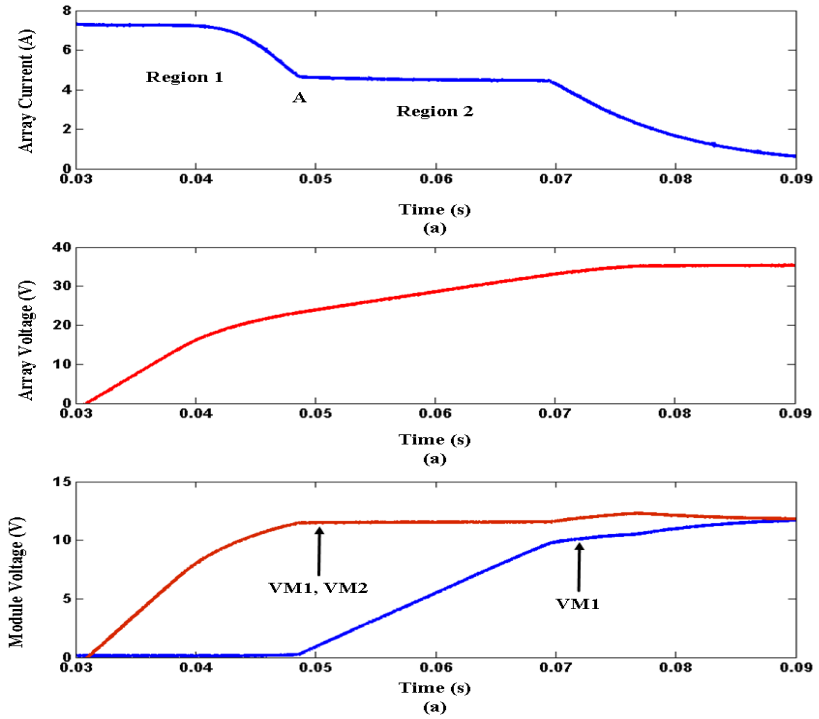

Fig. 7.7 Array current, voltage, and module voltage obtained capacitor charging method.

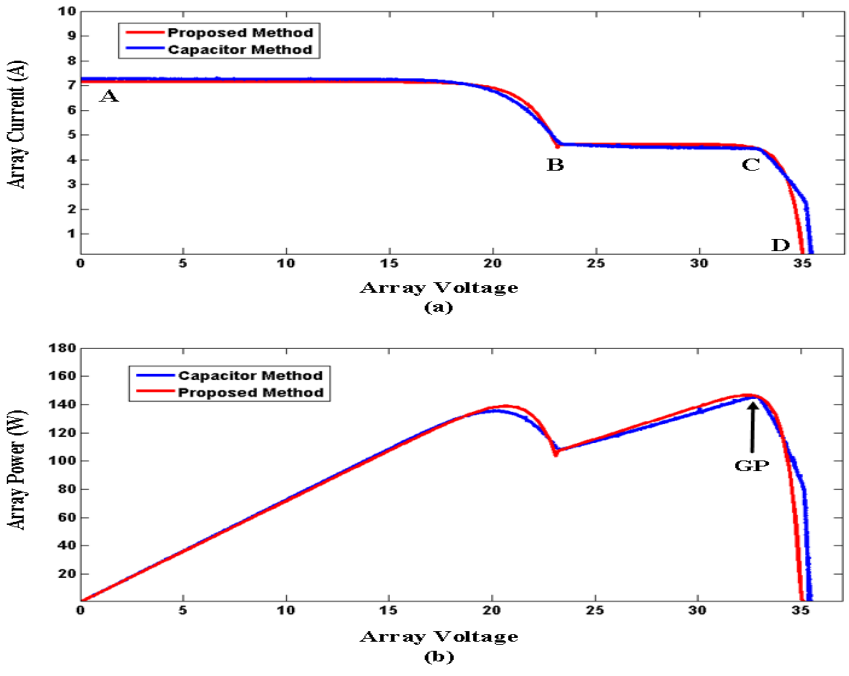

Fig. 7.8 *I-V* curve obtained from the capacitor charging method and the proposed method.

In this chapter, a scheme for finding the characteristic curve of a PV array, under the presence of voltage mismatch among the modules, has been presented. The procedure can also be applied for MPP tracking under any irradiance conditions. The performance of the proposed method has been confirmed through simulations and experiments. In the experimental verification, the proposed scheme has been compared with capacitor charging method. Experimental and simulation results reveal that the proposed algorithm can be applied for tracing the *I-V* curve and finding the global MPP successfully under any kind of irradiance conditions.

7.6 Economic Analysis of Practical Implementation of the Proposed Scheme

The algorithm given in this chapter is applicable for long strings and also for Distributed MPPT (DMPPT) applications. The actual cost of the additional hardware can only be ascertained depending upon the MPPT architecture. In this text we will perform economic analysis only in the case of DMPPT systems in which each panel acts as a substring and has its own MPP tracking algorithm. For monitoring the performance of PV systems an on-board device has been proposed in [57]. This board is mounted in each PV panel and the latter functions as a substring of a long PV string. The board is able to measure the PV panel's voltage, current, and temperature; it has a local MPP tracking hardware. Similarly, it can communicate with other boards and with the central control unit of the PV plant through RS 485 bus. A shortcoming of the system given in [57] is that the electrical curve of a PV panel cannot be obtained by the device. The method that is proposed in this chapter has an advantage that it can perform the monitoring, MPP tracking, and measuring the *I-V* curve in a single algorithm. However, we will present a list of hardware components utilized to ascertain the cost of the additional hardware that is used in the implementation of the algorithm given in this chapter. Table 7.1 gives the detail of the components used in [57].

Table 7.1 Details of components used for PV module monitoring in Ref. [57]

Device Name	Device's Function
ACS 712	Hall Effect based current sensor
PIC16F1825	Microcontroller for MPPT and communicating data with other boards and the central control unit
LMC 6062	Operational Amplifier
LM2675	Step down power converter
HCPL0601	Optical Couplers
TC1047A	Temperature Sensor

Table 7.2 Details of components required for monitoring the performance of a PV string

Component	Function	Total Nos	Per Unit Cost in Euros	Total Cost/Panel in Euros
AD 7124-4	Analog to Digital Converter, 4 Channel	1	9.6	9.6
SN65HVD1476	RS485	1	2	2
TC1047A	Temperature Sensor	1	0.48	0.48
HCPL0601	Optical Couplers, 2 Input	2	2.2	2.2
SN65HVD70	RS 485 Transceiver	1	2	2
Resistors and other passive components and PCB and Cabling	Component Assembling/Voltage Division/Signal Conditioning		8	8

In table 7.2 we give the estimated increase in cost per panel needed for the additional components. From the data given in this table we can see that additional cost of about 25 Euros per panel is needed. It means that by adopting the proposed scheme a cost of about 100 Euros/KW is incurred. For a typical home based MPPT [58] the total cost of 2000 Euros/KW is incurred. The proposed scheme increases the cost of PV installation by 5% but has additional features of diagnosis of the PV installations.

Chapter 8 MPPT and *I-V* Curve Tracing Algorithm Utilizing the Input Filter Capacitor of DC-DC Buck and Buck-Boost Converter

In this chapter, MPPT and I-V curve tracing algorithm is presented. The procedure described in this chapter extends the functionality of the input filter capacitor of DC-DC buck or buck-boost converter for finding the MPP and the characteristic curve under any kind of shading. This method is applicable to the applications in which the output of DC-DC converter is connected to storage devices like battery and/or supercapacitor.

8.1 PV Systems with Battery/Super Capacitor Storage

Stand-alone PV systems are used in areas which are far from the reach of the national grid. Extension of the national grid to these remote locations requires heavy expenditures and thus, stand-alone PV systems are the only alternative. These renewable energy systems provide power to different kinds of loads e.g. household applications, irrigation, and telephone communication repeater stations. The generation of power from the Sun is highly intermittent. Similarly, the nature of the load for which the stand-alone PV system is used may be highly variable. For example, the water irrigation systems utilize DC motors. The starting current of a DC motor is very high and may be beyond the capacity of the PV source. Owing to these reasons, battery backup is provided to maintain uninterrupted power at the output. For extending lifetime of the batteries, Hybrid Energy Storage Systems (HESS) are also used. HESS utilizes batteries as well as Super Capacitors (SC) to make optimal use of the storage system. SC has high power density allowing it to provide more energy for a short period of time (a few seconds) [52].

In many grid tied PV applications, the output of the DC-DC converter is connected to battery storage systems where the excessive power generated from the solar panels is stored and is provided to the load or grid in the time of need. The main benefit of this system is that, during the interruption of power generation from the PV system, the storage devices continue to supply power to the load or grid and the momentary power interruption does not create power quality issues.

8.2 Brief Description of Capacitor Charging based MPPT

A capacitor charging based MPPT is proposed in the previous work co-authored by the author in [53]. Brief descriptions of that work as well as some of its limitations are discussed here. The block diagram of the MPPT procedure is given in Fig. 8.1. As given in this figure, the PV array is connected to the DC-DC converter and a scanning circuit through MOSFET switches S1 and S2, respectively. It should be remembered that these switches are different from the MOSFET switch used inside the DC-DC converter. Under normal operation, S1 is closed while S2 is open. As S1 is normally conducting, a certain amount of power is lost in it due to its on-state resistance. The power is lost in the form of heat. It is therefore, necessary to design a special heat sink for S1. Moreover, high-side driver circuit is also required for this MOSFET, which increases the complexity of the circuit. Fig. 8.2 shows the scanning circuit in details. When the GP of the array is to be found, S1 is opened and the scanning circuit is connected to the array through S2. The resistors R1 and R2 are used for scaling the array voltage down to an appropriate value. The capacitor C_{EXT} is connected to the array through switch S2 for finding the GP. When the MPP is found, the normal operation of the PV system resumes at the new peak. Though it is not shown in the figure, a discharge resistor is used to discharge the external capacitor in order to make it ready for GP tracking again. Analog multiplier is used to multiply the array voltage and current. The output of the multiplier is connected with the input of a peak detector and trigger block [43]. During the charging evolution of C_{EXT}, when a peak at the output of the multiplier is encountered, the sample and hold amplifiers S&H1 and S&H2 are triggered into sampling mode. These amplifiers sample the array current and voltage corresponding to power peak. After the completion of the GP tracking procedure, the values of V_{MPP} and I_{MPP} are available at the outputs of S&H1 and S&H2 respectively. It is important that the sample and hold amplifiers should have short acquisition time (less than 1 μs) and low droop rate. After finding I_{MPP} and V_{MPP} the value of D_{MPP} is calculated using

Eq. (7.6). Once the operating point of the array is taken to the MPP, a conventional technique like P&O algorithm is invoked to maintain the operation around the power peak.

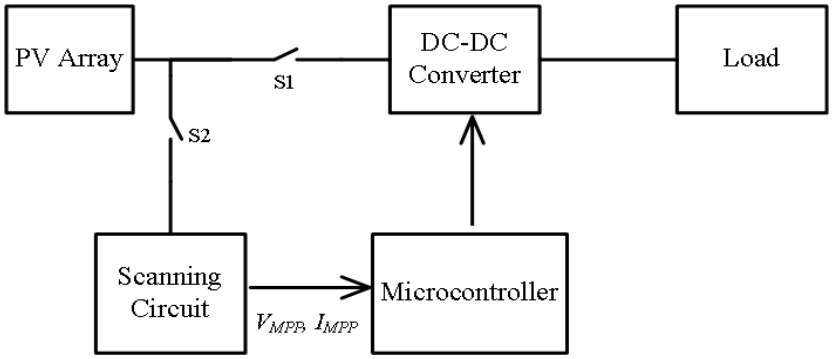

Fig. 8.1 Block diagram of capacitor charging based MPPT.

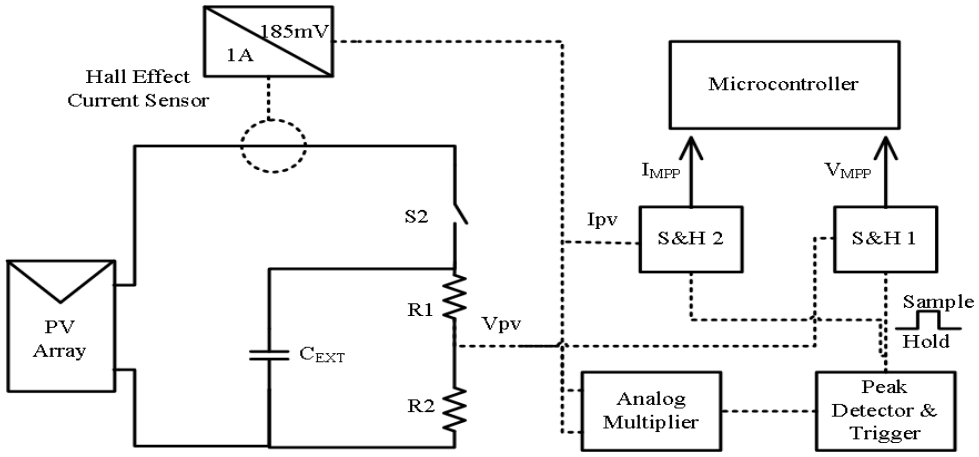

Fig. 8.2 Detailed diagram of the scanning circuit.

8.3 Rating of the External Capacitor and the Choice of DC-DC Converter Topology for the Proposed Scheme

In this section we derive an equation which relates the rating of the external capacitor to the time required for the external capacitor that is used for drawing the characteristic curve of a PV generator. For this purpose, we make a piecewise approximation of the *I-V* curve of a PV generator. By adopting a piecewise approximation of the *I–V* curve, the diode behaves like an open circuit in Fig. 8.3, when the operating points are in current source region of the characteristic curve of the generator to the maximum power point. Thus, the PV generator can be considered a current source from short circuit to near the MPP, neglecting also the current leakage in the parallel resistance. Moreover, from maximum power to open circuit conditions, the diode behavior together with the series resistance *Rs* is like a Thévenin equivalent. In this new simple model, the capacitance *C* is the only load connected to the generator, whereas the internal resistance R_C of the capacitor is assumed infinite.

(a) Transient Charging at Constant Current

An ideal current source supplies a resistance in series with a capacitor after the closing of the power breaker B in Fig. 8.3. The current is supplied by the parallel connection of N_P strings, as shown in Fig. 8.4 (a): every string gives $I_{ph} \approx I_{SC}$, which is the short circuit current of the N_C cells connected in series in each of the modules inside the string.

$$i(t) = I_{SC}N_P \qquad \text{for } 0 < t < t_0 \tag{8.1}$$

At the beginning of the transient, the capacitor acts like a short circuit with zero volts. The voltage across the capacitor increases until the end of this part of the transient. The signal *v(t)* is inversely proportional to the capacitance connected to the PV generator and directly proportional to solar irradiance falling on the generator i.e.

$$v(t) = \frac{1}{C}\int_0^{t_0} I_{SC}N_P dt = \frac{I_{SC}N_P}{C}t \quad \text{for } 0 < t < t_0 \tag{8.2}$$

This transient finishes at t_0, when the capacitor is charged to V_0: the definition of the pair (t_0, V_0) is given in the subsection that follows.

(b) Charging of the Capacitor in the Voltage Source Region

The second part of the capacitor charging commences at time t_0. In this part of the capacitor charging an ideal voltage source is supplying charge to the circuit comprising the Equivalent Resistance of the PV source and the external capacitor. The equivalent circuit in this portion of the transient is shown in Fig. 8.4 (b).

The behavior of the circuit is described by a first order differential equation, in which the unknown quantity is the capacitor voltage $v(t)$:

$$\frac{dv(t)}{dt} + \frac{v(t)}{R_{EQ}C} = \frac{N_S V_{OC}}{R_{EQ}C} \tag{8.3}$$

It should be remembered that the voltage signal must be continuous at time $t = t_0$, so the initial voltage $v(t = t_0)$ is the same voltage measured at the end of the previous part of the transient.

$$v(t = t_0) = V_0 = \frac{I_{SC}N_P t_0}{C} \tag{8.4}$$

Therefore, the evolution of the voltage across the capacitor is defined by the following equation, which is the solution of the differential Eq. (8.3), according to the boundary condition described by Eq. (8.4):

$$v(t) = V_{OC}N_S + \left(\frac{I_{SC}N_P t_0}{C} - V_{OC}N_S\right) exp\left(\frac{-(t-t_0)}{R_{EQ}C}\right) \quad \text{for } t_0 < t < \infty \tag{8.5}$$

The evolution of the current through the capacitor is:

$$i(t) = C\frac{dv(t)}{dt} = \left(\frac{N_S V_{OC}}{R_{EQ}} - \frac{N_P I_{SC} t_0}{R_{EQ}C}\right) \exp\left(\frac{-(t-t_0)}{R_{EQ}C}\right) \quad \text{for } t_0 < t < \infty \tag{8.6}$$

As is the case with voltage, the current must also be continuous at $t = t_0$

$$i(t = t_0) = N_P I_{SC} \tag{8.7}$$

The expression that links the capacitance value C with the switching time t_0, i.e., the time which defines the boundary between the two different transients, is given as:

$$C = \frac{N_P I_{SC}}{N_S V_{OC} - R_{EQ} N_P I_{SC}}\, t_0 \tag{8.8}$$

The final time t_f, which is the time taken after the closing of the switch till the moment the capacitor is fully charged, is the sum of the duration of the two transients. After the time t_0, the PV generator is assumed as a real voltage source and the behavior of the circuit is defined by a differential equation of the first order with a time constant $\tau = R_{EQ}C$. Thus, the final time t_f is given as:

$$t_f = t_0 + R_{EQ} C \tag{8.9}$$

Fig. 8.5 shows the actual and estimated waveforms of current and voltage during the charging of a capacitor by a commercial PV module. The signals are different, especially in the vicinity of the MPP. This difference is a result of the simplified model adopted here. The exponential voltage signal, in the second part of the capacitor charging, appears constant since the starting voltage is near the final voltage.

Combining Eq. (8.8) and (8.9) we obtain an equation which relates the size of the capacitor to the total time taken in full charging of the capacitor, i.e.

$$C = \frac{t_f I_{SC} N_P}{N_S V_{OC} + 4 R_{EQ} N_P I_{SC}} \tag{8.10}$$

In the above expression, the values of I_{SC} and V_{OC} for the STC can be found from the manufacturer's datasheet, N_S and N_P for a PV generator are also known. The only parameter is the value of R_{EQ}. Following the analysis in [42], it can be shown that:

$$R_{EQ} = \frac{V_{OC}-V_{MPP}}{I_{SC}} \frac{N_S}{N_P} \tag{8.11}$$

Substituting Eq. (8.11) into (8.10) we get an expression that relates the size of the external capacitor to the time t_f:

$$C = \frac{t_f I_{SC} N_P}{N_S V_{OC} + 4 \frac{V_{OC}-V_{MPP}}{I_{SC}} \frac{N_S}{N_P} N_P I_{SC}} \tag{8.12}$$

The value of V_{MPP} for crystalline silicon PV modules is about 80% of the V_{OC}. Thus, putting this value in Eq. (8.11) we get a simple relation for R_{EQ}, i.e.

$$R_{EQ} \approx \frac{V_{OC}-0.8V_{OC}}{I_{SC}} \frac{N_S}{N_P} = 0.2 \frac{N_S V_{OC}}{N_P I_{SC}} \tag{8.13}$$

Substituting Eq. (8.13) into (8.12), we obtain the simplified expression that relates the capacitance of the external capacitor to t_f:

$$C = A t_f \frac{N_P I_{SC}}{N_S V_{OC}} = 0.55\, t_f \frac{N_P I_{SC}}{N_S V_{OC}} \tag{8.14}$$

It is well known that the I_{SC} of an array is dependent on the irradiance and varies considerably. In deciding about the value of C, it should be chosen for lower values of irradiance, typically for about 200W/m^2 [53]. Similarly, the value of t_f should be taken to be less than the sampling period of the MPPT controller. For example, if the sampling period of the controller is 10 ms, then t_f should be taken to about 7 ms under 200 W/m^2. However, when there is full irradiance, the value of I_{SC} increases many times and that of t_f falls down. In this case, the circuit should be able to perform fast enough measurements. This issue will be discussed in detail later.

The three basic converter topologies of DC-DC converter are: Buck converter, Boost converter and Buck-Boost converter. Of the three types, the structure of the Buck and Buck-Boost converters allows the designers to use high value capacitor for filtering the input current. The reason for using high value capacitor is because of the pulsed nature of the input current. The ratings of components required for Buck and Boost converters for MPPT applications have been compared in [54] for the same voltage/current rating and switching frequency of the converter. It has

been shown that the value of the input capacitor for the step-down converter is ten times higher than that of the step-up converter. Therefore, owing to the higher capacitance of the input filter capacitor it can be utilized for tracing the *I-V* curve as well as MPP tracking under any kind of shading conditions.

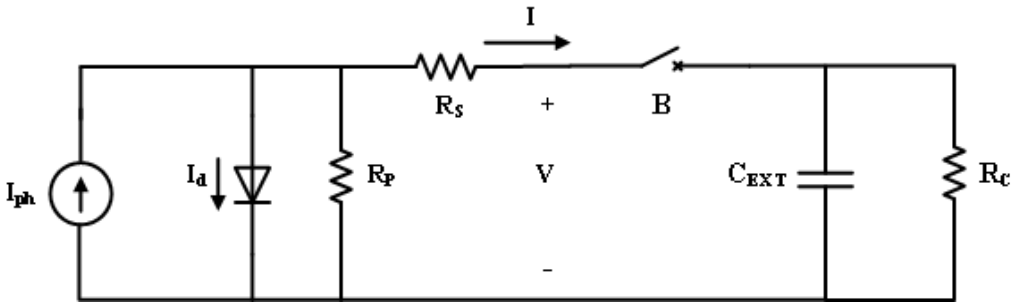

Fig. 8.3 Equivalent circuit of a PV generator supplying power to an external capacitor through a breaker.

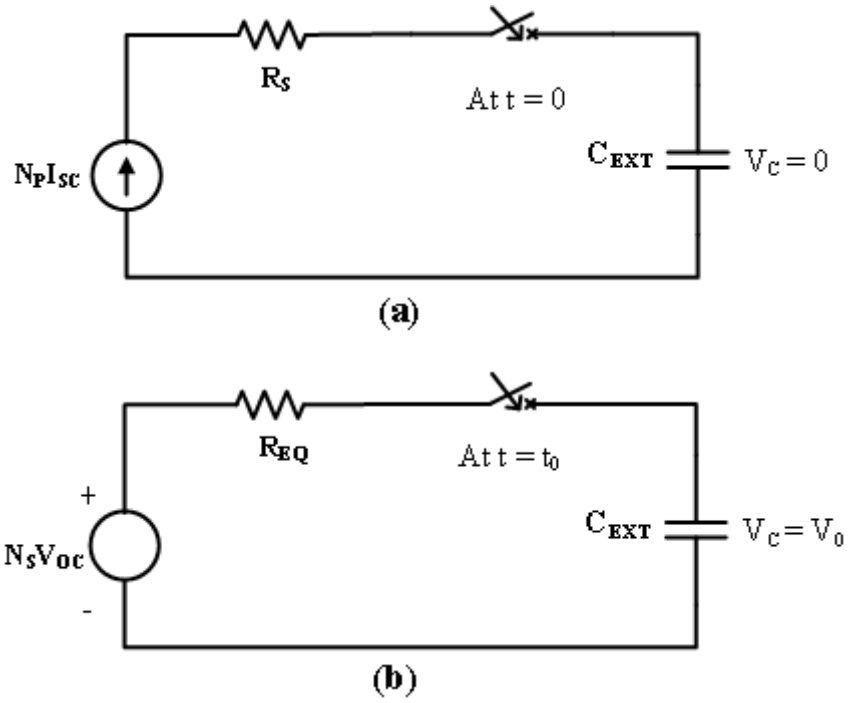

Fig. 8.4 Equivalent circuit of the capacitor connected to the PV. (a) Equivalent circuit for the current source region. (b) Equivalent circuit for voltage source region.

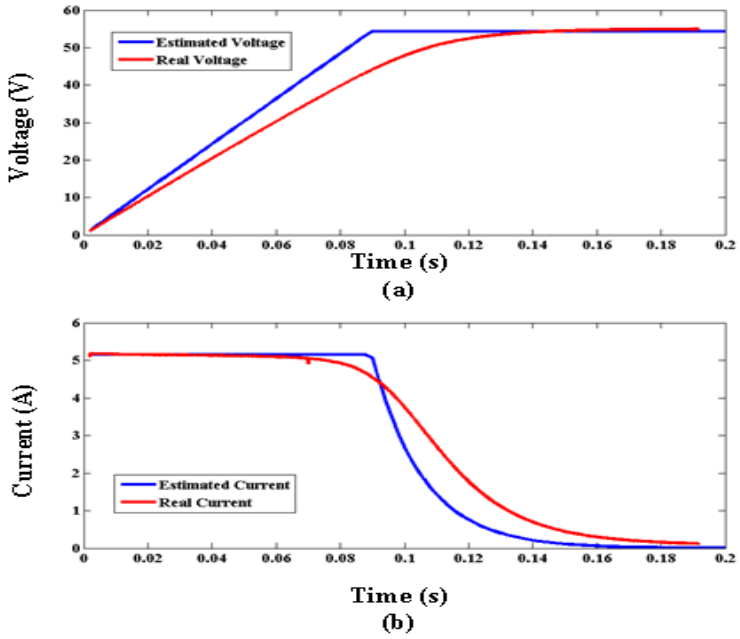

Fig. 8.5 Difference between the estimated and the real voltage and current signal during the capacitor charging for a polycrystalline silicon.

8.4 Proposed MPPT

The operation of the proposed scheme can be classified into two modes:

1. The curve tracing mode
2. The steady-state mode

It is during the curve tracing mode that the characteristic curve of the array is traced and its GP is found. This mode is invoked either at the beginning of the main program or when a sudden change in the output power of the PV array occurs. In this scenario, the array is first operated at a low voltage, i.e. close to the I_{SC}. This voltage should be lower than half of the rated voltage of a single series connected module. At lower voltage than this value no peak occurs in the characteristic curve of the array under any shading condition. Then, the duty cycle of DC-DC (Buck or Buck-Boost) converter is set to zero. When the main switch of the converter is in off-state, the load 'seen' by the array is the input filter capacitor holding a low voltage. In this way the array starts to charge the filter capacitor. During the charging of the capacitor its voltage, current, and power are constantly monitored. When the product of voltage and current is at its maximum,

the corresponding values of current and voltage are stored by the algorithm as I_{MPP} and V_{MPP} respectively. After the completion of this process, the algorithm then computes the duty cycle D_{MPP} for the operation of the array at the GP. Once the MPPT converges to the GP, the steady-state mode begins.

As discussed in the previous section, the time required for the input filter capacitor varies considerably depending upon the irradiance. In the design Eq. (8.14) the value of C is chosen for lower irradiance value. However, under full irradiance the circuit will have to perform fast measurement for obtaining accurate values of the array voltage and current. Thus, under full irradiance the measurement speed of the circuit become important. In order to deal with these design constraints, two possible solutions are presented here. The choice of either of these options depends upon the data conversion speed of the Analog to Digital Converter's (ADC) of the main microcontroller/DSP used in the hardware.

a. For microcontrollers with ADC conversion time >20μs

Some microcontrollers like those of PIC 18F family have low speed ADCs. The minimum time required for a single analog to digital conversion for this family of microcontrollers is about 34μs [55]. During the charging of the filter capacitor these microcontrollers cannot perform fast measurements and, hence, cannot acquire accurate values of I_{MPP} and V_{MPP}. To overcome this limitation of these controllers a scanning circuit is used for performing fast measurements [53].

In Fig. 8.6 is shown the whole circuit in details. It is important to note that the scanning circuit is identical to the one shown in section 8.2. The only difference is that in the new scheme the switch which was previously used for disconnecting the array from the load is eliminated. This reduces the complexity of the circuit and eliminates the conduction losses of the switch. When the PV system is operating in the steady-state around the GP, the scanning circuit is not in active mode and the microcontroller operates the PV system around its MPP using conventional P&O algorithm. When a sudden change in the irradiance occurs, this change is accompanied by reduction in the power from the PV array. As a result, the main MPPT program calls for the curve tracing subroutine. Before the subroutine the array is operated at a low voltage so as to allow the filter capacitor to discharge to a low value. During the curve tracing subroutine, the scanning circuit comes into active mode. The duty cycle of the converter is then set to zero and in this way, the PV array is isolated from the load and the array is allowed to

charge C_{in}. As discussed in the previous section, this momentary isolation does not affect the power supply to the load or grid if the PV system has battery backup or HESS. The operation of the scanning circuit has already been discussed in section 8.1. An advantage of the arrangement shown in Fig. 8.3 is that it can perform very fast measurements.

It is important to mention that, if the microcontroller can perform analog to digital conversion in 10µs–20µs, then the peak detector and trigger function can be performed by the controller and thus, the need for discrete peak detector and trigger blocks can be obviated.

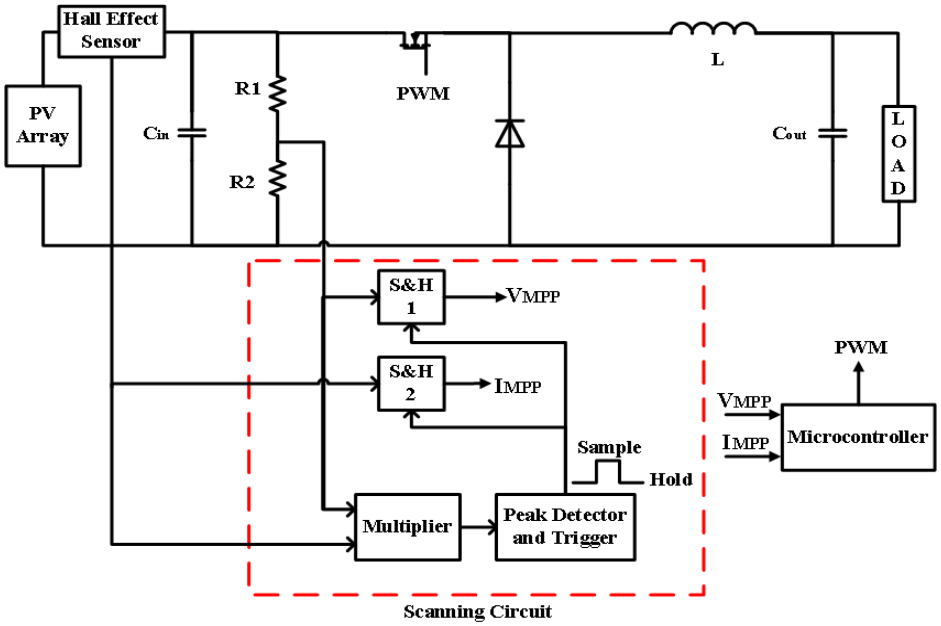

Fig. 8.6 Circuit diagram of the proposed algorithm employing the scanning circuit.

b. DSPs with ADC conversion time less than 10µs

If the controller used in the PV system has high speed ADC, the need for the scanning circuit shown in Fig. 8.6 is avoided. In this case, the entire scanning and measurement process is performed by the controller. The flowchart for this arrangement is shown in Fig. 8.7. Before the commencement of the subroutine, the filter capacitor is discharged to a low voltage. After that, the duty cycle of the DC-DC converter is set to zero for one sampling period. Afterwards, the array starts to charge the capacitor. In block 2, the values of I_{MPP} and V_{MPP} are

initialized to zero. Then, the voltage and current across the capacitor are sensed and are allocated to variables V_{PV} and I_{PV}, respectively. In block 4, the products $V_{PV} \times I_{PV}$ and $V_{MPP} \times I_{MPP}$ are compared. If the former quantity is more than the latter, the values of V_{PV} and I_{PV} are assigned to V_{MPP} and I_{MPP}, respectively. Then, in block 6, the current through C_{in} is sensed and if its value is greater than a predetermined threshold the program goes back to block 5 for the next iteration. If the current through C_{in} falls below a certain threshold value (for example, 0.1A), the program is stopped and the values of I_{MPP} and V_{MPP} are returned. In the same time the *I-V* curve of the array is also traced which can be used for getting any diagnostic information.

The main program for the MPPT is shown in Fig 8.8. As shown in this figure, the array is operated at low voltage. This operation allows the filter capacitor of the converter to discharge to low voltage value. As mentioned before, this voltage value should be set below 50% of the rated voltage of a single module. In block 3, R_o is calculated and then the system performs the curve tracing either through the scanning circuit or through program shown in Fig. 8.7. After the completion of the process, the value of the duty cycle of the converter is calculated using Eq. (7.6). In block 6, the PV system is operated at the MPP and after ensuring that the peak has been tracked the steady-state operation begins in block 7.

In the steady-state operation conventional P&O algorithm is invoked for performing fine tuning and changing the operating point of the system in case of small variations in the ambient conditions. The value of the perturbation step for the P&O algorithm is set to small value for reducing the oscillations around the GP. A timer overflow interrupt may also be used to invoke the GP tracking process periodically to perform the new tracking of GP.

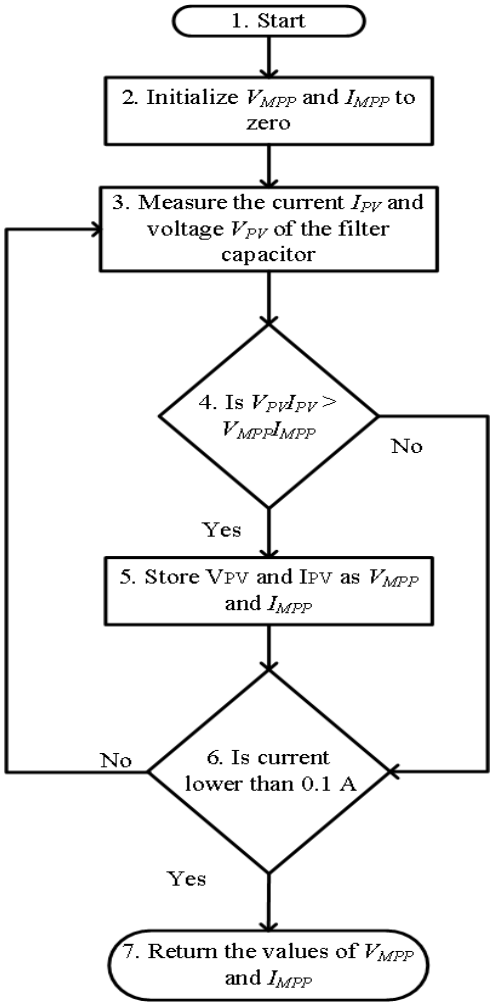

Fig. 8.7 Flowchart of the subroutine used to find MPP and the I-V curve using microcontroller/DSP with high speed ADC.

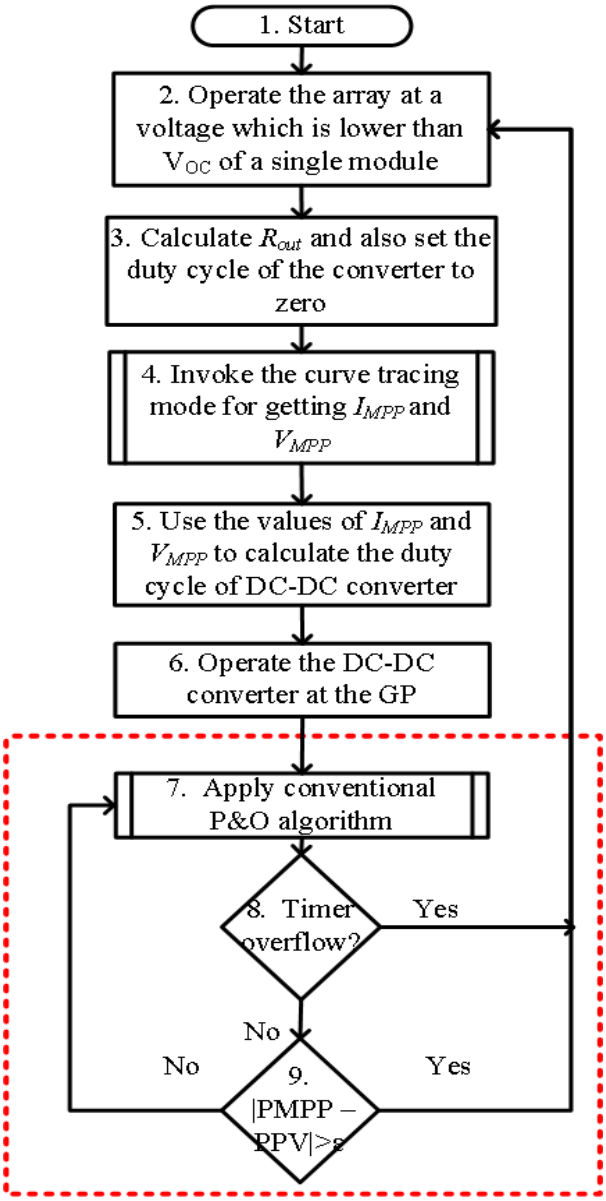

Fig. 8.8 Flow chart of the main program.

8.5 Simulation Results

For checking the performance of the proposed algorithm, simulations have been conducted in MATLAB/SIMULINK. The PV string has six series connected modules as given in Fig. 8.9. However, the number of series connected cells in each of the modules in the present situation is 20 and has rated V_{OC} and I_{SC} 12.2V

and 8.2A respectively. The voltage V_{OC} of the entire string is 73.2V under nominal conditions. DC-DC buck converter used in the simulations has switching frequency of 50 kHz. Sampling period of the MPPT controller is 10ms. The value of C_{in} of the converter is 150µF. Using Eq. (8.14), for low irradiance of 300W/m^2 the value of t_c for this value of the filter capacitor is about 7.3ms, which is lower than the sampling period of the MPPT controller. Under full irradiance t_f decreases to about 2.67ms which is long enough time to obtain adequately accurate values of V_{MPP} and I_{MPP}. Simulations were performed for the PV generator with irradiance pattern given in Fig. 8.9. In Fig. 8.10 is given the GP tracking process of the array with irradiance pattern shown in Fig. 8.9 (a). Before the beginning of the tracking process at t = 0.01s, the converter is operated at low voltage for discharging C_{in}. At t = 0.01s the duty cycle of the converter is set to zero and the capacitor is allowed to charge to the V_{OC} of the array. The algorithm shown in Fig. 8.4 is used for measurements of the voltage and current during the charging of the capacitor. Fig. 8.7 (a), (b), and (c) show the power, voltage and current during the GP tracking as a function of time respectively. Fig. 8.7 (b) and (c) also display V_{MPP} and I_{MPP}. As can be seen, the MPPT process first records the value of current and voltage corresponding to P1 as I_{MPP} and V_{MPP}. However, when peak P2 is met, its value is found to be greater than P1, the algorithm then stores the value of current and voltage at P2 as I_{MPP} and V_{MPP}. The peak P3 has lower value than P2 so this peak is ignored and the program returns the values of current and voltage corresponding to P2. Similarly, Fig. 8.11 shows the GP tracking process for the string with the irradiance pattern shown in Fig. 8.9 (b). The performance of the proposed scheme in tracking the single peak under uniform irradiance is given in Fig. 8.12.

The response of the MPPT to a step variation is revealed in Fig. 8.13. Fig. 8.13 (a), (b), (c), and (d) show the PV power, voltage, current and duty cycle of the DC-DC converter, respectively. Before t = 0.085s all the modules in the PV array are receiving 1000W/m^2 and the system is already operating around the GP with typical P&O algorithm. At t = 0.085s a step change in illumination takes place and now the modules M1, M2, and M3 get 300W/m^2; while M4, M5 and M6 take 1000W/m^2. This shading condition is similar to the one shown in Fig. 8.9 (b). In response to the variation, the decrease in power is sensed during the sampling interval at t = 0.09s. As discussed previously, the system is operated at low voltage in order to release the charge of the filter capacitor. This is executed from t = 0.09s to t = 0.10s. At t = 0.10s the duty cycle of the converter is set to zero. Now the only load seen by the PV generator is the input filter capacitor which has been discharged to a low voltage; and the capacitor is allowed to charge. During

the charging, the values of I_{MPP} and V_{MPP} are obtained in a manner discussed in the previous paragraph. At t = 0.11, the duty cycle of the converter is set to D_{MPP} attained from (7.6). From this time on, the steady state operation begins. This whole process of discovery of the GP requires only two sampling periods which is about 20ms.

The performance of the proposed MPPT was compared to the technique reported in [30] under identical conditions of irradiance. The tracking time of this technique is almost identical to [26], and [28]. Simulations were conducted for the array shown in Fig. 8.9 (b). As shown in Fig. 8.14, the time required for the technique in [23] is about 1.1s. This Fig. also shows that the steady-state operation begins at t = 1.1s. The steady state operation is based on conventional P&O algorithm.

The MPP tracking process which involves scanning the entire characteristic curve is shown in Fig. 8.15. The array is scanned from I_{SC} to V_{OC} and can be noticed that the process takes about 2s.

The difference in tracking time leads to the difference in loss of power during the MPP tracking. For comparing the power loss of the three methods discussed above the concept of normalized power loss is used. The normalized power loss is defined as:

$$P_{LOSS} = \frac{(\sum_{i=0}^{k} P_{max} - \sum_{i=0}^{k} P_{alg})}{\sum_{i=0}^{k} P_{max}} \times 100 \tag{8.15}$$

where P_{max} is the maximum available power from the array under given conditions, P_{alg} is the power extracted by a particular algorithm, and k is the number of iterations [17].

The power loss was calculated between two intervals, from the moment the GP tracking process started to the time when the slowest algorithm reached the steady state [25]. In this way the power loss in the interval when the GP tracking process started till t = 2s was calculated. These calculations revealed that the power loss due the proposed technique was only 2.36%. On the other hand, the power loss of the MPPT in [30] is 21.78% and the method which involves the scanning of the whole curve had a loss of 51.87%.

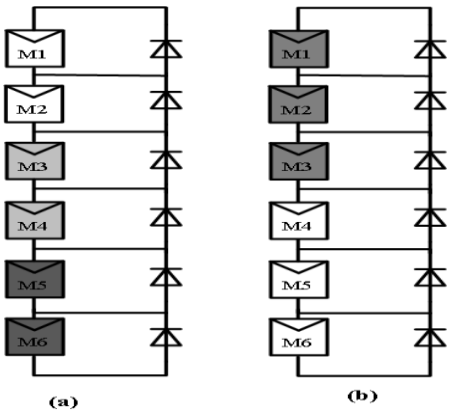

Fig. 8.9 PV array under different shading conditions. (a) Module M1 and M2 receive 1000 W/m^2, M3 and M4 receive 600 W/m^2, M5 and M6 receive 300 W/m^2. (b) M1, M2, and M3 have 300 W/m^2 irradiance; M4, M5, and M6 has 1000 W/m^2 irradiance.

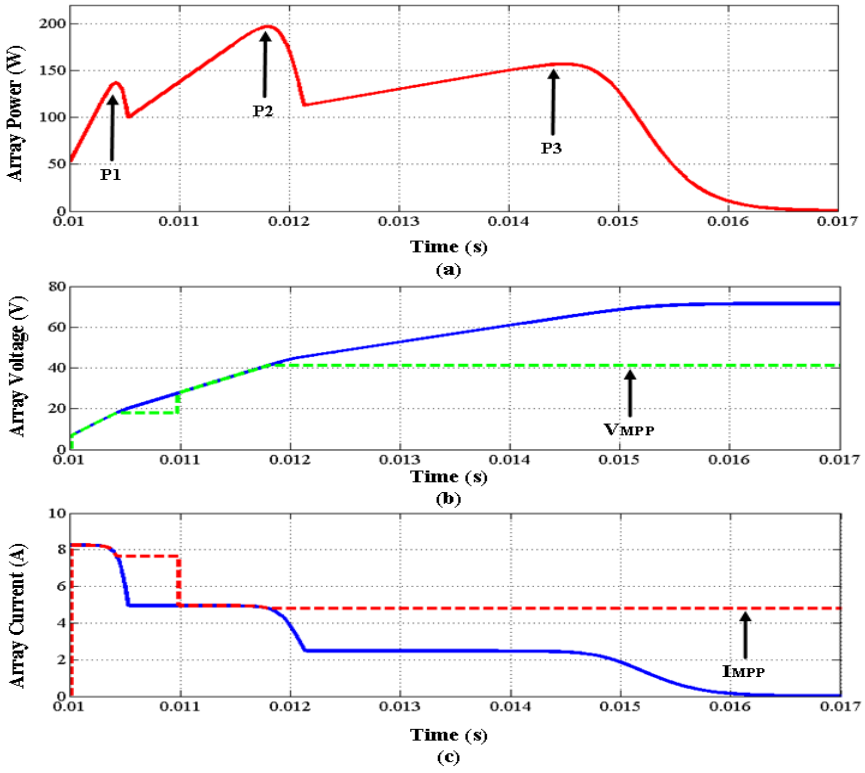

Fig. 8.10 MPP tracking and *I-V* curve tracing process of the array with irradiance pattern in Fig. 8.6 (a).

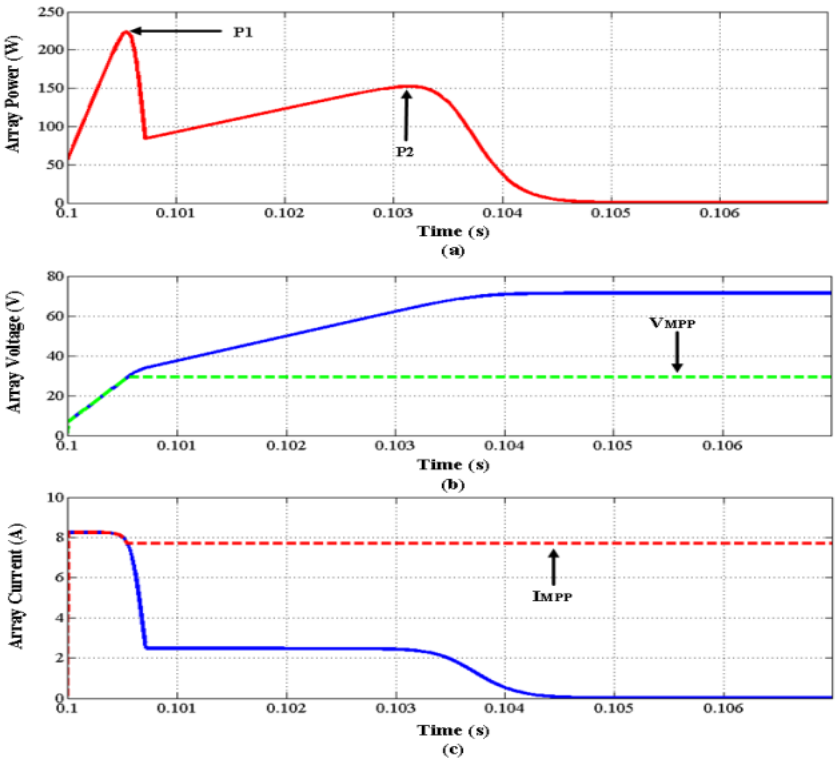

Fig. 8.11 MPP tracking and *I-V* curve tracing process of the array with irradiance pattern in Fig. 8.6 (b).

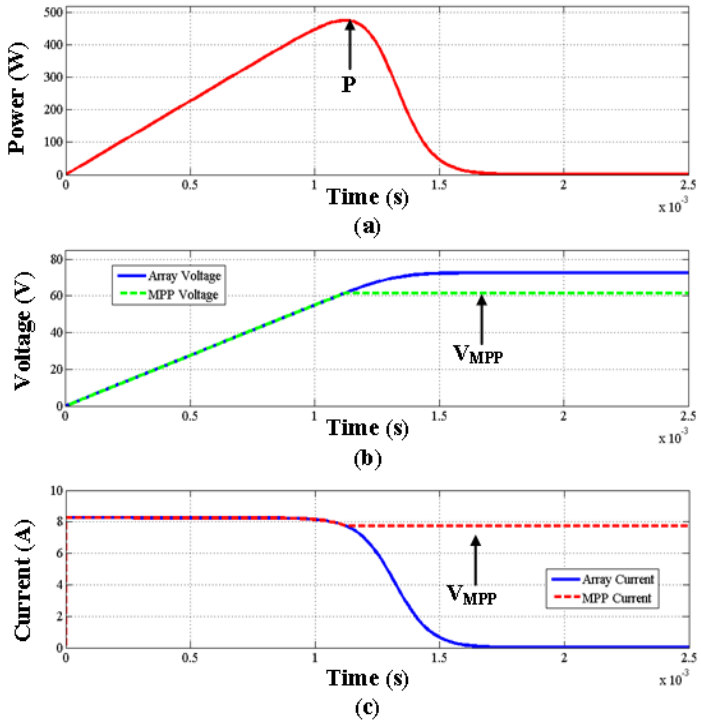

Fig. 8.12 MPP tracking during uniform irradiance.

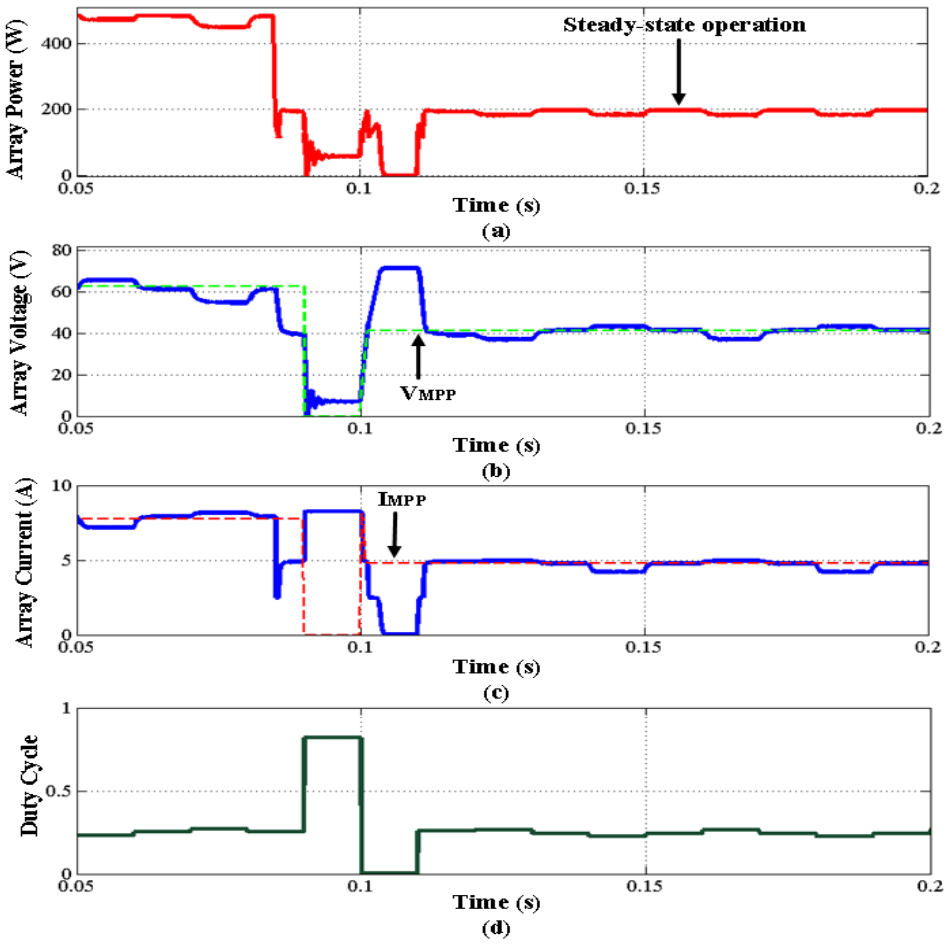

Fig. 8.13 Response of the proposed algorithm to step variation in irradiance.

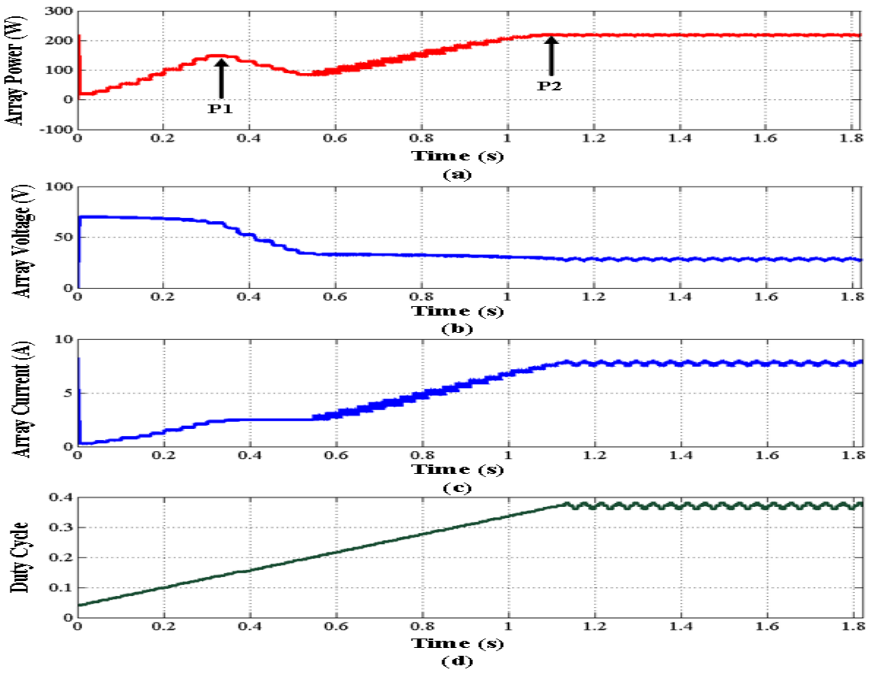

Fig. 8.14 MPP tracking process of the method proposed in [30].

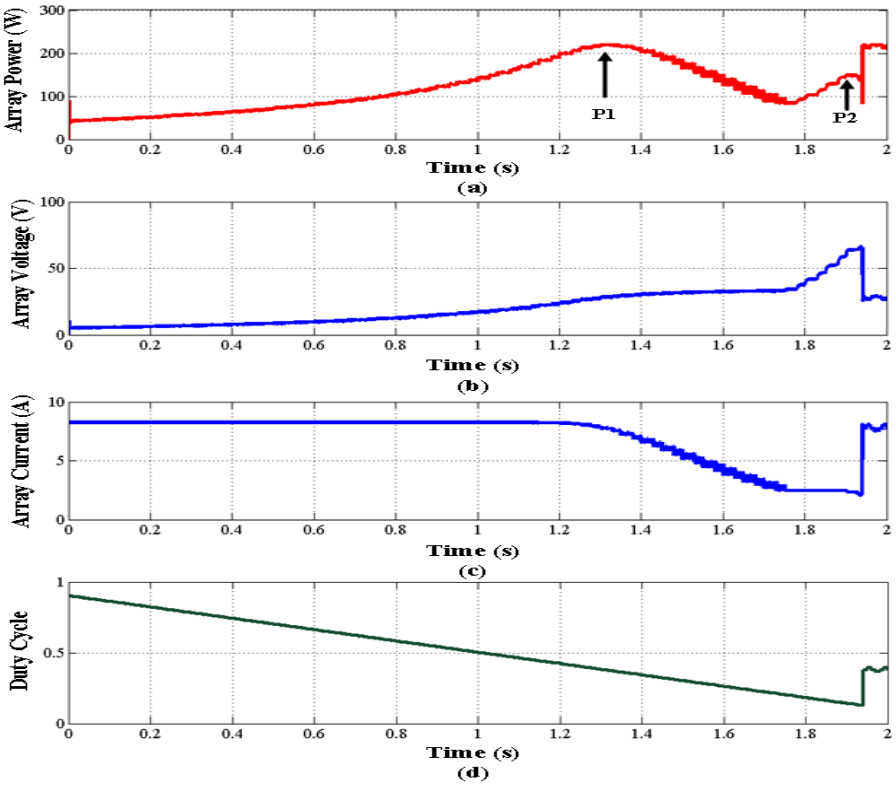

Fig. 8.15 MPP tracking process which involves scanning of the entire curve.

8.6 Experimental Results

For checking the performance of the proposed algorithm, experiments were conducted. The experimental set up is the same as given in the Chapter 7 with the exception that only the array voltage was measured instead of measuring the voltage across all the modules. As mentioned previously, when the duty cycle of DC-DC buck or buck boost converter is set to zero, the load seen by the PV source is C_{in}. For simplicity, only the capacitor is shown in Fig. 8.16.

Depending upon the switching frequency of DC-DC converter, the permissible input ripple voltage, and output current etc., the capacitance of the input filter capacitor of a buck or buck-boost converter may vary from a few tens to a few hundred microfarads. Further details for calculating the correct value of the capacitor can be found in [56]. For the experiments in this paper we have used the rating of the C_{in} = 100 μF. Due to the high conversion speed of the data acquisition device, the algorithm with flow chart shown in Fig. 8.4 is used for GP tracking.

Experiments were conducted under the following two irradiance patterns:

1. When the PV array is under lighter shading caused by a distant object. This scenario has been shown in Fig. 2.11 with the experimental *P-V* curve in Fig. 2.12.
2. When the array is under severe shading which is caused by an object near to the surface of the PV source. This has been shown in Fig. 2.13 and the experimentally determined *P-V* curve is shown in Fig. 2.14.

The GP tracking process of the first case is shown in Fig. 8.17. Fig. 8.17(a), (b), and (c) show the variation of power, voltage and current during the charging evolution of the capacitor. At the beginning of the tracking process, C_{in} had been discharged to about 5V. During the charging of the capacitor, the algorithm first encountered the peak P1 (which was a LP) and stored the values of current and voltage corresponding to that peak. However, as the capacitor was being charged, the algorithm found the value of power at P2 to be higher than P1. Therefore, the MPPT scheme stored the value of current and voltage corresponding to P2 as I_{MPP} and V_{MPP}, respectively. Similarly, Fig. 8.18 shows the GP tracking process when partial shading was caused by an object which was close to the surface of the PV source. As shown in this figure, during the charging of C_{in} the algorithm finds P1

first and stores the corresponding current and voltage. As P2 has lower value than P1, so it was ignored.

The experimental results reveal that the proposed MPPT is able to track the GP of a partially shaded PV array under any irradiance conditions. The results also reveal that, during the GP tracking process, the *I-V* curve of the array is also obtained under real-time conditions with negligible effect on the generation of power from the PV system. On the other hand, other methods that are used for obtaining the characteristics curve of the array are time consuming as well as dissipative.

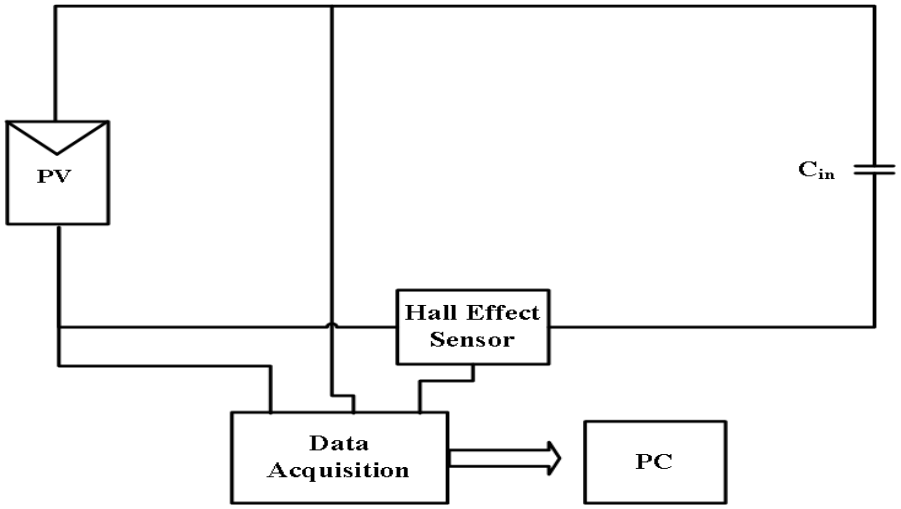

Fig. 8.16 Simplified diagram of the experimental setup.

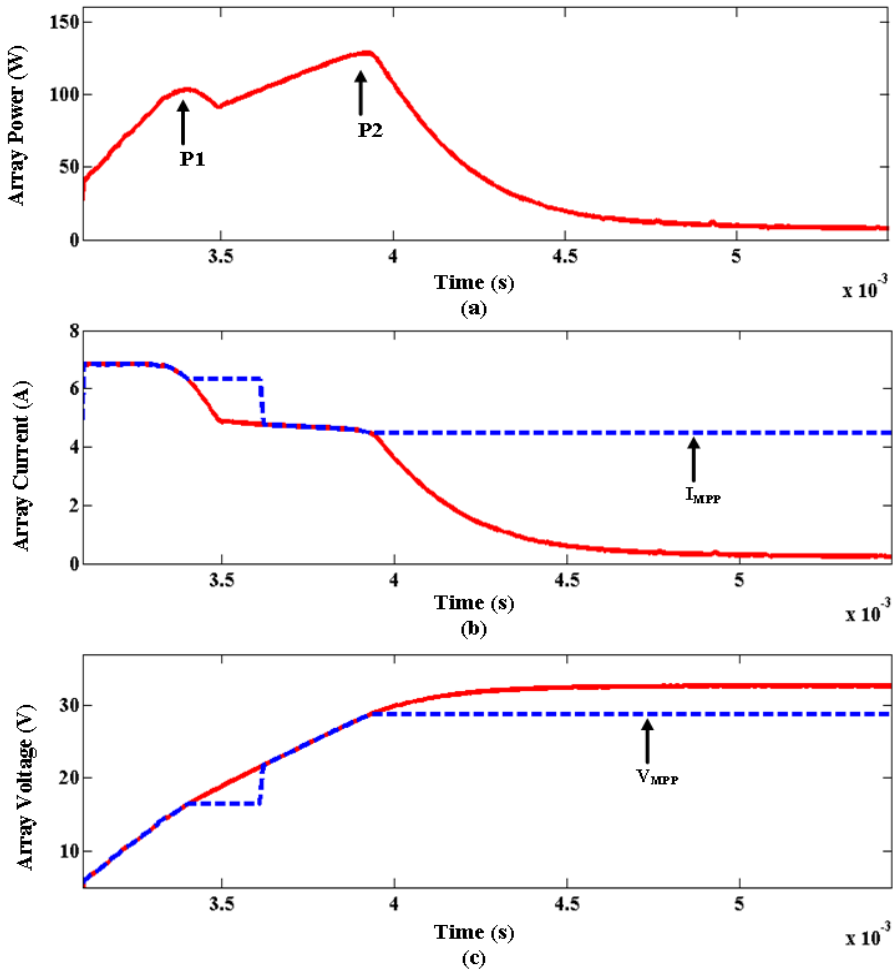

Fig. 8.17 Variation of array power, current, and voltage as a function of time during the charging of Cin in case of the shading pattern shown in Fig. 2.11.

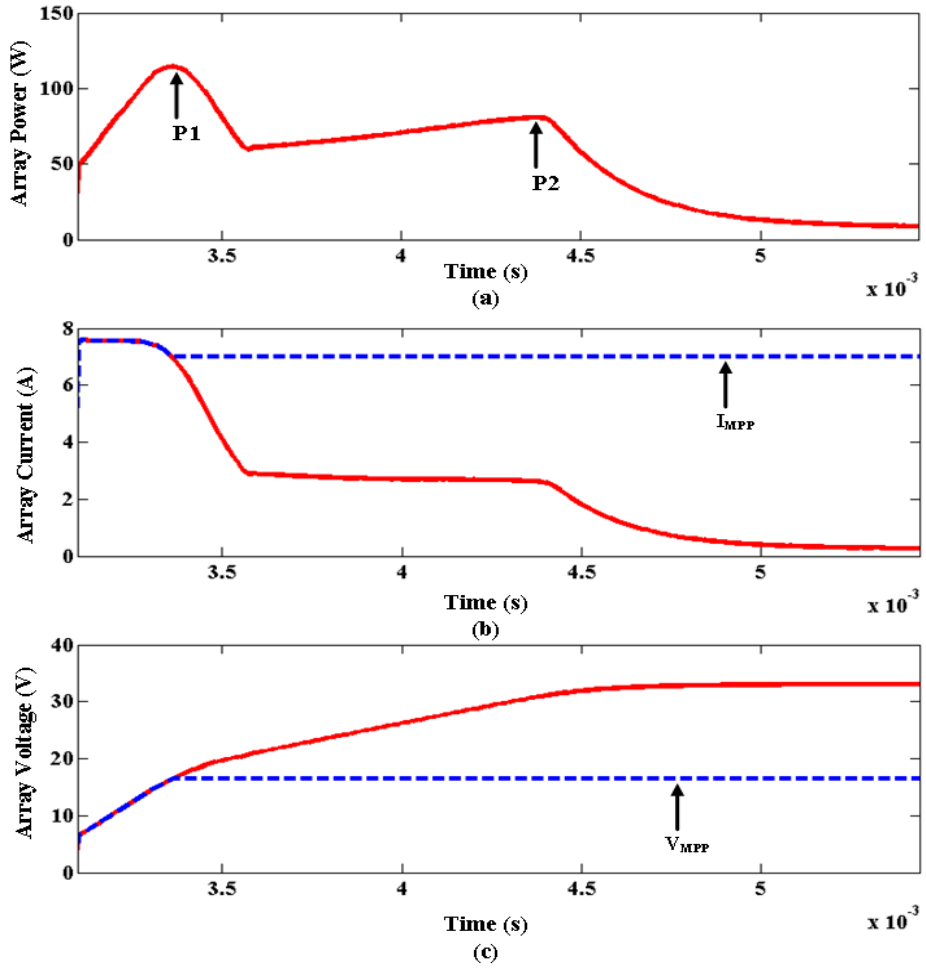

Fig. 8.18 Variation of array power, current, and voltage as a function of time during the charging of Cin in case of the shading pattern shown in Fig. 2.13.

In this chapter, a scheme for finding the *I-V* curve and the MPP under any shading conditions is presented. The equation which relates the capacitance of the capacitor which is used for obtaining the characteristic curve of the array is derived. The procedure proposed in this chapter makes use of the input filter capacitor of buck or buck-boost converter for performing these tasks. The performance of the algorithm is checked through simulation and experimental results. Simulation results confirming the performance of the presented scheme under different kinds of partial shading and uniform irradiance conditions have been presented. The method has also been compared to some of those which have been reported in the literature. From the results we can conclude that the presented

scheme performs the scanning of the whole curve and finding the MPP under any kind of shading conditions much faster than other methods.

Conclusion

In the past decade or so, we have seen an exponential increase in the installed capacity of the PV generating plants globally. This increase is attributed to many factors like: awareness about the emission of pollutant to the atmosphere, the decreasing cost of PV generators and other components involved in the conversion process, and provision of incentives by various governments for installation of PV plants. Notwithstanding the increase in the installed capacity, the main challenges in the full utilization of the solar energy are:

- Low conversion efficiency of PV cells.
- Nonlinear *I-V* characteristic of PV modules.
- MPP tracking during the partial shading conditions.
- During the operation under the field conditions, the PV generators are subject to severe thermomechanical stresses. These stresses make the solar modules prone to various defects.
- Online detection of PV faults.

MPPTs are used for optimal extraction of power from the solar arrays. Various conventional MPPT schemes operate efficiently under uniform irradiance conditions. However, when the array is partially shaded, multiple peaks appear in its *P-V* characteristics. Tracking of the global peak in the presence of multiple peaks is quite challenging. If a conventional MPPT algorithm converges to a local peak instead of global, there is a considerable power loss. The ability of MPPTs to track the global peak under partially shaded conditions is essential to avoid the power loss. One of the important attributes of MPPT algorithms is the speed of convergence to the global peak. Decreasing the convergence speed of MPPT algorithm is one of the issues that have been addressed in this thesis.

For controlling and monitoring purposes the I-V curve of the PV plants is acquired frequently. An abnormal electrical curve can also indicate the presence of a defect in the PV array. Many methods have been reported in the literature, which are used for finding the electrical curve of PV panels. One of the shortcomings of these mechanisms is that the normal operation of the plant is interrupted during the measurement of the curve. In this way, these tests cannot be performed too frequently because of the loss of power that is involved.

In this text a scheme has been proposed which finds the electrical characteristic curve of the module from online measurements. These measurements are performed during the MPP tracking. Therefore, the methods presented in this text perform the dual task of MPP tracking and finding the electrical curve of the PV generators in a single algorithm. The proposed schemes have been confirmed through experimental and simulation results.

References

1. Ibrahim Dincer, "Renewable energy and sustainable development: a crucial review" *Renewable and Sustainable Energy Reviews 4 (2000) pp. 157-175*.
2. Anon. Our common future. *Oxford University Press, Oxford: World Commission on Environment and Development, 1987.*
3. Renewables 2016 Global Status Report, Renewable Energy Policy Network for the 21st Century. Available online at: http://www.ren21.net/wp-content/uploads/2016/10/REN21_GSR2016_FullReport_en_11.pdf
4. G. Petrone, G. Spagnuolo, R. Teodorescu, M. Vitelli, "Reliability issues in photovoltaic power processing systems" *IEEE Trans. Industrial Electron., Vol. 55, No. 7, pp. 2569-2580, July 2008.*
5. N. G. Dhere, "Reliability of PV modules and balance of system components," in *Proc. 31st IEEE Photovolt. Spec. Conf., pp. 1570-76. Jan 2005.*
6. John A. Tsanakas, Long Ha, Claudia Buerhop, "Faults and infrared thermographic diagnosis in operating c-Si photovoltaic modules: A review of research and future challenges," *Renewable and Sustainable Energy Reviews 62, pp. 695-709, 2016.*
7. A. Burgio, D. Menniti, C. Picardi, and A. Pennarelli, "A novel integrated configuration of grid-connected photovoltaic plant with UPS: Reliability estimation," in *Proc. Int. Conf. Clean Electr. Power, pp. 142-147, May 2007.*
8. G. O. Anderson, "The role, reliability, and limitations of solar photovoltaic systems in Botswana," in *Proc. 9th Int. Conf. Harmonics Qual. Power, pp. 973-982, Oct 2000.*
9. A. B. Maish, C. Atcitty, S. Hester, D. Greenberg, D. Osborn, and D. Collier, "Photovoltaic system reliability," in *Proc. 26th IEEE Photovolt. Spec. Conf., pp. 1049-1054, 1997.*

10. W. Bower, "Inverters ─ critical photovoltaic balance of system components: status, issues, and new-millennium opportunities," *Prog. Phtovolt. Res. Appl., vol. 8, no. 1, pp. 113-126, 2000.*
11. W. Bower, R. West, and A. Dickerson, "Innovative PV micro-inverter topology eliminates electrolytic capacitors for longer lifetime," in *Proc. IEEE 4th World Conf. Photovolt. Energy Convers., vol. 2, pp. 2038-2041, May 2006.*
12. T. Shimizu, K. Wada, and N. Nakamura, "A fly-back type single phase utility interactive inverter with low frequency ripple current reduction on the DC input for an AC photovoltaic module system," in *Proc. IEEE 33rd Annu. Power Electron. Spec. Conf., vol. 3, pp. 1483-1488, Jun 2002.*
13. F. Chan, H. Calleja, and E. Martinez, "Grid connected PV systems: A reliability-based comparison," in *Proc. IEEE Int. Symp. Ind. Electron., pp. 1583-1588. Jul 2006.*
14. J. Prashant Ram, N. Rajeskar, Masfumi Miyatake, "Design and overview of maximum power point tracking techniques in wind and solar photovoltaic systems" *Renewable and Sustainable Energy Reviews 70, pp. 1138-1159, 2017.*
15. T. Esram and P. L. Chapman, "Comparison of photovoltaic array maximum power point tracking techniques," *IEEE Trans. Energy Convers.,* vol. 22, pp. 439-449, Jun, 2007.
16. H. Kim, S. Kim, C. K. Kwon, Y. J. Min, C. Kim, and S. W. Kim, "An energy efficient fast maximum power point tracking circuit in an 800 μW photovoltaic energy harvester," I*EEE Trans. Power Electron.* vol. 28, pp. 2927-2935, Jun, 2013.
17. Y. Hong, T. Yoo, K. Chac, K. Back, and Y. S. Kim, "Efficient maximum power point tracking for a distributed system under rapidly changing environmental conditions," *IEEE Trans. Power Electron*. vol. 30, pp. 4209-4218, 2015.
18. A. K. Abdelsalam, A. M. Massoud, S. Ahmed, and P. N. Enjeti, "High-performance adaptive perturb and observe MPPT technique for photovoltaic-based microgrids," *IEEE Trans. Power Electron*. vol. 26, pp. 1010-1021, April, 2011.
19. A. Murtaza, M. Chiaberge, M. D. Giuseppe, and D. Boero, "A duty cycle optimization based maximum power point tracking technique for photovoltaic systems," *Electrical Power and Energy Systems*, vol. 59, pp. 141-154, July, 2014.

20. Ahmad, J.; Spertino, F.; Ciocia, A.; Di Leo, P., “A maximum power point tracker for module integrated PV systems under rapidly changing irradiance conditions,” in *Proc. 5th International Conference on Smart Grid and Clean Energy Technologies, ICSGCE 2015, pp. 7-11*.
21. K. Ishaque, Z. Salam, “A review of maximum power point tracking techniques of PV system for uniform insolation and partial shading condition,” *Renewable and Sustainable Energy Reviews 19(2013), pp. 475-488.*
22. Azadeh Safari, Saad Mekhilef, “Simulation and hardware implementation of incremental conductance MPPT with direct control method using Cuk converter,” *IEEE Trans. Power Electron, vol. 58, pp. 1154-1161, April, 2011.*
23. E. Koutroulis, "A new technique for tracking the global maximum power point of PV arrays under partial shading conditions," *IEEE Journal of Photovoltaics, Volume 2, Issue 2, April 2012, PP. 184-190.*
24. Ali Bidram, Ali Davoudi, Robert S. Balog, “Control and circuit techniques to mitigate partial shading effects in photovoltaic arrays”, *IEEE Journal of Photovoltaics, Vol. 2, No. 4, October 2012.*
25. K. S. Parlak, Hayrettin Can, "A new MPPT Method for PV array under parially shaded conditions," *3rd IEEE Symposium on Power Electronics for Distributed Generation Systems, pp. 437-441, 2012.*
26. H. Patel, V. Agarwal, “Maximum power point tracking scheme for PV systems operating under partially shaded conditions,” *IEEE Transactions on Industrial Electronics, vol. 55, Issue 4, pp. 1689-1698, 2008.*
27. A. Kouchaki, H. Iman-Eini, B. Asaei, “A new maximum power point tracking strategy for PV arrays under uniform and non-uniform insolation conditions”, *Solar Energy, 91 (2013), pp. 221-232.*
28. K. S. Tey, S. Mekhilef, “Modified Incremental Conductance algorithm for photovoltaic systems under partial shading conditions and load variation,” IEEE Trans. Industrial Electron. vol. 61, no. 10, Oct. 2014.
29. F. Spertino, Jawad Ahmad, P. Di Leo, A. Ciocia, “A method for obtaining the *I-V* curve of photovoltaic arrays from module voltages and its application for MPP tracking,” *Sol. Energy, vol. 139, December 2016, pp. 489-505.*
30. Kai Chen, Shulin Tian, Yuhua Cheng, Libing Bai, “An improved MPPT controller for photovoltaic system under partial shading conditions,” *IEEE*

Transactions on Sustainable Energy, Vol. 5, No. 3, July 2014, pp. 978-985.

31. Jawad Ahmad, F. Spertino, P. Di Leo, A. Ciocia, "A variable step size Perturb and Observe based MPPT for partially shaded photovoltaic arrays," *International Exhibition and Conference for Power Electronics, Intelligent Motion, Renewable Energy and Energy Management, 2016, pp. 1-8.*
32. Jawad Ahmad, F. Spertino, P. Di Leo, A. Ciocia, "An efficient maximum power point tracking algorithm for photovoltaic arrays under partial shading conditions," *IEEE International Power Electronics and Motions Control Conference, 2016, pp. 322-327.*
33. DD. Nguyen, B. Lehman, and S. Kamarthi, "Solar photovoltaic array's shadow evaluation using neural network with on-site measurement," in *Proc. Electr. Power conf., pp. 44-49, 2007.*
34. K. Punitha, D. Devraj, and S. Sakhtivel, "Artificial neural network based modified incremental conductance algorithm for maximum power point tracking in photovoltaic system under partial shading conditions," *Energy 62(2013), pp. 330-340.*
35. T. L. Nguyen and K. S. Low, " A global maximum power point tracking scheme employing DIRECT search algorithm for photovoltaic systems," *IEEE Trans. Ind. Electron. vol. 57, no. 10, pp. 3456-3467, Oct. 2010.*
36. J. W. Bishop, "Computer simulation of effects of electrical mismatches in photovoltaic cell interconnection circuit," *Sol. Cells 25 (1988), pp. 73-89.*
37. Damiamo La Manna, Vincenzo Li Vigni, Eleonora Riva Sanseverino, Vincenzo, Di Dio, Pietro Romano, "Reconfigurable electrical interconnection strategies for photovoltaic arrays," *Renewable and Sustainable Energy Reviews, 33(2014), pp. 412-426.*
38. Georgios N. Psarros, Efstratios I. Batzelis, and Stavros A. Papathanassiou, "Partial shading analysis of multistring PV arrays and derivation of simplified MPP Expressions," *IEEE Transactions on Sustainable Energy, vol. 6, No. 2, Apr. 2015, pp. 499-507.*
39. P. Robert C. N., and P. David J., "Submodule integrated distributed maximum power point tracking for solar photovoltaic applications," *IEEE Trans. Power Electron. vol. 28, pp-2957-2967, Jun 2013.*
40. E. Duran, M. Piliogine, M. Sidrach-de-Cardoan, J. Galan, J. M. Andujar, "Different methods to obtain the *I-V* curve of the PV modules: A review," *In Proc. 33rd IEEE PVSC, pp. 1-6, 2008.*

41. A. Q. Malik, S. J. Bin Haji Damit, “Outdoor testing of single crystalline silicon solar cells,” *Renewable Energy, 28, 2003, pp. 1433-1445.*

42. F. Spertino, Jawad Ahmad, A. Ciocia, P. Di Leo, Ali F. Murtaza, M. Chiaberge, “Capacitor charging method for *I-V* curve tracer and MPPT in photovoltaic systems,” *Sol. Energy, vol. 119, September 2015, pp. 461-473.*

43. Yingying Kuai, S. Yuvarajan, "An electronic load for testing photovoltaic panels," *Journal of Power Sources, vol. 154, Issue 1, pp. 308-13, 2006.*

44. E. Duran, J. Galan, M. Sidrach-de-Cardona, J. M. Andujar, “ A new application of the buck-boost-derived converters to obtain the I-V curve of PV modules,” in *Proc. 38th IEEE PESC, pp. 413-417, 2007.*

45. N. Femia, D. Giranozio, G. Petrone, G. Spagnuolo, and M. Vitelli, “Optimized one cycle control in phtovoltaic grid connected applications,” *IEEE Trans. Aerosp. Electron. Syst., vol. 42, no. 3, pp. 954-972, Jul. 2006.*

46. A. Wyote, J. Nins, and R. Belmans, “Partial shadowing of photovoltaic arrays with different system configurations: Literature review and field test results,” *Sol. Energy, vol. 74, no. 3, pp. 217-223, Mar. 2003.*

47. L. A. Hecktheuer, A. Krenzinger, C. W. M. Prieb, “Methodology for photovoltaic modules characterization and shading effect analysis,” *Journal of Brazilian Society of Mechanical Sciences, 24(1), 2002.*

48. M. G. Villalva, J. R. Gazoli, and E. R. Filho, “Comprehensive approach to modelling and simulation of photovoltaic arrays,” *IEEE Trans. Power Elctron. vol. 24, pp. 1198-1208, May 2009.*

49. A. Orioli, A. and Gi Gangi, “A procedure to calculate the five parameter model of crystalline silicon photovoltaic modules on the basis of the tabular performance data,” *Applied Energy, vol. 102, pp. 1160-1177, Feb. 2013.*

50. J. Accarino, G. Petrone, C. A. Ramos-Paga, and G. Spagnuolo, “Symbolic algebra for the calculation of the series and parallel resistances in PV module model” *In Proc. Clean Electric Power, International Conference on, pp. 62-66, 2013.*

51. Mutlu Boztepe, Francesc Guijoan, Guillermo Velasco-Quesada, Santiago Silvestre, Aissa Chouder, Engin Karatepe, “Global MPPT scheme for photovoltaic string inverters based on restricted voltage window search algorithm” *IEEE Trans. Ind. Electron. vol. 61, No. 7, Jul. 2014.*

52. M. E. Glavin, W. G. Hurley, “Optimisation of a photovoltaic battery ultracapacitor hybrid energy storag e system”, *Solar Energy, vol. 86, pp. 3009-3020, 2012.*

53. F. Spertino, Jawad Ahmad, A. Ciocia, P. Di Leo, “A technique for tracking the global maximum power point tracking of photovoltaic arrays under partial shading conditions,” *Power Electronics for Distributed Generation Systems (PEDG), IEEE Internationsl Symposium on, pp. 1-5, 2015*.

54. Weidong Xiao, Nathan Ozog, William G Dunford, “Topology study of photovoltaic interface for maximum power poitn tracking,” *IEEE Trans. Ind. Electrons., vol. 54, no. 3, pp. 1696-1704, Jun 2007.*

55. Dogan Ibrahim, “Advanced PIC microcontroller projects in C,” *Elsevier/Newness Inc.*

56. Jason Arrigo, “Input and output capacitor selection”, Application Note, Texas Instruments. Feb. 2006.

57. L. Ciani, L. Cristaldi, M. Faifer, M. Lazzaroni, M. Rossi, “Design and implementation of a on-board device for photovoltaic panel monitoring,” *In Proc. IEEE Instrumentation and Measurement Technology Conference, May, 2013.*

58. A. Ciocia, Jawad Ahmad, G. Chicco, P. Di Leo, F. Spertino, “Optimal size of photovoltaic systems with storage for office and residential loads in the Italian net-billing scheme,” *Accepted for publication at IEEE UPEC 2016.*

59. S. Moballegh, J. Jiang, “Modelling, prediction, and experimental validations of power peaks of PV arrays under partial shading conditions,” *IEEE Transactions on Sustainable Energy, vol. 5, no. 1, pp. 293-300, Jan 2014.*

List of Publications

1. F. Spertino, Jawad Ahmad, P. Di Leo, A. Ciocia, "A method for obtaining the *I-V* curve of photovoltaic arrays from module voltages and its application for MPP tracking," *Sol. Energy, vol. 139, December 2016, pp. 489-505.*

2. F. Spertino, Jawad Ahmad, A. Ciocia, P. Di Leo, Ali F. Murtaza, M. Chiaberge, "Capacitor charging method for *I-V* curve tracer and MPPT in photovoltaic systems," *Sol. Energy, vol. 119, September 2015, pp. 461-473.*

3. Jawad Ahmad, F. Spertino, P. Di Leo, A. Ciocia, "A module voltage based maximum power point tracking algorithm for photovoltaic arrays under partial shading conditions," *IEEE International Conference on Power and Electrical Engineering of Riga Technical University, October 2016.*

4. Jawad Ahmad, F. Spertino, P. Di Leo, A. Ciocia, "An efficient maximum power point tracking algorithm for photovoltaic arrays under partial shading conditions," *IEEE International Power Electronics and Motions Control Conference, 2016, pp. 322-327.*

5. Jawad Ahmad, F. Spertino, P. Di Leo, A. Ciocia, "A variable step size Perturb and Observe based MPPT for partially shaded photovoltaic arrays," *International Exhibition and Conference for Power Electronics, Intelligent Motion, Renewable Energy and Energy Management, 2016, pp. 1-8.*

6. F. Spertino, Jawad Ahmad, A. Ciocia, P. Di Leo, "A technique for tracking the global maximum power point tracking of photovoltaic arrays under partial shading conditions," *Power Electronics for Distributed Generation Systems (PEDG), IEEE Internationsl Symposium on, pp. 1-5, 2015.*

7. Ahmad, J.; Spertino, F.; Ciocia, A.; Di Leo, P., “A maximum power point tracker for module integrated PV systems under rapidly changing irradiance conditions,” in *Proc. 5th International Conference on Smart Grid and Clean Energy Technologies, ICSGCE 2015, pp. 7-11*.

8. Ahmad, J; Ciocia, A; Spertino, F; “ A maximum power point tracker of photovoltaic arrays under partial shading conditions, ” in Proc. *Industrial Engineering and Operations Management (IEOM), 2015 IEEE International Conference on, pages 1-5.*